AN INVESTIGATION INTO DYNAMIC STABILITY OF WATERBORNE AIRCRAFT ON TAKE-OFF AND LANDING

Jafar A.H. Masri

PhD

2020

AN INVESTIGATION INTO DYNAMIC STABILITY OF WATERBORNE AIRCRAFT ON TAKE-OFF AND LANDING

Jafar A.H. Masri

A thesis submitted in partial fulfilment of the requirements of the University of Northumbria at Newcastle for the degree of Doctor of Philosophy

Research undertaken in the Faculty of Engineering and Environment

March 2020

Abstract

This research contributes to the knowledge of dynamic stability of waterborne aircraft and ground effect phenomenon. Hereto an analytical and computational study has been performed during which the motion of waterborne aircraft in take-off and landing is predicted. An analytical tool that can be used to predict the nonlinear heaving and pitching motions of seaplanes is presented. First, the heaving and pitching equations of motion are presented in their general Lagrangian form. Then, the equations are simplified to a form of nonlinear equations known as the forced Duffing equations with cubic nonlinearity. The system of motion is assumed to be driven by a sinusoidal head sea wave. The equations are then solved using the Poincare-Lindstedt perturbation method. The analytical solution is verified with CFD simulations performed on Ansys Fluent and AQWA. The solution is used to extend Savitsky's method to predict porpoising which is a form of dynamic instability found in high-speed boats and seaplanes.

The results of the analytical tool are in very good agreement with the results obtained from Fluent and AQWA. However, as the motion is assumed to be 2D in Fluent, heaving amplitude is slightly over predicted. Moreover, the frequency of oscillations of the 2D simulations is found to be unsteady. The unsteadiness in frequency increases with the increase of the length of the hull. Nevertheless, the amplitude of the pitch motion is slightly less than the amplitude predicted analytically. The discrepancy in the results is due to the characteristics of the 2D simulations that assumes that sea water will only pass underneath the hull which will make the buoyancy force greater as less damping is experienced. This is also a consequence of the fact that parameters within the analytical model of heave and pitch are calculated using a strip theory which considers only hydrodynamic effects, while Fluent also incorporate aerodynamic contributions. Similarly, AQWA is a 3D platform that only takes in consideration hydrodynamic effects. Hence, the results of AQWA are slightly less in amplitude than that predicted analytically. In addition, it was found that the frequency of oscillations obtained using AQWA increases with time while in the analytical approach, the frequency of oscillations can only be

assumed to be constant for the whole period of motion. The increment in the oscillations indicates that porpoising is taking place. Nevertheless, it was found that heaving terms control the amplitude of motion and pitching terms control frequency of oscillations. The pitching nonlinear term has an effect on the amplitude of motion but not significant. Finally, the analytical method of Savitsky that is used to predict the porpoising stability limit is extended to find the porpoising limit for a wider range of pitch angles. In addition, the porpoising limit is predicted for a planing hull that is moving under the effect of head sea waves. When the seaplane is moving through head sea waves at a fixed pitch angle, porpoising takes place at a lower speed than what Savitsky has predicted.

List of Publications

- J. Masri, L. Dala and B. Huard, "Analytical prediction of heave and pitch motions of seaplanes advancing through head-sea waves," accepted for publication in Aerospace Science and Technology journal.
- J. Masri, L. Dala and B. Huard, "Effect of nonlinearity and coupling on frequency and amplitude of heave and pitch motions of sea-crafts under resonant periodic forcing," to be submitted to the journal of Applied Mathematical Modelling (under preparation).
- J. Masri, L. Dala and B. Huard, "Analytical prediction of heaving and pitching motions of seaplanes," in *Aerospace Europe2020 Conf.*, Bordeaux, France, Feb. 25-28, 2020.
- J. Masri, L. Dala and B. Huard, "A review of the analytical methods used for seaplanes' performance prediction," *Aircraft Engineering and Aerospace Technology*, vol. 91, no. 6, pp. 820-833, 2019.
- J. Masri, L. Dala and B. Huard, "A review of the analytical methods used for seaplanes performance prediction," in *6th Aircraft Structural Design Conf.*, Bristol, UK, Oct. 9-11, 2018.

Declaration

I hereby declare that this research is my own original work and has not been submitted before for any other award. I also confirm that this work fully acknowledges opinions, ideas and contributions from all sources used and have cited these in the Reference section.

Any ethical clearance for the research presented in this thesis has been approved. Approval has been sought and granted by the Faculty Ethics Committee on 09/05/2018.

I declare that the word count of this thesis is 34360 excluding references, footnotes and appendices.

Name: Jafar A.H. Masri

Signature:

Date: March 2020

Acknowledgement

First and foremost, I would like to thank my supervisor Prof. Laurent Dala for his tremendous help, encouragement and support. His technical knowledge, everlasting enthusiasm and integrity of character have provided invaluable contribution throughout this Ph.D. research. The joy and enthusiasm he has for his research was contagious and motivational for me, even during tough times. I am also thankful for the excellent example he has provided as a successful professor and person.

I would also like to thank my co-supervisor Dr. Benoit Huard for his patience, motivation, and immense knowledge. His help in the mathematical part of the work was indispensable. I would like to thank him for giving me the opportunity to teach with him. I could not have imagined having a better supervisory team for my Ph.D. study.

My sincere thanks goes to all the members of the Department of Mechanical and Construction Engineering at Northumbria University, staff and students, for creating the environment, within I have been very lucky to work.

I thank the Faculty of Engineering of Environment at Northumbria University for funding my Ph.D. research. I will be grateful for this University for the rest of my life.

Last but not least, I would like to thank my family for their encouragement and support during the many rainy days.

Contents

List of Figures

List of Tables

Nomenclature

- g: Acceleration of gravity (m/s²)
- V: Velocity (m/s)
- V_m: Mean velocity (m/s)
- B or b: Seaplane beam (m)
- S: Wetted surface area (m²)
- A: Aspect ratio = $\frac{b^2}{S}$
- Δ or m: Seaplane mass (kg)
- ∇: Static volume of displacement (m^3)
- $C_{L\beta}$: Lift coefficient, dead-rise surface
- C_{Lo}: Lift coefficient, zero dead-rise
- λ: Wetted length-beam ratio
- λ_y: Dimensionless distance between stagnation point and transom
- L_w: Wetted length (m)
- L_k: Keel length (m)
- L_m: Mean wetted length (m)
- L_c: Chine length (m)
- C_f: Friction-drag coefficient
- C_p: Centre of dynamic pressure (m)
- ε: Inclination of thrust line relative to keel line (deg), or a small non-dimensional parameter
- ρ: Density of fluid (kg/m³)
- F_n: Froude Number = $\frac{V}{\sqrt{gb}}$
- $F_{n\nabla}$: Volumetric Froude Number = $\frac{V}{\sqrt{g\sqrt[3]{\nabla}}}$
- R_e: Reynold's number = $\frac{V_m \lambda b}{v}$
- $\emptyset$: Roll angle (deg)
- β: Dead-rise angle (deg)

- τ: Trim angle (deg)
- D_f: Fluid friction drag (N)
- v: Kinematic viscosity of fluid (m²/s), or pitch rotational angle (rad)
- P_{max}: Maximum pressure at stagnation point (Pa)
- q: Pressure along the keel line (Pa)
- P_L: Pressure behind the stagnation point (Pa)
- P_T: Pressure at the transom (Pa)
- M: Moment (N.m)
- η: Displacement coordinate vector
- $\dot{\eta}$: Velocity coordinate vector
- $\ddot{\eta}$: Acceleration coordinate vector
- F_3: Amplitude of the exciting force (heave)
- F_5: Amplitude of the exciting moment (pitch)
- I_{55}: Mass moment of inertia (kg.m²)
- ω: Circular frequency of the encounter (rad/sec)

CHAPTER 1

1. INTRODUCTION

1.1 Research Background

The modern transport market can be divided into two categories: the first one has the ability to reach high speed but with low-payload capacity, such as airplanes, and the second one has high-payload capacity but operates in the low speed regime, such as cargo ships. With the increasing number of passengers and the need for more freight transport around the world, logistics and transport companies are pressured to increase the number of flights. This, however, has led to a major increase in global air traffic, while the aviation industry is under pressure to reduce noise and emissions. In fact, the rising concerns about noise and air pollution in the areas close to large airports are affecting the capacity and expansion of airports. One of the potential solutions for this issue is to build airports away from populated areas in offshore locations which means moving take-off and landing paths over water. However, the cost of land reclamation and the need for new terminal buildings and pathways to be constructed is very expensive. These reasons, combined with environmental concerns over fuel efficiency has led researchers to look for hybrid technologies capable of closing this gap in the market.

A substantial alternative that would end the need for such expensive infrastructure expenditure would be the use of waterborne crafts. Since the beginning of the nineteenth century, the concept of waterborne vehicles has been widely investigated due to its ability to cover a wide range of applications as well as its ability to combine between the characteristics of aeroplanes and hydroplanes. Moreover, as almost 71% of the earth's surface is water, the waterborne aircraft could provide access to almost every part of the world.

Waterborne aircraft is essentially a ship that has the ability to fly just above water with a speed close to normal airplanes. The increase in speed relative to normal ships comes from the increased lift force acting on the lower surface of the craft while traveling in the region close to water or any underlying surface. This phenomenon is called ground effect and known for its substantial lift-to-drag ratio that makes the hybrid combination of a huge cargo ship and a fast airplane possible. This hybrid configuration was most notably used in the development of the "Ekranoplan" designed by the Soviet Union in the beginning of the 1960s [1]. The configuration is also known as seaplane, sea-craft, ground effect vehicle (GEV) or wing-in-ground effect vehicle (WIG). A sea-craft flying in the ground effect region is shown in Figure 1.

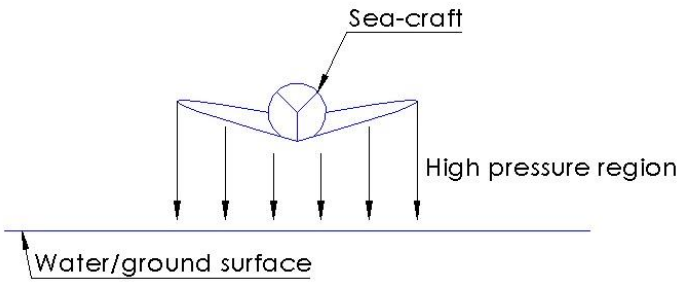

Figure 1. Sea-craft in ground effect

The benefits of a hybrid design capable of sustaining high-speeds while carrying significant amount of cargo are extremely tangible. Not only financial, but also humanitarian needs vindicate a worthy amount of research into this field. Considerable work has been done, mainly in Russia, on the ground effect machines. Other work has focused on cushion vehicle or hydro-planing hulls. Whilst vital progress has been made, some issues still prevent the hybrid vehicles to take a significant market share from conventional ships of airplanes. Most importantly, there is still much which is not understood about the take-off and landing characteristics when the craft is under sea wave effects.

Nonlinear behaviour is very common in real-life engineering applications such as the circular motion of a spring-mass-pendulum system and the free vibration of cantilever beams [2]. Initially, the analytical foundations of nonlinear

theory built on the pioneering work of Poincare [3] and Lyapunov [4] at the end of the 19th century. In classical mechanics, the dynamical analysis is the study of time-evolving processes and their corresponding equations of motion. Thus, the nonlinear dynamical system is presented as a nonlinear equation (or system of equations) which then stand as a model of the process. A well-known example of nonlinear dynamical system is the forced Duffing equation [2], which serves as a prototype for anharmonic oscillations such as the one encountered when dealing with the motion of sea-crafts through head sea waves.

1.2 Problem Statement

A large number of analytical, numerical and experimental investigations have been carried out in the area of waterborne aircraft dynamics. However, the previous studies have many limitations and only applicable under some considerations and assumptions. There is insufficient work to define the nonlinear dynamic characteristics of motion of these crafts in take-off and landing when the craft is under the effect of sea waves. The current research will analytically study the take-off and landing characteristics of waterborne aircraft and develop a nonlinear mathematical model taking into consideration sea wave effect. This will allow the effect of nonlinearity and coupling in the two equations of heave and pitch to be explained and quantified. Also, the porpoising stability limit defined in Savitsky hydrodynamic stability analysis will be expanded through the analytical solution obtained. The porpoising stability limit is a key design parameter for waterborne aircraft and expanding this limit will enhance the dynamic and static stability of this configuration.

1.3 Aim and Objectives

The aim of this research is to analytically investigate the dynamic stability of waterborne aircraft during take-off and landing through obtaining analytical solutions to the two nonlinear equations of heave and pitch motions. The two equations are driven by an external force/moment that is assumed to be caused by sinusoidal head sea waves. Focus is given to only heaving and pitching because at

a speed-to-length ratio of less than 4 (take-off and landing speeds), the hydrodynamic coefficients associated with motions in other directions are neglected [5]. As a result, the dynamic stability of sea-crafts during take-off and landing is examined from heave and pitch motions. Heaving and pitching due to moving through head sea waves are illustrated in Figure 2. Heaving can be defined as the translational (linear) motion in the vertical direction while pitching is the rotational (angular) motion about the centre of gravity of the sea-craft [6].

Figure 2. Sea-crafts' heaving and pitching motions

The aim of this research will be achieved by completing the following objectives:

1. Derive and justify a nonlinear mathematical model of heave and pitch motions of sea-crafts.
2. Apply the perturbation method of Poincare-Lindstedt to obtain periodic analytical solution to the two nonlinear equations of heave and pitch. The method will be applied to the coupled and uncoupled forms of the equations to better quantify the effect of coupling.
3. Verify the analytical tool through comparing the analytical results obtained from Poincare-Lindstedt perturbation method with numerical results obtained from Ansys Fluent CFD software and Ansys AQWA.
4. Examine the effect of coupling and nonlinearity on frequency of oscillations and amplitude of motion. This will give an insight into the design parameters that can be used to enhance stability.
5. Extend Savitsky's method to predict the porpoising stability limit of seaplanes.

1.4 Contribution to Knowledge

The novelty of this research lies in the evaluation of the dynamic stability of seaplanes by the use a perturbation technique to solve the nonlinear equations of motion driven by sinusoidal head sea waves. In addition, the effect of coupling and nonlinearity on the motion of sea-crafts is examined. This should provide a deeper understanding of the nonlinear phenomenon associated with motion through head sea waves in which the effect of the nonlinear and coupling coefficients on the amplitude of the external force/moment is explained. Moreover, Savitsky analysis is extended to predict the porpoising stability limit from the nonlinear analytical pitch equation. Savitsky performed 2D analysis to obtain the porpoising stability limit from linear empirical relations which are limited to a certain range of speed and geometrical aspects. However, in this research, the applicability range is expanded using the nonlinear analytical solution of pitch rotational motion. Not only that, but also the understanding of the hydrodynamic characteristics of seaplanes as well as their dynamic stability is enhanced which contributed to the knowledge of the ground effect phenomenon. In addition, a detailed review of the conventional analytical methods used to study the performance of waterborne crafts is documented.

1.5 Thesis Outline

The thesis is organised as follows: in chapter 2, necessary background topics are introduced in which ground effect phenomenon is discussed and its applications presented. State-of-the-art analytical prediction techniques are presented and finally, the limitations of the analytical methods used to study the hydrodynamic performance of high-speed planing hulls are discussed. Chapter 3 presents the analytical mechanics of waterborne aircraft in which the structural response of the six-degree-of-freedom system is explained. The strip theory which is used to calculate the hydrodynamic coefficients of the equation of motion is illustrated. Chapter 4 presents the analytical approach used to obtain the solution to the nonlinear equations of heave and pitch motions. The Duffing equations and its applications are explained. The analytical methods used to study nonlinear ordinary

differential equations are discussed. The perturbation method of Poincare-Lindstedt used in this research is described and the solution to nonlinear heave and pitch system of equations of motion is presented. In Chapter 5, the CFD investigations carried out in this research are illustrated. The steps of performing CFD simulations using Ansys Fluent are explained. Not only that, but also the steps of performing Ansys AQWA simulations of motion are presented. The analytical and CFD results obtained are presented and discussed in Chapter 6. The results are verified using Ansys Fluent and Ansys AQWA. In this chapter, the analytical model presented in this research is used to extend the method of Savitsky in which the porpoising stability limit of high-speed planing hulls is predicted. Chapter 7 presents the conclusions drawn from this research and provides some guidance on possible areas of improvements and future research.

CHAPTER 2

2. LITERATURE REVIEW

2.1 Introduction

A significant number of scientist and engineers around the world have worked on the development of ground effect vehicles and concluded that this technology has an important impact on the transport segment, such as Rozhdestvensky [7], Hahn et al. [8], Ollila [9] and Ford [10]. In order to develop a mathematical model to study the dynamic stability of ground effect vehicles, it is necessary to understand the basic principles and performance characteristics of those vehicles. This chapter details previous publications and information pertaining to ground effect vehicles development, design characteristics and performance prediction which will enhance the understanding of the physics of ground effect vehicles.

2.2 Ground Effect Phenomenon

When a craft flies next to the surface of water or ground, it is influenced by the surface effect aero-hydrodynamics which develop high lift-to-drag ratio. As shown in Figure 3, the deceleration of air trapped between the ground and the wing surface causes significant increase in pressure on the under-surface of the wing [1]. Thus, ground effect (GE) can be defined as an increase in the lift-to-drag ratio of a lifting surface flying at a small relative distance from an underlying surface [7].

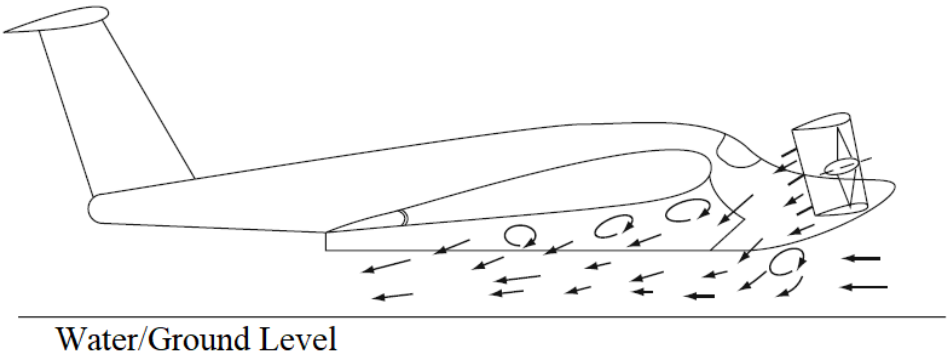

Figure 3. Ground effect concept [1]

This enhancement in the lift-to-drag ratio is mainly due to two reasons. First of all, as previously mentioned, lift increases as a result of the higher pressure experienced by the lower surface of the lifting body which consequently increases the lift-to-drag ratio. Secondly, drag deteriorates due to the fact that when flying next to a surface, wingtip vortices will not be able to spin around the wing so that less vortex drag will be generated. In this case, the vortices will impact the ground and cause an air cushion underneath the wing which will increase the pressure underneath the wing and hence, improve the lift-to-drag ratio. Moreover, it should be noted that creating wingtip vortices and the consequent downwash takes energy from the wings which causes more aerodynamic drag. This explains why less drag is experienced when flying in the ground effect region. Figure 4 shows a plane under the effect of wingtip vortices when flying at an altitude and when flying close to ground [1].

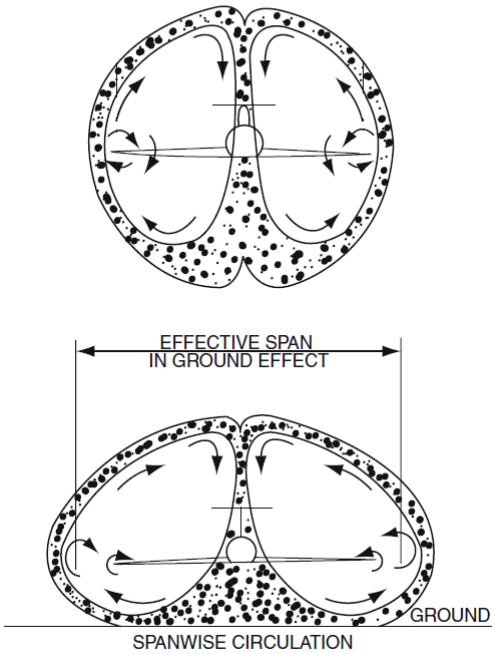

Figure 4. Wingtip vortices in GE [1]

Ground effect phenomenon was investigated by Bagley [11] who analytically and experimentally examined the pressure distribution on two-dimensional wings near the surface of ground. After that, Carter [12] conducted experimental testing on aerofoils with end plates and concluded the following:

1. An increase in the slope of the lift curve is experienced as the aerofoil approaches the ground.
2. If end plates are added to the aerofoil, a further increase in the slope of the lift curve and a considerable decrease in the induced drag are experienced which largely increase the lift-to-drag ratio. This is because wingtip vortices will not spin around the wing of the vehicle but will impact the ground which will create a region of high pressure underneath the vehicle.
3. The skin friction drag remains constant as the aerofoil approaches the ground.
4. As the height above the ground is reduced, the static longitudinal stability is increased at higher angles of attack due to the high-pressure region created underneath the vehicle.

It can be concluded that GE is the effect of aero-dynamic and aero-elastic forces on platforms flying very close to underlying surfaces. This effect is due to the reduction in wingtip vortices and increase in pressure underneath the vehicle which results in more lift force to be generated, less induced drag to be experienced and consequently less total aerodynamic drag to be encountered [13].

2.3 Wing-in-ground Effect Vehicles

2.3.1 Definition

Yun, Bliault and Doo [1] define the wing-in-ground (WIG) effect vehicle as one that creates load-carrying air cushion under its wings while flying just above the surface of water or ground. The latter goes on to claim that this configuration offers another step upwards in service speed which could reach almost 100 knots. Rozhdestvensky [7] defines the WIG effect vehicle as one with an engine which is designed to fly next to ground or water surface by taking advantage of ground effect. Maimun et al. [14] studied the aerodynamic characteristics of ground effect vehicles and claim that a GEV is one of high speed low altitude flying vehicle that could take-off and land on any relatively flat surface such as land, water or ice.

2.3.2 History and Development

Ground effect was already being used in flight machines in 1903 when the Wright brothers encountered the GE under what was known as “cushioning effect” or “pancake” landing. In 1930, the Dornier DO-X seaplane has experienced GE during its transatlantic flights [9]. The phenomenon was then highlighted as an enhancement in performance when flying close to a surface. After that, T. Kaario built a ground effect vehicle in Finland in 1935 [15]. It was the first purposefully designed vehicle to exploit GE. The vehicle was called “Aerosledge No.8” and it was a single seater and capable of reaching 12 knots over ice or water [7]. The vehicle is shown in Figure 5. However, due to the greater interest in passenger aircraft, seaplanes and high-speed boats were not developed further.

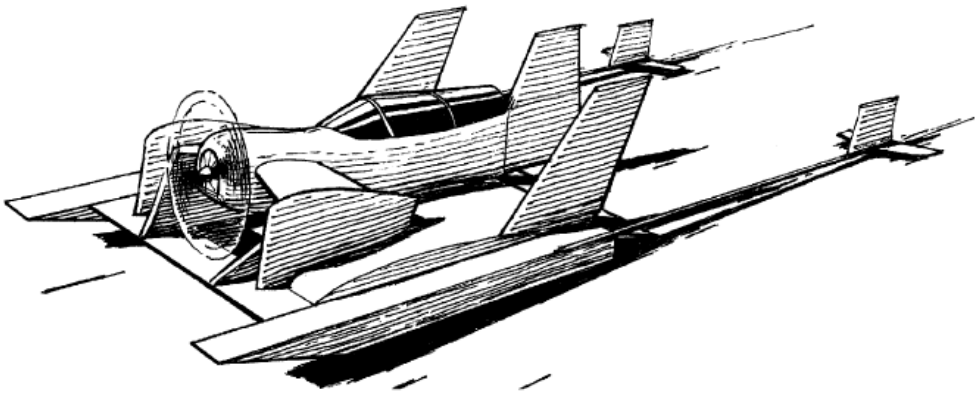

Figure 5. Aeroseldge No.8 GE vehicle [7]

At the beginning of the 1960s, R.E Alexeyev started his development programme in Russia focusing on a new military craft called Ekranoplan [7]. The work was carried out at the Central Hydrofoil Design Bureau in the Soviet Union and it was the world's first major research and development project targeting WIG effect vehicles [1]. The first concept developed by Alexeyev was inspired by high speed boats. The latter proposed to add aircraft-like wings to the hull of a high speed boat so that more lift will be generated. As a result, the craft will then take-off and glide just above the surface of water supported by GE.

Alexeyev noticed that the most important factor to stabilise the WIG effect vehicle is lift force variation on the distance from the wing to the water surface (screen or "ekran" in Russian). This variation allows the vehicle to fly steadily at a fixed distance from the water surface. This was regarded as the most critical design challenge in the development of WIG effect crafts [7]. Figure 6 illustrates this behaviour. It shows the effect of aspect ratio on the lift-to-drag ratio while taking in consideration the height above the ground as a ratio of height to mean chord. The lift-to-drag ratio increases in direct proportion with the aspect ratio and in inverse proportion with the height-to-chord.

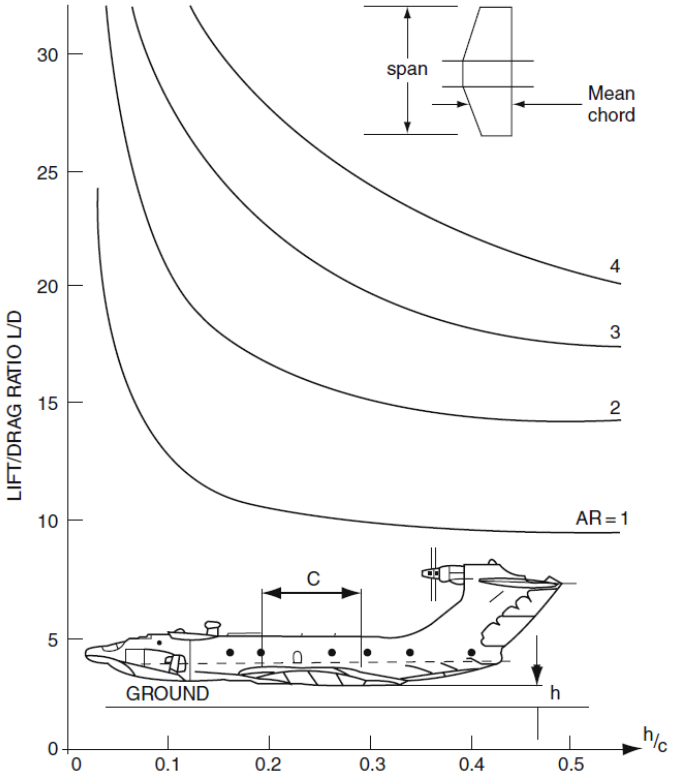

Figure 6. Lift-to-drag ratio against flying height [1]

Alexeyev and his team succeeded in the design and construction of the first WIG effect vehicle, SM-1 in 1960. The vehicle has a 20 m long cylindrical fuselage and two wings in a tandem arrangement and weighs almost 2.8 ton. It managed to reach 200 km/h over calm water [1]. A schematic diagram of SM-1 is presented in Figure 7.

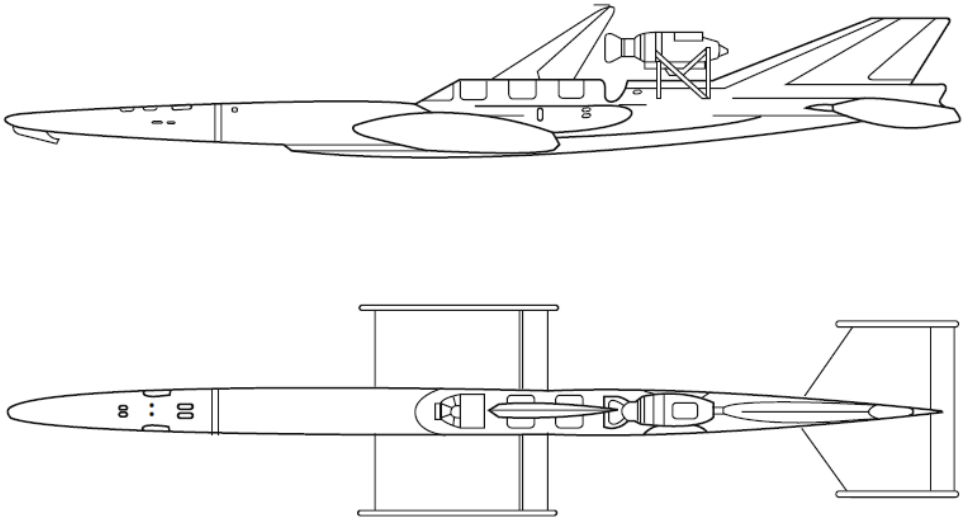

Figure 7. The SM-1 Ekranoplan [1]

SM-1 has proved the basic principles of GE and allowed the team to learn more about the concept. However, SM-1 had experienced several issues through testing till it crashed in January 1962 due to engine failure. In order to overcome the technical problems in SM-1, a new aerodynamic design was proposed. The new Ekranoplan has one main wing supported the craft in exploiting GE and another horizontal tail at the top of a vertical fin outside GE region to maintain longitudinal stability. Also, a new jet engine was mounted at the bow to deliver high pressure air through a diffuser into the area under the wing. The new design was called SM-2 and completed in March 1962 [1]. A schematic diagram of SM-2 is shown in Figure 8.

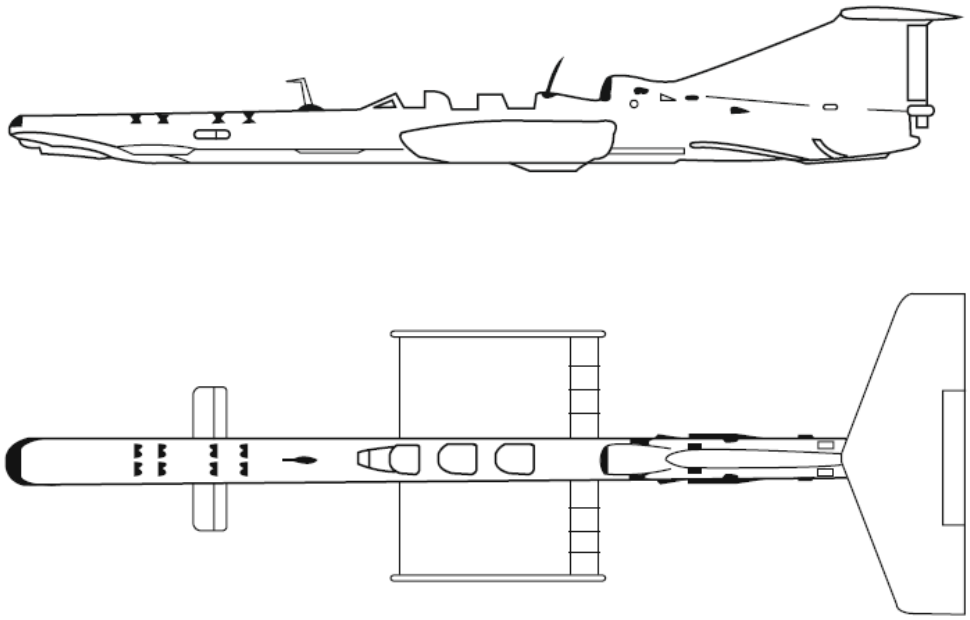

Figure 8. The SM-2 Ekranoplan [1]

Unfortunately, the SM-2 was partially damaged in a fire accident and was subsequently modified. The modified version was called SM-2P and it was given a rectangular wing, the tail size was increased and a second engine was installed. This craft showed better stability in cruising [1].

In 1962, SM-3 was designed and built to succeed the SM-2. It has a much longer, low aspect ratio main lifting wing and smaller tail wing. The engine is now mounted at the front of the nose of the fuselage with the exhausts blown under the leading edge of the lifting wing [1]. The SM-3 is presented in Figure 9.

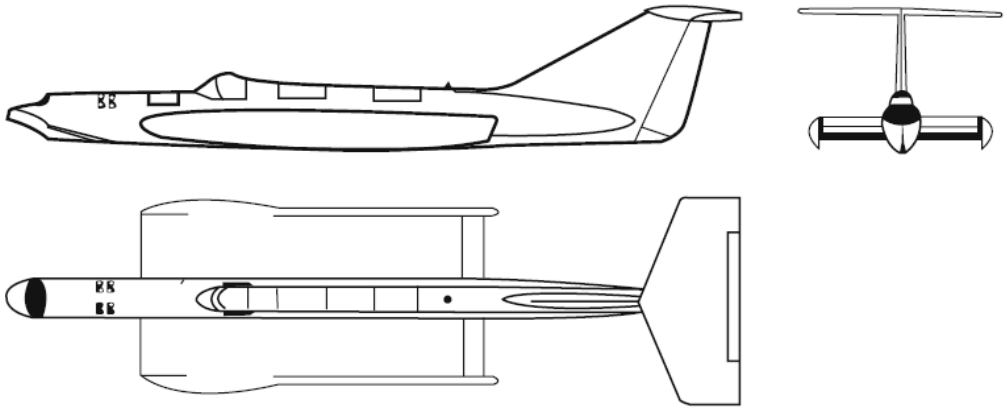

Figure 9. The SM-3 Ekranoplan [1]

This configuration showed much improved lifting capability but the low aspect ratio was not the best solution especially at high speeds. In addition, when flying at a distance of 1.5 m and above from the water, the SM-3 was unstable in yaw [1].

After that, a new configuration was developed based on the SM-2. It was called the SM-4 and had a larger jet engine to enhance take-off ability. The design was very promising and made Alexeyev believe that the hydrodynamic and aerodynamic characteristics of WIG effect vehicles are predictable enough that a huge step to a much larger production Ekranoplan was possible. As a result, the KM or the “Caspian Sea Monster” was next. The craft was 92.3 m long and weighed 544 ton. It was capable of accommodating 900 passenger and reaching a speed of 300 knots. Nevertheless, the KM had 10 huge turbojet engines with 13 ton thrust, 8 were mounted at the bow for take-off and 2 were mounted at the stern for cruising [1]. The KM is shown in Figure 10.

Figure 10. The KM Ekranoplan [1]

The craft was built in the “Chikarov” Naval Construction Facility very close to Gorky city and was completed in 1966. The first test took place in the Caspian Sea coast in October 1966. The craft was able to achieve a speed of 450 km/h without any stability problem. The take-off happened at a speed of 140 km/h using the 8 turbojet engines mounted at the bow. Thrust nozzles are turned down during take-off to blow under the lifting wing to create air cushion so that lift could be increased. Once the craft leaves the sea, thrust nozzles are turned back to their horizontal position to provide more thrust to accelerate. Landing procedure is very simple, it is the reverse procedure of take-off. First of all, thrust power is reduced so that the craft could slow down. Secondly, bow jets’ nozzles are turned down to increase pressure under the main wing. After that, cruising engines are turned down so that the craft could settle on its dynamic air cushion. Then, speed is reduced and the craft cruise in displacement mode just like a ship [1].

In order to examine the stability of the craft, Alexeyev stopped the engine and let the craft ditch without human intervention. The craft was able to land horizontally and safely and it gave the passengers on board much better confidence. Moreover, the craft had much improved manoeuvrability, it managed to complete a 360° turn without any issue [1].

The KM completed a 14-year operational career safely and successfully. However, during a test in 1980, the pilot changed to cruise mode before the KM actually enters the GE region which made the craft to lose speed and decelerate quickly and eventually touch the water at a relatively high speed which caused the craft to crash into the sea. The structure was damaged beyond repair and sank in the Caspian Sea [1].

The success of the KM made the team design a smaller WIG effect craft, the heavy-duty landing craft “Orlyonok”. It was constructed in 1973 with 120 ton weight, two engines hidden in the bow part of fuselage and a cruising propulsion mounted at the intersection of the vertical stabiliser and the tail plane [7]. A general profile and a picture of the Orlyonok are shown in Figures 11 and 12 respectively.

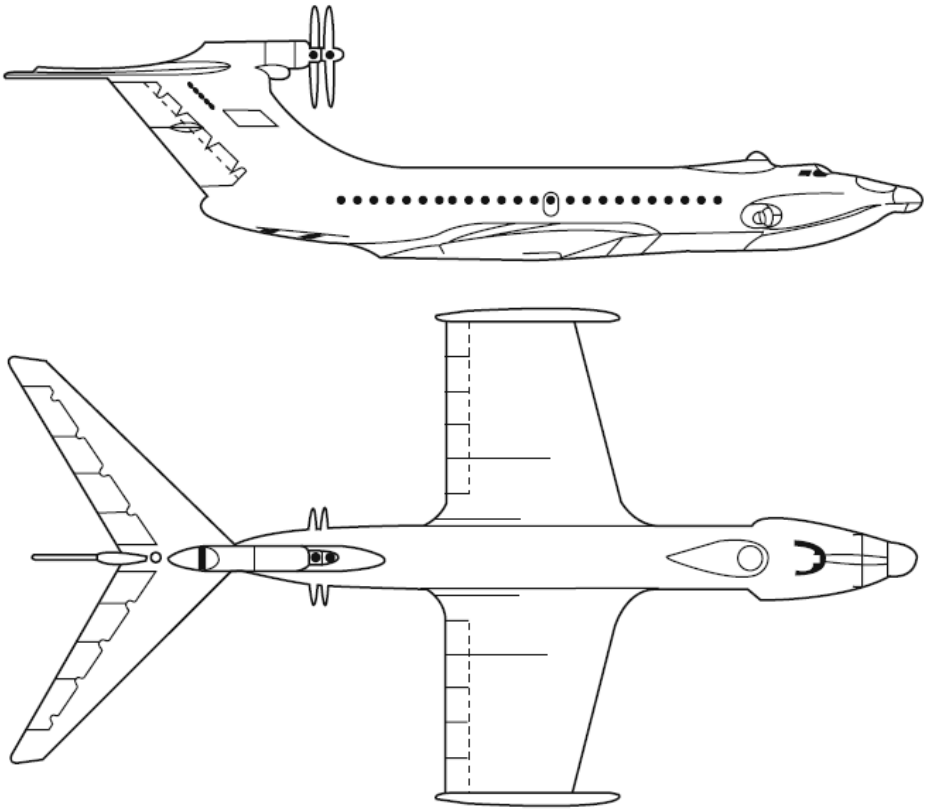

Figure 11. Orlyonok general profile [1]

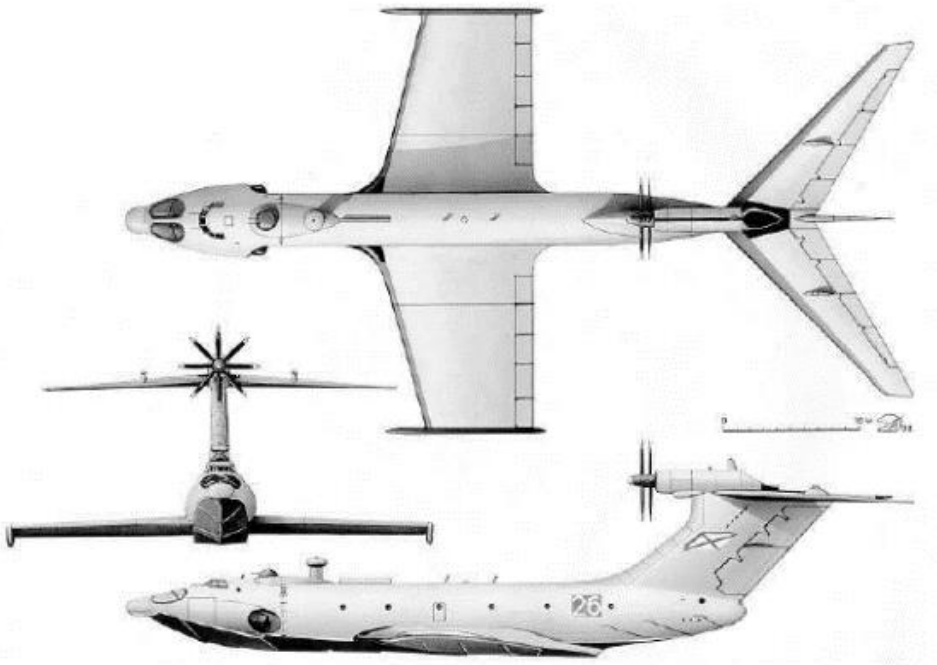

Figure 12. The Orlyonok Ekranoplan [16]

The Orlyonok showed improved manoeuvrability especially at low speed due to the improved rear engine and lower weight. But after a few runs, the craft made a strong impact with a wave resulting in a serious damage. Alexeyev claimed that the accident was caused by a pilot error [1].

In 1987, the development programme of Ekranoplans continued and staff at the Russian Central Navy designed a military WIG effect craft called “Lun” [1]. It was based on its predecessor the Orlyonok but with 8 engines at the front for take-off and 2 at the rear for cruising. It showed better seakeeping because of its more dynamically balanced design and larger size. In addition, the craft performed much better under the effect of sea waves of up to 3 m height [7]. The Lun is shown in Figure 13.

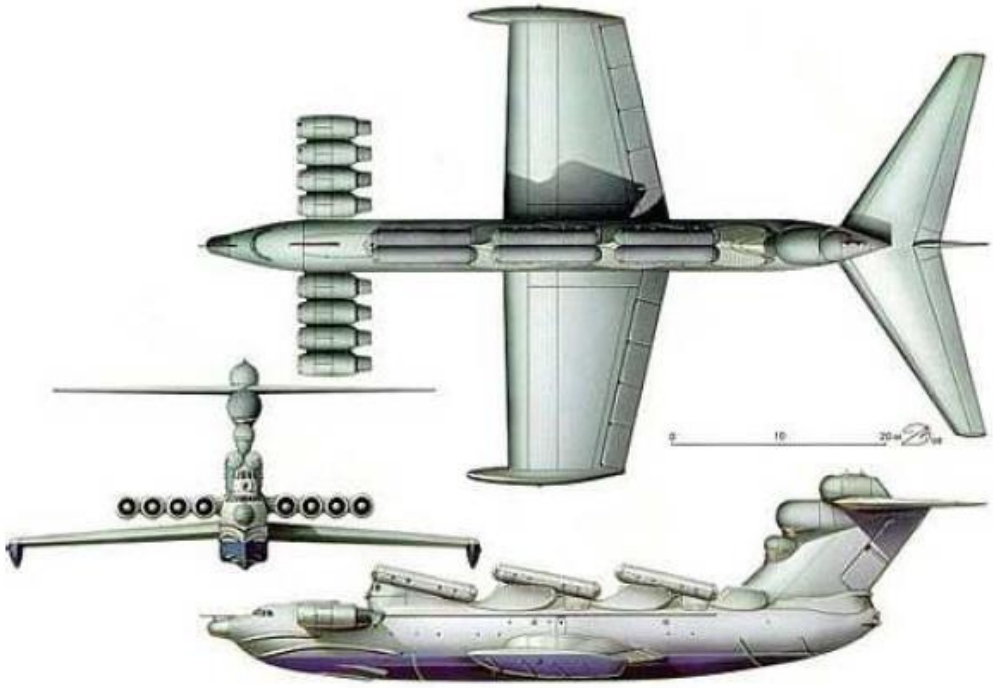

Figure 13. The Lun Ekranoplan [10]

Because of lack of funding, the Russian Navy was unable to continue developing WIG effect crafts. However, after the accident of the nuclear submarine "Comsomoloz" in 1989, Russian officials concluded that WIG crafts, with their high-speed capabilities, would be the best option to be used as salvage vehicles in remote areas [1].

WIG effect crafts were also developed in countries such as China, Germany, England and the USA. A more extensive historical review of WIG effect crafts can be found in [1], [7] and [9].

2.3.3 Technical Terms

To enhance the understanding of GE and WIG vehicles, a few technical terms relating to this technology are defined next:

1. Dynamic air cushion: it is the high-pressure region generated between the lifting body and the below water or ground surface as the body travels in the

improved aerodynamic effect region. This cushion can be generated in two ways:

- Geometrically: The lifting body can be shaped in a way so that air can be retained underneath the body. This was known previously as the captured air bubble (CAB) concept of the 1960s [10]. An example of a CAB vehicle is shown in Figure 14.

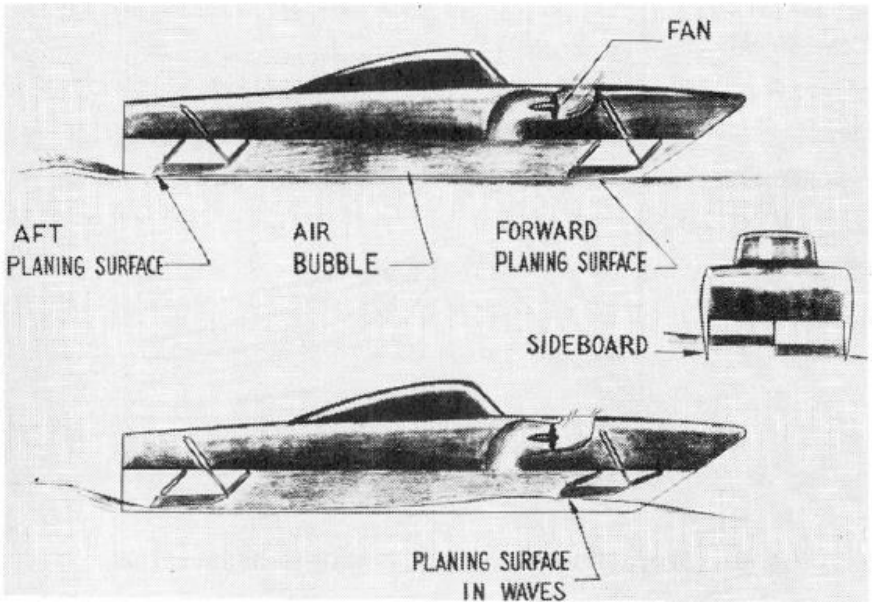

Figure 14. Captured air bubble (CAB) vehicle over water [10]

- Aerodynamically: in this way, air is blown underneath the lifting wing at a much higher speed than the body's forward speed. This way enhances lift by lowering he wing flaps and wing tip fences and by adjusting wing geometry. This was the basic principle for the Russian WIG effect craft programme [1].

2. Static air cushion: this is the high pressure region generated by air jets, propellers or fans that are mounted between a lifting body and water or ground surface (directed towards the water or ground surface when the craft is at standstill) [1]. A WIG effect craft designed to create static air cushion

will close the main wing flap when accelerating from a standstill to assist in generating the static air cushion.

3. Hump speed point: as the seaplane accelerates from zero velocity, there is some speed at which the water resistance becomes maximum. This point is known as “hump speed point”. It is the point where the lift force shifts from being predominantly buoyant to being dynamic (hydrostatic to hydrodynamic). This is a key point in WIG effect craft design success [17-19]. The variation of water drag with vehicle speed and with engine thrust for a hypothetical WIG vehicle is explained in the conceptual curves in Figure 15.

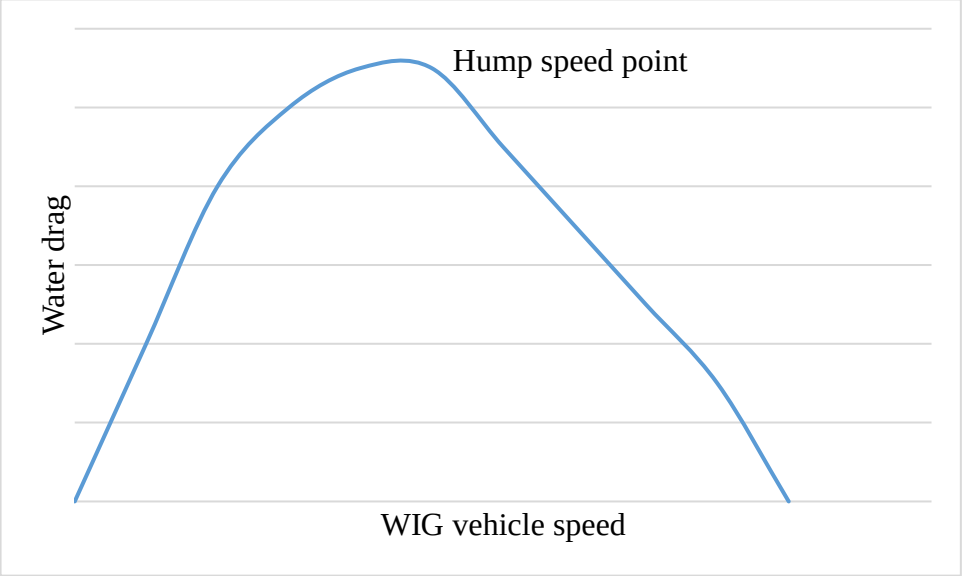

Figure 15. Variation of water drag with speed and thrust

4. Porpoising: WIG effect vehicles have a unique instability phenomenon called porpoising which, according to Faltinsen [19], can be defined as a periodic, bounded vertical motion that a craft might show at take-off and landing speeds. A schematic of porpoising is shown in Figure 16. This phenomenon can be seen as an oscillatory motion in the heave and pitch axes and can cause severe damage to the structure of the craft. In some cases, if the hull is leaving water and returning at negative trim angle, the craft will submarine [20]. Stability issues of WIG effect vehicles can be fateful even in calm water. Loss

of longitudinal stability can cause self-induced heave and pitch oscillations (porpoising) and submergence of the bow area [21]. Therefore, it is very important to predict the behaviour of WIG effect vehicles in the design stage. More details about porpoising can be found in [5, 21, 22, 23].

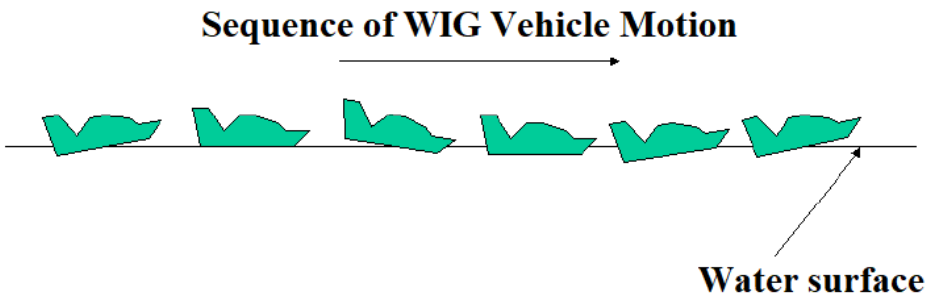

Figure 16. Schematic of Porpoising [21]

5. Froude Number (F_n): it is a dimensionless number used in hydrodynamics to study the influence of gravity on fluid motion [24]. It is defined based on the speed-to-length ratio as follows:

$$F_n = \frac{U}{\sqrt{gL}} \tag{2.1}$$

where U is the forward speed, g is the acceleration of gravity and L is the length of the craft's hull. It can also be based on the beam length of the hull or the volume of displacement [19].

2.3.4 Types

The wish to develop an optimum configuration of a WIG effect vehicle that generates low drag and provides sufficient stability in all possible speeds has led to a wide range of ground effect vehicle concepts. Clearly, the objective of every design is to perfectly exploit GE. However, the differences are in the lifting methods used to operate near water or ground surfaces and in the methods used to maximise the lift to overcome the hump speed point. The different types proposed over the

past years have different names and are known by acronyms. The variations may be summarised as follows:

- Wing-in-ground (WIG): this is the most common name of crafts with GE technology. Crafts designed with deep chord lifting wing and side buoys or plates are known as WIG vehicles. These crafts have no especial lift improvement features like propellers or fans to blow under the main wing. They have the advantage of lower capital and running cost compared to the other types. This design fits very well in the civil applications as it is configured to operate in the lower speed and load ranges [25]. An example of this type is the Lippisch X-114 developed in Germany for tourism purposes [26]. The model is shown in Figure 17.

Figure 17. Lippisch X-114 WIG [26]

- Ekranoplan or power augmented wing-in-ground effect craft (PARWIG): The PARWIG is a very good example of a GE machine that could be designed with improved performance and operating characteristics. It has bow-mounted propellers that make the generation of air cushion under the wing possible at even zero forward speed. This improves the take-off ability and eliminates the hump drag [1]. Most of the configurations are built for military applications (high speed and load capacity) [7]. These vehicles use propellers to create a static air cushion underneath the main wing to generate lift as

described before in section 2.3.2. An example of this type is the KM Ekranoplan presented in Figure 10.

- Dynamic-air-cushion craft (DACC) or Ground-effect-machine (GEM): this configuration flies in the high-pressure region very close to the underlying surface. The craft in this case has a large cushion length-to-beam ratio. In addition, it has one or two lifting wings with small aspect ratio. The propellers are usually mounted at the front in order to blow high pressure air into the cushion underneath the craft. This configuration has the advantage of added take-off ability as it starts to enter the in-surface effect at lower speed compared to other types. The Russian "Volga-2" (shown in Figure 18) is considered a DACC [27].

Figure 18. Volga-2 DACC craft [27]

- Dynamic air cushion wing-in-ground effect craft (DACWIG): this is a hybrid design that combines the characteristics of both the DACC and the PARWIG. It is designed to take the high-speed ability and good cruising stability of the PARWIG, and the easier manoeuvring and less capital cost of the DACC. This configuration operates in the strong ground effect zone close to the water surface, and it is unable to operate out of the GE region which makes it less complicated due to the un-needed stability and control systems. A typical

craft of this type is the Chinese DACWIG presented in Figure 19 and known as the SWAN [28, 29, 30].

Figure 19. The SWAN [28]

2.3.5 Operational Modes

The modes of operation of GE machines, over different surfaces and at different speeds, are presented in Figure 20.

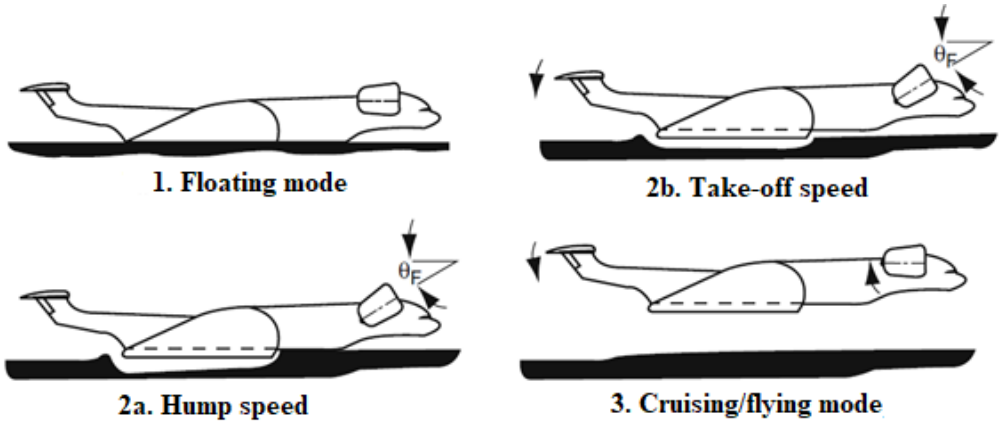

Figure 20. WIG vehicles operational modes [1]

The operational modes of WIG effect vehicles can be explained as follows:

1. Floating mode: this mode is used for manoeuvring on water at low speed after launching or approaching terminal.
2. Air cushion-borne mode: the craft is moving on water at medium speed. This mode is used for manoeuvring over narrow water ways and also when

accelerating for take-off. There are two points at which the overall performance is highly affected due to the peak drag experienced:

a. Hump speed: this point is explained previously in section 2.3.3. In basic words, the hydrodynamic resistance becomes maximum at this speed point. The pilot should make an effort to pass this hump speed as quickly as possible.
b. Take-off speed: this is the point where lift becomes high enough to overcome hump drag. The craft will then leave water surface to enter true flying mode in GE region. At this point, daylight clearance will exist between the craft's hull and water surface. Also, hydrodynamic resistance will noticeably drop allowing the craft to accelerate to cruising/flying mode.

3. Cruising/flying mode: the craft is operating in the GE region at high speed. Stability and behaviour in this mode is highly affected by the vehicle configuration and thrust power.

2.3.6 Alternative Technologies

There are several other vehicle types that were developed to provide fast marine transportation. The most common alternatives to WIG effect vehicles are as follows:

1. The Hydrofoil: this alternative craft has foils attached to its hull that act as an aircraft's wings in water. The foils operate in water which causes high water-friction drag. In contrast to WIG vehicles, this technology does not use the GE to generate lift. Its speed is limited to a maximum of 50 knots due to the cavitation barrier on the foil upper surface [31]. The fully-submerged hydrofoil shown in Figure 21 and known as the "Jetfoil" is the most famous example of hydrofoil crafts [31].

Figure 21. The “Jetfoil” hydrofoil craft [1]

2. The surface effect ship (SES): the side hulls of this craft are designed to generate an air cushion and reduce the water wave-making. However, it still has very significant water-friction drag. This technology has the advantage of much larger payload compared to hydrofoils. It can reach a maximum speed of 100 knots [31]. The SES Bell Halter 110 is shown in Figure 22.

Figure 22. The Bell Halter 110 SES craft [1]

3. The Hovercraft: it is also known as air cushion vehicle (ACV). As shown in Figure 23, this configuration uses fans to blow air into a cavity in a similar way to the SES. However, it has flexible skirts around the air cushion periphery which are used to isolate the craft from the surrounding water surface so that it can operate over both water and ground [31].

Figure 23. BHC AP1-88 hovercraft [1]

2.3.7 Advantages and limitations

Before discussing the advantages and limitations of WIG effect vehicles over other technologies, it may be helpful to first distinguish the WIG effect vehicles from other marine vehicles and airplanes. A WIG vehicle next to a conventional airplane is shown in Figure 24. The features that distinguish WIG vehicles from other technologies are listed below the Figure:

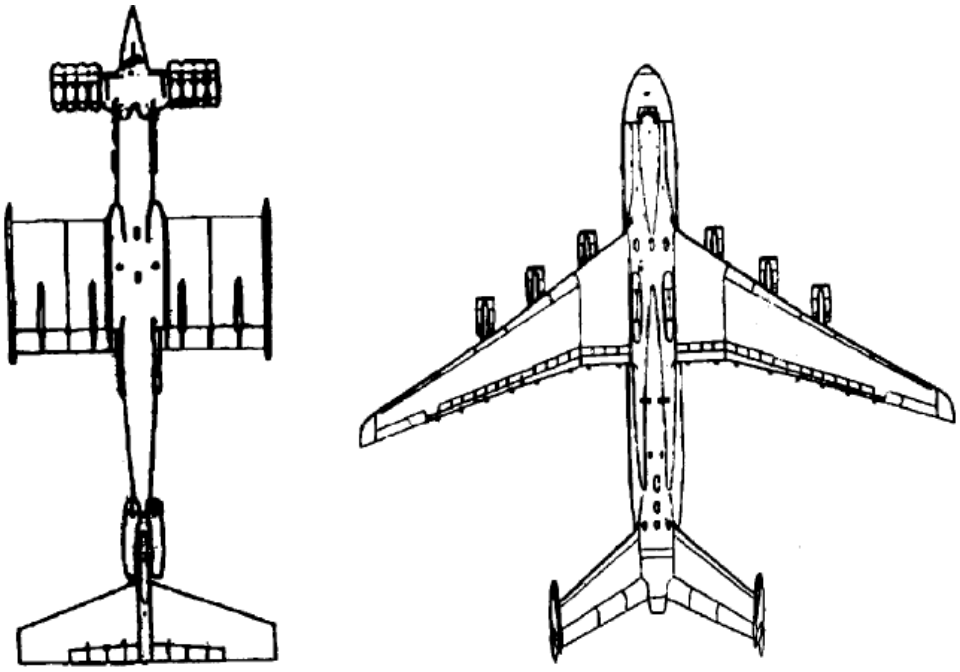

Figure 24. WIG vehicle vs airplane [7]

1. The main wing is low attached to the hull and has wide shape with small aspect ratio. Also, boundary plates (usually float plates) are attached to the main wing to enhance its aerodynamics when moving close to water. This is to restrict air underneath the craft in order to create the high pressure region (air cushion) [31].
2. Improved tail assembly. The fin (or sometimes fins) is high and has a rudder. Also, a horizontal stabiliser is attached to the fin at utmost height.
3. The bottom of the hull is made with increased strength to withstand the hydrodynamic loads.
4. The WIG effect vehicle has specific equipment and specific software for automatic control to enhance and expedite taking-off from water, stability, efficiency and safety.
5. Adjustable bow-mounted propellers to allow for air blow under the main wing for increased take-off ability. This can also be done by installing deflectors or leading edge slats.

The most important advantages of GE machines over other technologies are as follows:

1. Much improved safety because of the ability to ditch over water in case of an emergency which means especial life-support systems for crew and passenger are not required.
2. Specific transport operations and expensive runways are not needed as WIG effect vehicles can use any naval port or shore as their base of operation because they have the ability to fly, float on water and land on shore.
3. Much improved comfort level is possible.
4. Less expensive cargo and passenger transportation can be achieved. Nevertheless, with this technology, the touristic and commercial opportunities are endless.
5. Improved fuel consumption due to the high-lift-to-drag ratio experienced.

Despite that, GE vehicles have a few limitations such as:

1. WIG effect vehicles need calm seas to operate. High waves can be a big challenge when designing a WIG craft.
2. Very long journeys are not possible without refuelling which pose a practical challenge.
3. The cost of designing and producing a WIG effect vehicle is very high compared to a conventional ship or aircraft.

2.4 Aerodynamic Aspects of WIG Effect Vehicles

Aeroplanes usually experience four forces: lift force, drag force, gravitational force and thrust force. The gravitational force depends on the weight of the craft and it is always directed towards the earth. The thrust force depends on the engine and the type of propulsion system of the craft. The lift and drag forces depend on the shape of the craft, the air conditions, the velocity of the craft and other factors. Lift is directed opposite to the weight and drag is opposite to the thrust.

In terms of aerodynamics, GE is the improved performance of forces of a lifting body with respect to the freestream results, which is applicable when operating next to an underlying surface. As illustrated in Figure 25, the aerodynamic forces experienced by aeroplanes are categorised into two components: lift normal to the freestream and drag parallel to the freestream. When operating close to a surface, the incoming fluid flow is restricted under the lower surface of the wing which increases the pressure and thus produces more lift compared to the freestream results. Moreover, the induced drag is reduced due to the reduction in downwash as explained previously in section 2.2. This change in aerodynamics between conventional airplanes and WIG effect vehicles is demonstrated in Figure 26 [32].

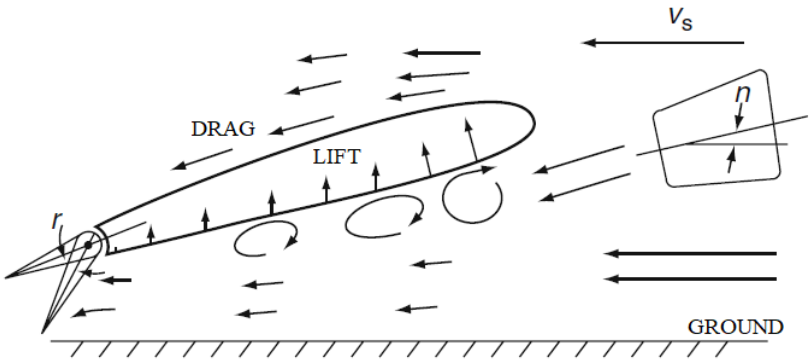

Figure 25. Aerodynamic forces experienced by WIG vehicles [1]

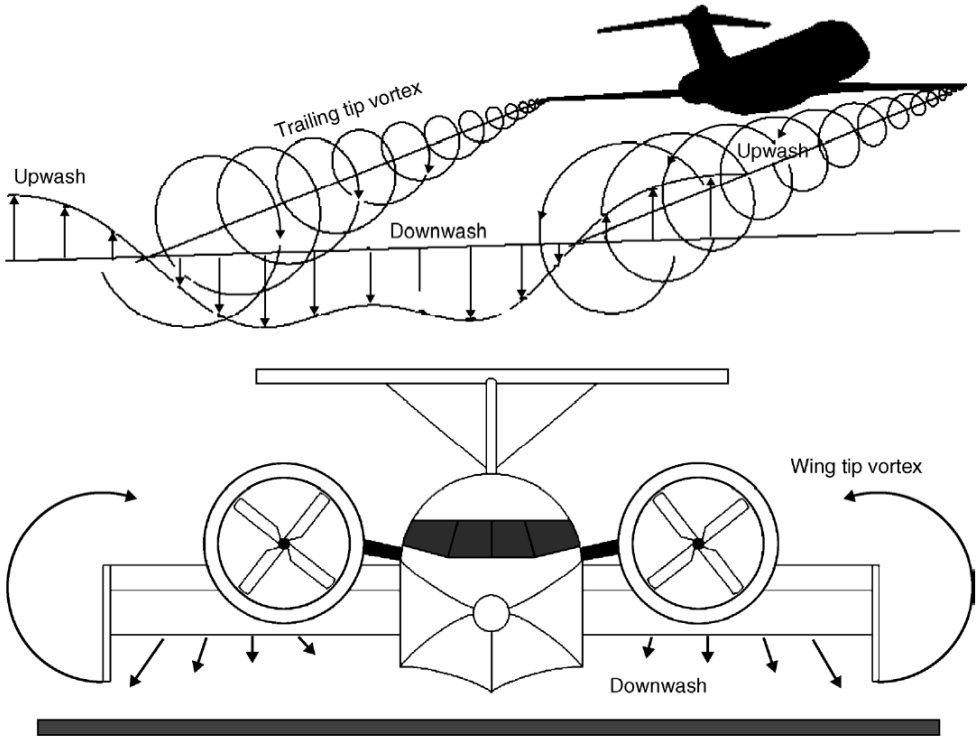

Figure 26. Aerodynamics of WIG vehicles vs normal airplanes [32]

The study of WIG effect craft aerodynamics is concerned with the effects of the three-dimensional flow field on the overall performance produced by the presence of the underlying surface. In order to understand the aerodynamics of WIG effect vehicles, it may be helpful to first explain the terminology. The aerodynamic performance of a WIG vehicle can be described by a few terms such as:

- Wingspan: as shown in Figure 27, it is the horizontal distance between the tips of the two wings of a craft [33].

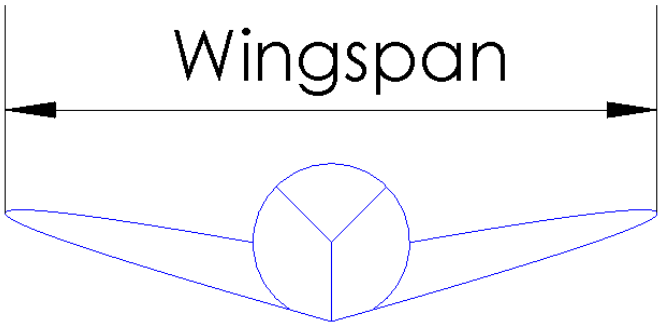

Figure 27. Wingspan of a WIG craft

- Angle of attack: it is the angle between the oncoming air or relative wind and a reference line on the airplane or wing as shown in Figure 28 [33].
- Chord length: as presented in Figure 28, this parameter refers to the distance between the leading edge and the trailing edge of a wing or aerofoil [33].

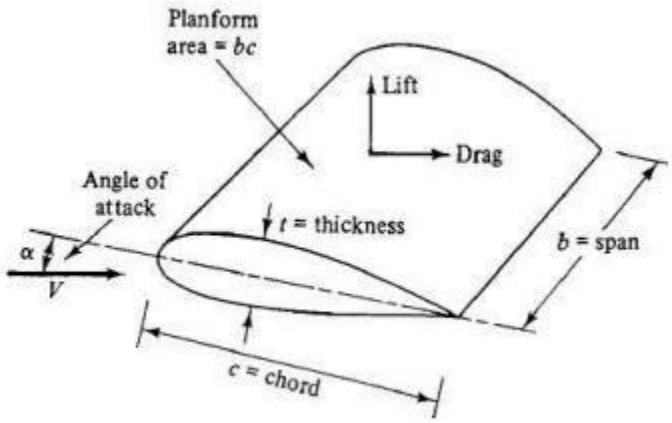

Figure 28. Aerodynamic parameters of WIG vehicles [33]

- Wing loading factor: is the WIG vehicle weight per unit area of wing.
- The aspect ratio (AR): is the ratio of the wing's span to its mean chord.
- Stagnation point: it is a point at the leading edge on an aerofoil where the local velocity of stream or wind stagnates (brought to a standstill). In other words, it is the point where the flow field splits, flow above the stagnation

point goes to the upper surface of the aerofoil and flow below the stagnation point goes to the lower surface of the aerofoil [34].

It should be mentioned that the impact of ground effect starts when the craft is on a distance equals the wingspan from the underlying surface [31].

In the next sub-sections, the aerodynamic aspects that define the performance of WIG effect vehicles and their performance prediction methods will be discussed.

2.4.1 Aerodynamic Lift

Lift can be defined as the mechanical aerodynamic force that holds the vehicle in the air. It is produced by motion of a flying body through air and it is always in the direction opposite to the weight of the body. Lift force is generated from every part of the vehicle body but the major part of it is generated by the wings. Aerodynamic lift is a vector force that has a magnitude and a direction. In terms of direction, lift force passes through the centre of pressure of the craft and it is always normal to the flow direction. On the other hand, the magnitude of the lift force is affected by wingspan, angle of attack, height above the underlying surface, wing loading factor, aspect ratio and vehicle speed [34, 35].

Lift force depends on Newton's third law of action and reaction. It passes through the centre of pressure of the craft and it is always normal to the flow direction. This explains that lift is an interaction between a moving fluid and a body with mass. The body should be in contact with the fluid. Otherwise, no lift can be generated. Also, lift is generated by the difference in velocity between the craft and the fluid which means that no lift is generated if there is no motion between the craft and the fluid [34].

When the lifting geometry of a WIG effect craft is well designed, it provides an enhanced lift for smaller ground clearance. For instance, wings with flat lower surface generate optimum ground effect. This explains some of the differences between the different configurations of WIG vehicles. Moreover, as previously

demonstrated in Figure 6, for a given wing area, lift is larger for a wing with larger aspect ratio.

The impact of GE on the lift of a WIG effect vehicle can be explained by a graph of lift coefficient versus vehicle's altitude and angle of attack. For a typical WIG vehicle, the coefficient of lift varying with angle of attack and ratio of altitude to mean chord is shown in Figure 29 [32].

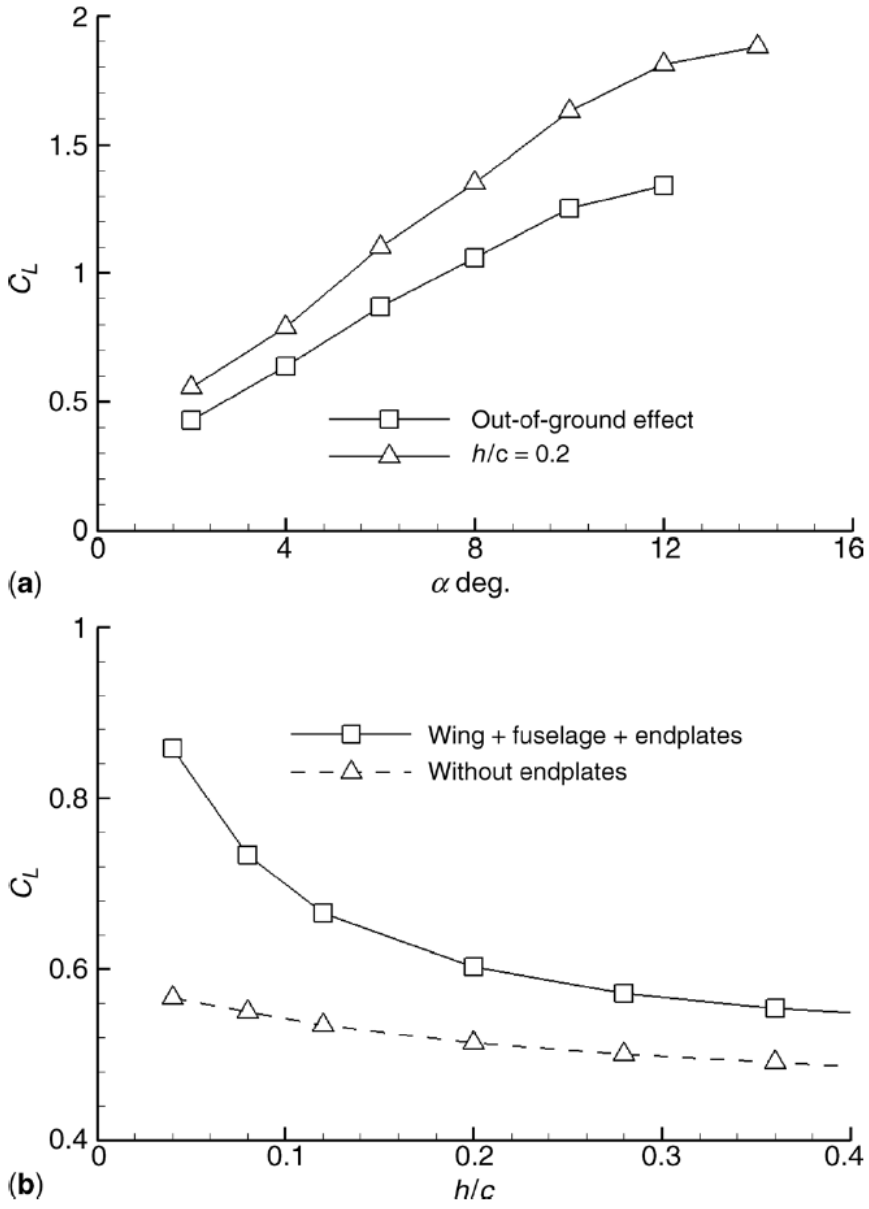

Figure 29. Lift coefficient varying with (a) angle of attack; (b) height/chord [25]

It can be observed from Figure 29 that the lift coefficient increases inversely with craft's height-to-chord ratio and directly with the angle of attack for a given WIG geometry.

2.4.2 Aerodynamic Drag

The aerodynamic drag is defined as a mechanical force that opposes a body motion through air. Drag is generated from every part of the vehicle's body as a result of fluid interaction with the solid body of the vehicle and it is always opposite to the direction of motion of the vehicle. The difference in velocity between the craft and the fluid is the main reason of the aerodynamic drag. Nevertheless, drag can also be described as a friction force because the main source of drag is the skin friction between the molecules of the fluid and the solid body surface of the craft. The skin friction drag highly depends on the properties of both the body of the craft and the fluid. A rough surface would produce more skin friction drag than a smooth one. In terms of fluid, the magnitude of friction force depends on many factors, some of these factors also affect the magnitude of the lift force but others are unique to aerodynamic drag such as viscosity, compressibility, mass of fluid and craft speed. Drag force is also a vector quantity and therefore it has a magnitude and a direction [35].

The most critical factor that aerodynamic drag is influenced by is the viscosity of the fluid which can significantly affect the aerodynamic resistance to motion. This can be explained as follows: as the craft travels through air, air molecules stick to the surface of the craft and create a layer of air near the surface known as a boundary layer. This can be defined as a thin layer of fluid near the surface of the craft in which the velocity changes from zero at the surface to the freestream value away from the surface. Boundary layer build up is shown in Figure 30 [36].

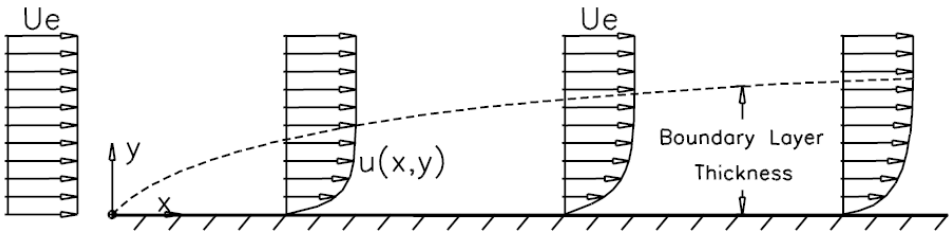

Figure 30. Schematic of boundary layer formation on a flat plate [36]

Boundary layer can change the shape of the craft because the flow of air reacts to the edge of the boundary layer as a physical surface. However, the fluid flow conditions in and near the boundary layer are unsteady which means it changes with time [35].

Reynolds number represents the magnitude of the viscous forces to the motion of the fluid flow. The magnitude of these forces depends on the geometry and the speed of the craft. Reynolds number is used to specify the condition of fluid flow as laminar or turbulent. Reynolds number is defined as the ratio of inertial forces (which is the resistance to change or motion) to viscous forces (which is the friction force between a layer and a fluid). It can be expressed as follows [35]:

$$R_e = \frac{inertia\ forces}{viscous\ forces} = \frac{\rho.U.L}{\mu} = \frac{U.L}{v} \qquad (2.2)$$

where ρ is the viscosity of the fluid, U is the speed of the fluid, L is the chord length, v is the kinematic viscosity, μ is the absolute viscosity which is the density multiplied by the kinematic viscosity.

For WIG effect vehicles, drag force is measured by its induced vortex component and it depends on the mutual relationship between chord length, wingspan and height from underlying surface. According to Rozhdestvensky [7], for a vehicle with high chord length, drag increases as the vehicle comes closer to the underlying surface as a result of the high-pressure region created underneath its body. However, the latter goes on to claim that for a harmonically designed WIG vehicle, drag decreases with decreasing flying height for a constant lift. This is because near an underlying surface, lift-to-drag ratio increases with both the

increase of aspect ratio and with the decrease of flying height. This is supported by Yun, Bliault and Doo [1] who state that aerodynamic drag of WIG vehicles is highly dependent on the aspect ratio (AR). For a WIG vehicle with aspect ratio above 1, the drag decreases with increasing flying height. But when the AR = 1, the drag becomes independent of flying height. However, when the AR is less than 1, the drag increases with increasing altitude [1, 7].

2.4.3 Lift-to-Drag Ratio

Lift-to-drag ratio can be defined as the quantity that measures the efficiency of the craft. A WIG vehicle can have a high lift-to-drag ratio only if it generates a large amount of lift or a small amount of drag. The higher the lift force generated the more payload the craft can carry. Also, the higher the lift-to-drag ratio the less fuel is consumed and the longer distance the flight can cover. Generally, lift-to-drag ratio equals the lift coefficient C_L over the drag coefficient C_D as shown in the following equation [35]:

$$\frac{L}{D} = \frac{0.5.C_L.\rho.V^2.A}{0.5.C_D.\rho.V^2.A} = \frac{C_L}{C_D} \tag{2.3}$$

where V is the speed of the craft, A is the frontal area (the surface area that the fluid interacts with) and ρ is the density of air.

Yun, Bliault and Doo [1] suggest that lift-to-drag ratio is proportional to the aspect ratio for a fixed angle of attack and ground clearance. The effect of aspect ratio, ground clearance and angle of attack on the lift-to-drag ratio for a rectangular platform is shown in Figure 31.

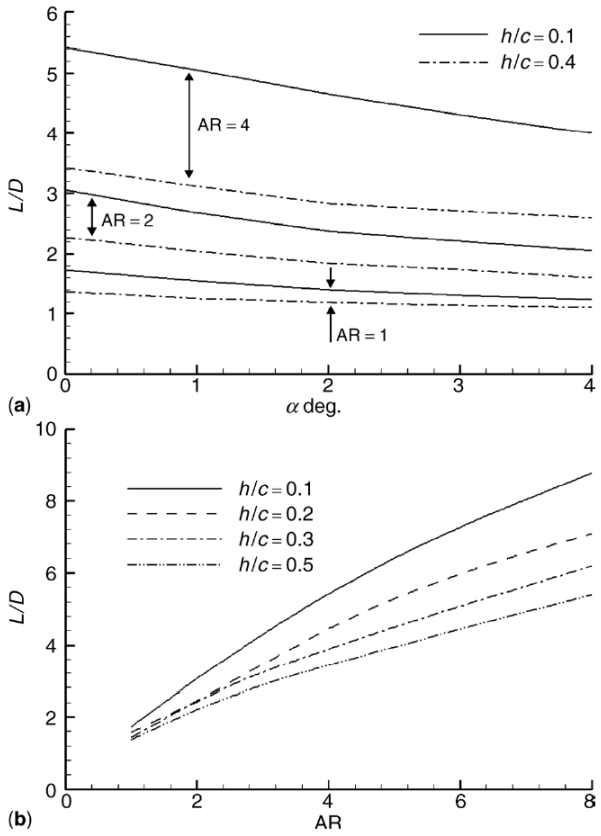

Figure 31. Lift-to-drag ratio relationship with (a) angle of attack (b) AR for different flying heights [32]

2.4.4 Endplates Effects

Endplates are a very important aerodynamic feature of WIG effect vehicles because, for a WIG vehicle with long chord, the air cushion underneath the vehicle is positively affected by the difference in pressure between the upper and lower surfaces of the wing. Endplates are used to reduce the loss of pressure from underneath the vehicle. In addition, endplates play a significant role in the increase of effective aspect ratio. The smaller the aspect ratio, the more useful the endplates in preventing pressure loss. Also, if endplates are designed to be portable (retractable), they could be used in static stability control and motion [37].

2.4.5 Sea Waves Effect

There are many important situations that should be considered when a WIG effect vehicle operates over a sea environment such as take-off and landing on waves. Although insufficient research has been done on this area, the following points have been concluded from the literature [37, 38]:

- When a WIG effect vehicle flies above a wavy sea, it experiences an additional unsteady lift which changes periodically depending on amplitude. This is due to the shape of sea waves which continuously changes between peak (highest amplitude value) and trough (lowest amplitude value).
- The total wave-induced lift for a flat wing over the wave overall period is positive. This explains why a wing would have additional lift when operating over a sea wave. This is due to the nonlinear characteristics of GE phenomenon whereby the average lift increment due to wave crests is relatively larger than the lift decrement due to wave troughs.
- The amplitude of the unsteady wave-induced lift depends on the ratio of wavelength to chord-length of the wing. As the ratio increases, the amplitude decreases.
- The wave-induced lift response of the WIG vehicle depends on the vehicle's weight, the flying height, angle of attack and on the wave characteristics (length and amplitude). For instance, a vehicle with large weight will not be affected by water waves unless the waves are very long.
- The vertical wind generated by the orbital motion of the air particles excited by the water waves imposes a significant impact on the aerodynamic performance of WIG vehicles. This effect depends on the wave amplitude, wind speed and difference in velocity between the water wave and the WIG vehicle.
- Finally, roughness of sea water negatively affects the performance of the vehicle because ground clearance must be increased in order to avoid contact with water waves crests.

2.4.6 Aerodynamic Performance Prediction Methods

The aerodynamic characteristics of WIG effect vehicles can be examined using different methods to analyse the behaviour of these vehicles under desired conditions. Mathematical, numerical or experimental investigations can be applied to describe the performance of WIG effect crafts. Recently, the remarkable growth of computing power along with Computational Fluid Dynamics (CFD) allowed the designers to make considerable progress in performance prediction. However, the analytical methods are still very vital especially in the design stage and can be used to create a performance prediction tool. The analytical methods are used to calculate lift, drag and centre of pressure of WIG effect vehicles. The most common analytical procedures used to describe the aerodynamic behaviour of WIG crafts are the following [39]:

- Conformal mapping.
- Vortex theory.
- Asymptotic expansions.
- Pressure distribution calculation.
- Computational panel methods.

Cummings et al. [37] argue that the most common methods used to describe the three-dimensional aerodynamic vortex of a body in air are the Vortex Lattice method (VLM) and the Panel method. Those methods are efficient and capable of providing noticeable insight into wing and craft components aerodynamics. They are based on Laplace's equations and subjected to the same principal theoretical restrictions such as being only applicable to two-dimensional problems. Moreover, both methods are solved numerically which means that answers cannot be obtained without finding the numerical solution of a matrix which is too large for basic hand calculations. However, there are a few differences between the two methods such as: VLM focuses on the lifting effects without paying much attention to the thickness and the wing is assumed to be a combination of thin surfaces. On the other hand, the Panel method has no limitations on thickness [39].

Priyanto et al. [40] measured the wing aerodynamic drag on a WIG effect craft and state that the methods that can be used to model a wing motion in proximity to the ground are simple channel models, analytical asymptotic approaches, potential panel methods and modern finite volume methods. Also, the work presented in [40] concluded that the total aerodynamic drag force on a wing near an underlying surface is divided into two components which are drag force of wing which is caused by dynamic air cushion pressure and drag force of fuselage which is due to the forces acting on the hull above water. The tail drag was neglected in this research [40]. More details about the aerodynamic performance of WIG effect vehicles can be found in [32-44].

2.5 Hydrodynamic Aspects of WIG Effect Vehicles

The first studies in the development of WIG vehicles were done on high speed planing hulls which have similar performance characteristics as WIG vehicles as they are both designed to glide on top of water and take advantage of the positive dynamic lift produced by their motion. Thus, it is important to study the hydrodynamic characteristics of planing hulls before undertaking the design of a GE machine. In the last century, fundamental research on the hydrodynamics of water-based aircraft has been carried out. The first experimental research on planing surfaces was conducted by Baker in 1912 [45]. This is followed by wider investigations carried by Sottorf in 1932 [46]. After that, more examinations on the topic were carried out by Shoemaker [47], Sambraus [48], Sedov [49], Locke [50], Korvin-Kroukovsky et al. [51] and Murray [52]. Subsequently, in 1964, Savitsky [53] discussed the hydrodynamic characteristics of planing surfaces and presented a method to predict the performance of prismatic planing surfaces [54].

Planing starts when accelerating to a sufficiently high speed so that the centre of gravity of the hull is lifted above its normal still-floatation height. A planing surface is designed to be supported by the dynamic reactions between the body and the water [55]. There are two different types of pressure forces acting on the hull of a WIG craft. The first one is the hydrostatic force (buoyancy force). According to Archimedes principle, the hydrostatic force acting on a body that is fully or partially

submerged in water equals the weight of the water that the body displaces. The buoyancy force is always in the upward direction and passes through the centre of mass of the body. The second force is the hydrodynamic force which depends on the fluid flow around the hull and proportional to the speed square [55]. On the other hand, the total hydrodynamic pressure drag of seaplanes is composed of two different types. The first one is the pressure drag developed by water pressure acting normal to the inclined hull. The second one is the viscous drag acting tangentially to the bottom of the hull and is the result of fluid friction [52]. Figure 32 shows the different forces acting on a planing surface in viscous water.

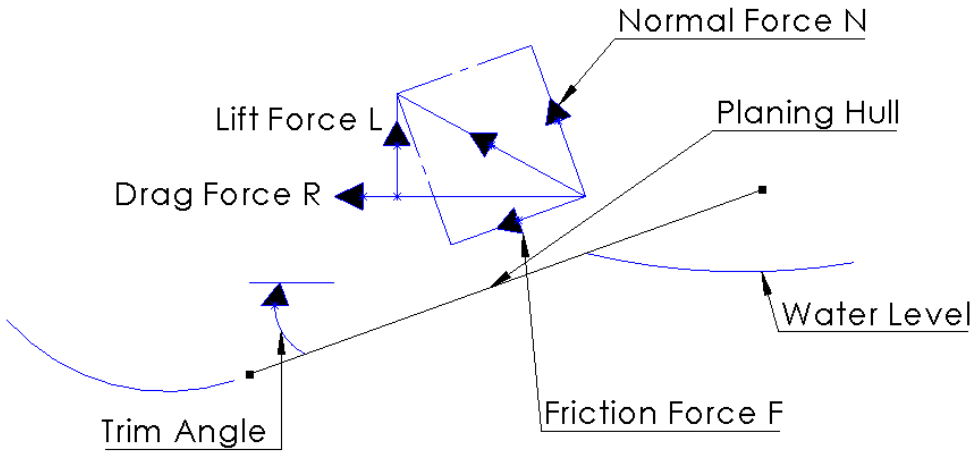

Figure 32. Forces acting on a planing surface

The motion of WIG effect vehicles is distinguished by many unique characteristics that exist because these vehicles operate in two media, air and water. When the WIG vehicle is floating on water, the motion introduces additional complications. As explained in Figure 33, WIG vehicles go through a transition process from a steady state mode in which the vehicle is under static buoyancy (the displacement range) to a dynamic planing mode (the planing range).

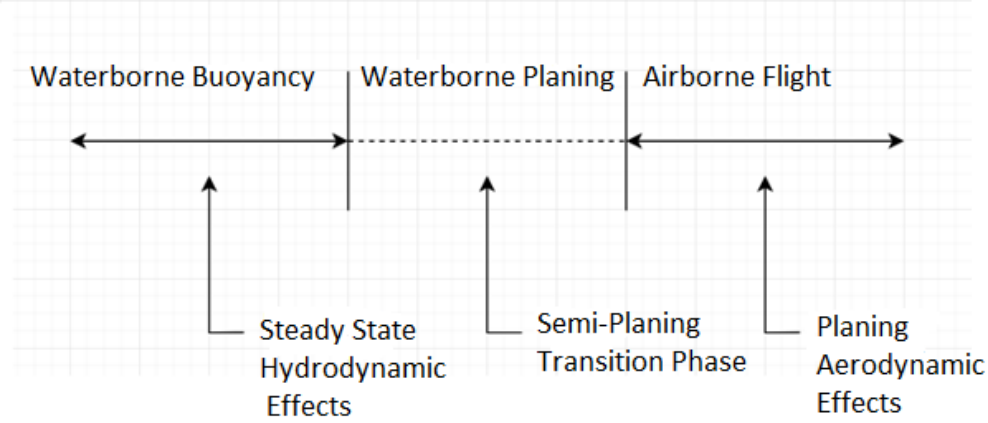

Figure 33. WIG vehicles operating phases [56]

The vehicle must be designed to accomplish this transition smoothly and successfully between the three basic regimes which are waterborne buoyancy, waterborne planing and airborne flight. In order to differentiate between the three modes, the motion of WIG effect vehicles is classified according to Froude Number (F_n) as follows [56]:

- $F_n > 0.4$: This is the displacement range. The seaplane is moving through water by pushing the water aside. In this range, there are two types of pressure forces acting on the seaplane, the hydrostatic force (buoyancy force) and the hydrodynamic force. However, the hydrostatic force (restoring force) is dominant in this region relative to the hydrodynamic forces (added mass and damping forces). The seaplane must be capable of withstanding moments introduced by the action of wind and wave while travelling in this speed range.
- $0.4 < F_n < 1.0$: In this speed range the seaplane enters the planing mode (also known as semi-planing or semi-displacement mode). As the speed increases, the weight of the seaplane becomes mainly supported by hydrodynamic forces while the hydrostatic force becomes less dominant. Each of the forces has a different centre of pressure. Nevertheless, aerodynamic effects start to play a role in lifting the seaplane off water in this region. The main challenges in the design of seaplanes are in this speed range. The seaplane must be capable of accelerating to take-off while keeping

stability about all axes of motion. Also, as the seaplane accelerates from zero velocity, there is some speed at which the water resistance becomes maximum. This point is known as "hump speed point". It is the point where the lift force shifts from being predominantly buoyant to being dynamic (hydrostatic to hydrodynamic). If the seaplane is not very well designed to over-take this issue, it will not be able to take-off.

- $F_n > 1.0$: This is the fully planing range where the weight of the seaplane is mainly supported by aerodynamic forces.

Almeter [54] carried out a study about the resistance prediction methods of planing hulls and suggested an analytical method to study their performance which will be discussed later in this section. In this study, the author has defined the basic speed regimes that a planing hull can operate in according to the volumetric Froude Number ($F_{n\nabla}$) as follows [54]:

- Pre-planing: it is also called the displacement mode. It is the hydrodynamic effect region and can be experienced up to $F_{n\nabla} = 2.5$. Most of the weight of the hull is supported by hydrostatic forces (buoyancy).
- Semi-planing: it is also known as semi-displacement mode. It is the transition phase and can be experienced in the range of $2.5 < F_{n\nabla} < 4.0$. In this case, the weight of the hull is supported by both hydrostatic (buoyancy) and hydrodynamic forces. As the speed increases the contribution of hydrodynamic forces in lifting the weight of the craft increases while the hydrostatic forces contribution decreases.
- Fully-planing: it is the aerodynamic effect region. It can be experienced when $F_{n\nabla} \geq 4.0$. At higher speeds, the weight of the hull is supported by aerodynamic forces only.

It can be understood from Almeter's study that when the seaplane is hydroplaning, the pressure forces acting on the surface of the hull are buoyancy and dynamic pressure. Each of the forces has a different centre of pressure. The buoyancy force has a centre of hydrostatic pressure, while dynamic forces have a centre of hydrodynamic pressure as shown in Figure 34 [54].

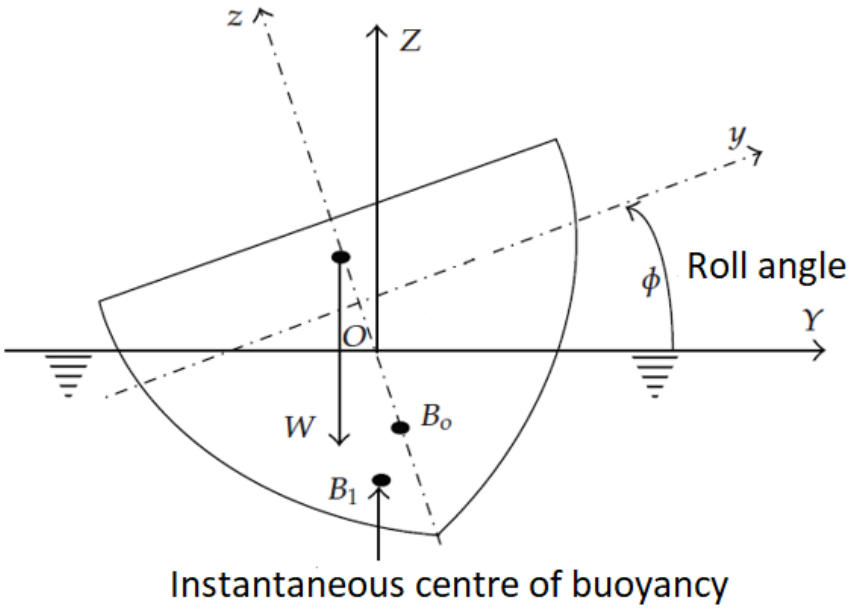

Figure 34. The centre of hydrodynamic and hydrostatic pressures [57]

The basic hull design of seaplanes demonstrates a hull that assists in lifting off the craft in the water. Priyanto et al. [40] state that when a hull is in planing mode, there is a tendency that it trims at a certain angle. This means that the front of the hull will lift out of water and the rear part of the hull will immerse partially in water. Figure 35 explains the difference between a hull in the planing and pre-planing (displacement) modes. The hydrodynamic lift and resistance will be encountered at the rear part of the hull where the front will be affected by aerodynamic forces [40].

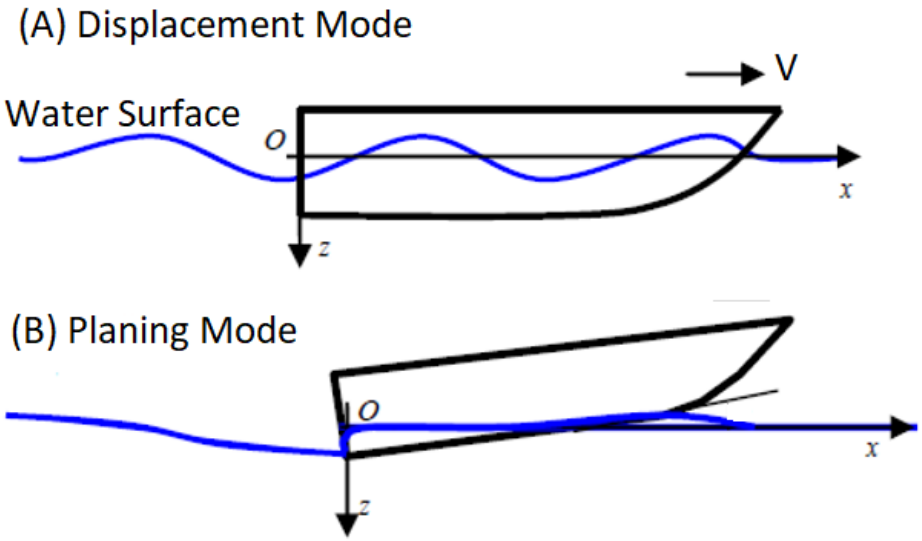

Figure 35. A planing hull in (A) Displacement mode (B) Planing mode [40]

Hydrodynamic drag on a body moving through water can be defined as a force acting in the direction opposite to the direction of motion of the body. This force is sometimes called "resistance to motion". The system of fluid (in this research its water) is given a uniform velocity opposite to the direction of the body (WIG vehicle). This velocity brings the body to rest, while at infinity the fluid assumes a velocity equal and opposite to that velocity the body had before. In this case, as the superposition of such a uniform rectilinear motion cannot have any dynamic consequences, the drag of the body does not change whether the fluid is moving and the body is at rest or whether the fluid is at rest and the body is moving [35].

The first hydrodynamic resistance law was proposed by Newton. The law assumes that the drag is due to inertia, which is the case when a body is moving through fluid with relatively low viscosity like water or air. As a result, the hydrodynamic drag can be calculated using the following equation [35]:

$$D = fA\rho v^2 \tag{2.4}$$

where D is the drag force, f is the factor of proportionality (usually assumed $\frac{1}{2}$), A is the projected area of the body in the direction motion and v is the forward velocity.

There are several forms of hydrodynamic drag that influence the performance of planing hulls such as [58]:

- Skin friction: it is the drag due to viscous properties of fluid. The basic principles of this drag are the same as the drag in normal aeroplanes. The wetted area of the WIG effect vehicle's body imparts a velocity gradient on the flow of fluid around it which creates a boundary layer similar to that explained in section 2.4.2.
- Wave drag: it is usually generated by the vehicle's hull while travelling through water. It is proportional to the hull length and it affects the performance significantly when traveling in the displacement mode.
- Pressure drag: this drag is due to the pressure difference between the leading edge and trailing edge of the vehicle's hull. When traveling in displacement mode, this drag is caused by the separation of fluid particle at the trailing edge of the hull. When traveling in planing mode, the pressure drag is due to the generation of lift as the bow of the hull starts to incline which increases the difference in pressure between the two sides of the hull.
- Appendage drag: it is generated due to the additional hardware below waterline such as rudders, propellers and roll control surfaces. This drag is almost negligible when studying the hydrodynamic performance of WIG effect vehicles because they are usually controlled by aerodynamic rudders and driven with aero engines.

2.5.1 Hydrodynamic Performance Prediction Methods

The performance of planing hulls is predicted by studying the relations between different variables such as speed, displacement, longitudinal length, beam length, trim angle, dead-rise angle and longitudinal centre of gravity. These variables are called the basic dimensions (geometry) and loading of the planing hull. The shape of the hull can be concave, convex or straight, and can have high warp or high beam taper. Resistance prediction methods can generally be classified into the following categories [54]:

1. Analytical methods (also called empirical prediction methods).
2. Graphical prediction methods.
3. Planing hull series prediction methods.
4. Numerical methods.
5. Statistical methods.
6. Experimental methods.

It is important in the design stage to choose the most applicable performance prediction method that conforms to the shape, operating conditions and geometry of the planing hull [54]. The hydrodynamic analysis techniques for seaplanes available in the open literature are summarised in the next diagram.

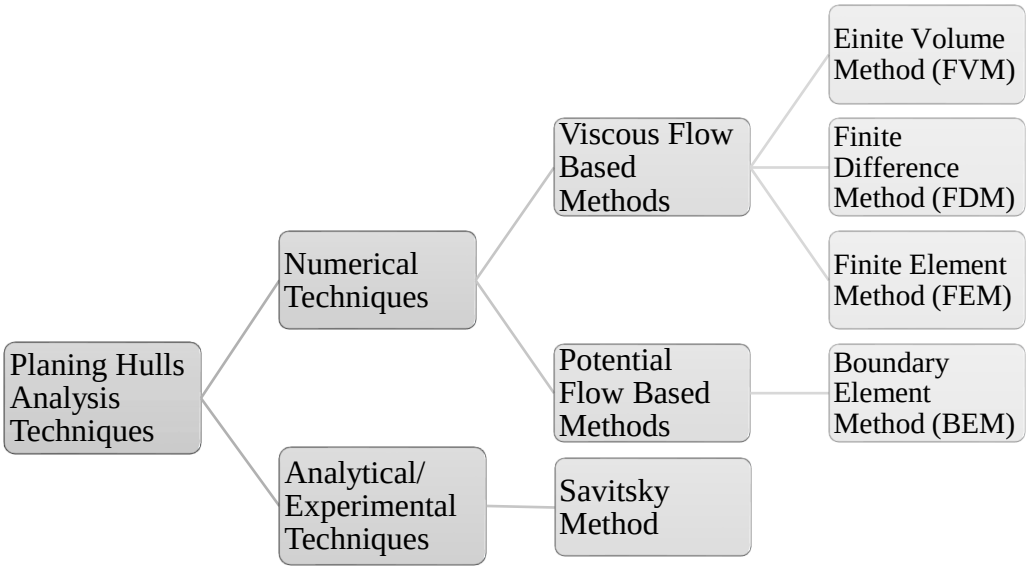

Figure 36. Hydrodynamic performance prediction methods [59]

In the next sub-sections, the analytical methods available in the literature will be discussed.

2.5.1.1 Savitsky Method

Savitsky [53] states that the horizontal centre of buoyancy is 33% of the wetted length forward of the transom. The work in [53] also suggests that the horizontal centre of dynamic pressure is 75% forward of the transom in case of a small angle of attack. The pressure distribution on a planing surface is presented in Figure 37. The Figure shows that the centre of dynamic pressure is approximately at a point 75% forward of the transom. As the speed increases, the forces start to change from hydrostatic to hydrodynamic. This means that at higher speeds the buoyancy force can be neglected, and the centre of pressure moves from the centre of buoyancy to the centre of dynamic pressure [53].

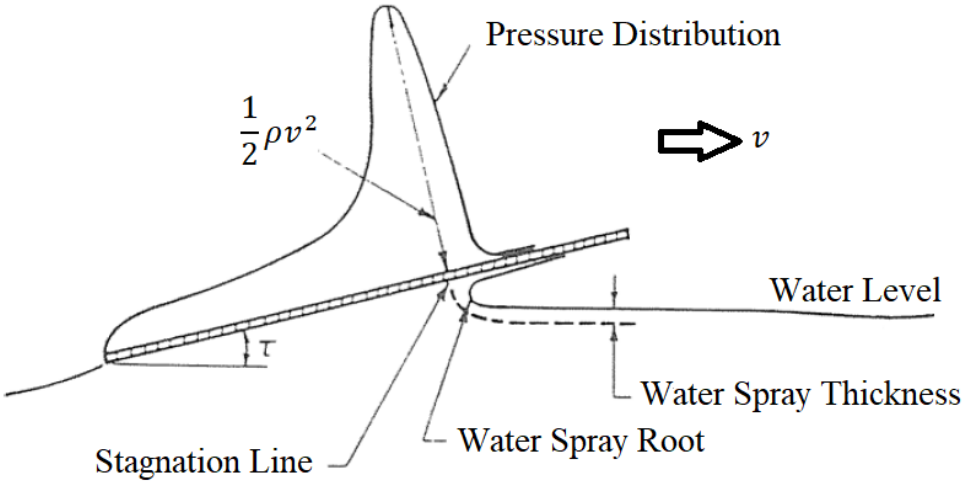

Figure 37. Pressure distribution on a planing surface [53]

The equations developed by Savitsky describe the wetted area, lift force, drag force, centre of pressure and the porpoising stability limits of hard chine prismatic planing plate in terms of its dead-rise angle, trim angle, speed and weight. This method is based on the dynamic lift equations first developed by Sedov [49]. Once the shape and geometry of the hull are defined, it becomes easier to predict its performance. Figure 38 shows the basic terms that describe a planing hull according to Savitsky.

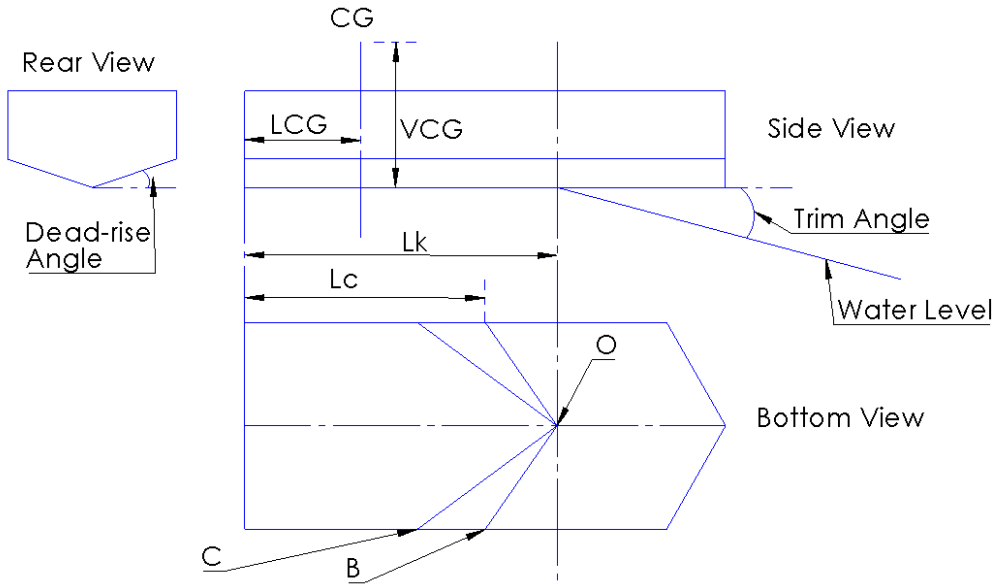

Figure 38. Planing hull design characteristics [53]

The Figure demonstrates that the intersection of the bottom surface with the undisturbed water surface is along the two sloping lines (O-C) between the keel and chines. It can also be observed from Figure 38 that for a V-shaped planing hull, there is no noticeable evidence of water pile-up at the keel line. When the hull starts to rise and have a larger trim angle, the water will pile-up at the keel. Also, along the spray root line (O-B) there is a tendency of the water surface to rise before the initial point of contact with water O. Savitsky [53] argues that the spray root line is slightly convex. However, it can be assumed straight. As a result, the mean wetted length of a dead-rise planing surface can be defined as the average of the keel length and chine length calculated from the back of the hull (transom) to the point of intersection with spray root line (O-B).

As presented in Figure 39, the total hydrodynamic drag on a planing hull has two components:

- The fluid friction drag D_f.
- The pressure drag $\frac{D_f}{cos\tau}$.

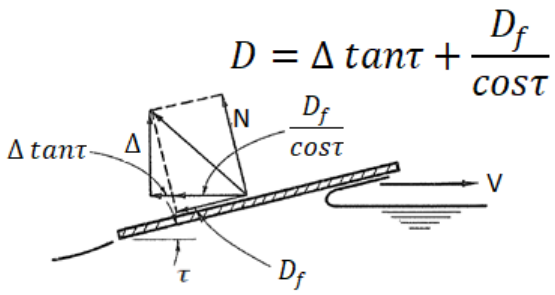

Figure 39. Hydrodynamic drag components [53]

In order to develop his equations, Savitsky [53] studied the equilibrium of planing surfaces. First of all, he assumed that the planing hull is moving in a constant speed with no acceleration in any direction. Secondly, the planing hull is considered to have a constant dead-rise angle (β), a constant equilibrium trim angle (τ_e) and a constant beam length (B) for the whole wetted planing area. Nevertheless, Savitsky's theory only investigates the hydrodynamic conditions. This means that the weight of the hull is balanced only by the hydrodynamic lift forces. According to Savitsky [53], equilibrium is achieved when the following conditions apply:

1. The summation of forces in the vertical direction is zero.
2. The summation of forces in the horizontal direction is zero.
3. The summation of moments about the centre of gravity CG is zero (pitching moment equilibrium).

Figure 40 shows the different forces and parameters Savitsky [53] has used in the development of his method.

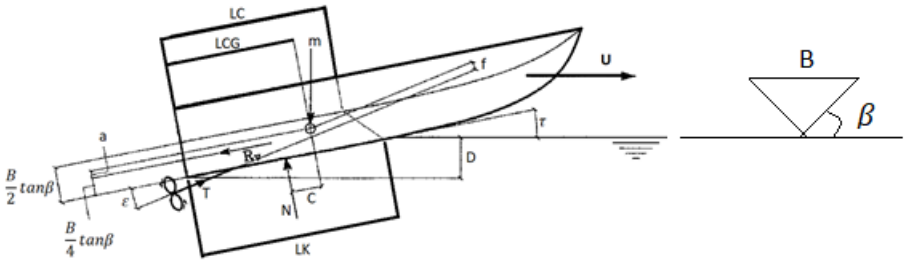

Figure 40. Schematic analysis of a planing hull [53]

It is worth mentioning that in his analysis, Savitsky [53] considered the beam to be more important than the length of the hull because the wetted length of the hull does not remain constant. It varies with trim angle, loading and speed while the wetted beam generally remains constant. This means that he classified the basic speed regimes that a planing hull can operate in according to the beam Froude Number. Moreover, the latter points out that at high speeds, it is possible to change the wetted length of the planing hull without changing its hydrodynamic characteristics. This assumption was also supported by Murray [52]. In addition, Savitsky [53] used Froude law of similitude to produce the planing coefficients and symbols in his analysis. It can be noted that these analyses can be applied to study the performance of water-based aircraft.

By applying the equilibrium principle, the equilibrium trim angle (τ_e) can be calculated and the performance characteristics of the planing hull can be predicted. The procedure of Savitsky method can be explained as follows:

1. The geometry of the hull is defined in which the following variables are specified:

    - The total mass of the boat m (or can be expressed as Δ).
    - The beam length b.
    - The longitudinal distance of centre of gravity measured from the transom LCG.
    - The vertical distance of centre of gravity measured from the keel VCG.
    - The dead-rise angle β.
    - The trim angle τ.
    - The velocity of the craft V.
    - The inclination of thrust line relative to keel line ε.

2. Then a few variables are calculated in the same order as follows:

    - The speed coefficient (which is the beam Froude number):

$$C_v = \frac{V}{\sqrt{gb}} \tag{2.5}$$

- The lift coefficient of dead-rise planing surface:

$$C_{L\beta} = \frac{mg}{\frac{1}{2}V^2 b^2 \rho} \tag{2.6}$$

- The lift coefficient of an equivalent flat plate C_{Lo} is calculated from the following equation:

$$C_{Lo} = C_{L\beta} + 0.0065\beta C_{Lo}^{0.6} \tag{2.7}$$

- The wetted length-beam ratio λ is calculated from the following equation:

$$C_{Lo} = \tau^{1.1}\left[0.012\lambda^{0.5} + \frac{0.0055\lambda^{2.5}}{C_v^2}\right] \tag{2.8}$$

Then, the wetted length is calculated from the following equation: $L_w = \lambda b$

- The mean velocity over the bottom of the planing surface is calculated from the following equation:

$$V_m = V\left[1 - \frac{0.012\lambda^{0.5}\tau^{1.1} - 0.0065\beta(0.012\lambda^{0.5}\tau^{1.1})^{0.6}}{\lambda\cos(\tau)}\right]^{0.5} \tag{2.9}$$

- The friction drag coefficient is calculated as follows:

$$C_f = \frac{0.075}{(log_{10}(R_e) - 2)^2} \tag{2.10}$$

where R_e is Reynold's number and can be calculated as:

$$R_e = \frac{V_m \lambda b}{v} \tag{2.11}$$

- The water friction drag D_f can be calculated from the following equation:

$$D_f = \frac{1}{2}\frac{\rho V_m^2 \lambda b^2}{\cos(\beta)}\left(C_f + \Delta C_f\right) \tag{2.12}$$

where ΔC_f is ATTC standard roughness = 0.0004

- Then, the total hydrodynamic drag can be calculated as follows:

$$D = mg\ tan(\tau) + \frac{D_f}{\cos(\tau)} \tag{2.13}$$

- After that, the centre of dynamic pressure is found from:

$$C_p = 0.75 - \frac{1}{\frac{5.21 C_v^2}{\lambda^2} + 2.39} \tag{2.14}$$

- Then the two distances a and c shown in Figure 40 are calculated from:

$$c = LCG - C_p \lambda b \tag{2.15}$$

$$a = VCG - \frac{b}{4}\tan(\beta) \tag{2.16}$$

The equation of equilibrium of pitching moment is then solved as follows:

$$M_{tot} = mg\left[\frac{c}{\cos(\tau)}(1 - \sin(\tau)\sin(\tau + \varepsilon)) - f sin(\tau)\right] + D_f(a - f) \tag{2.17}$$

- If the equation satisfies the equilibrium (sum of moments = 0) then the wetted length of keel L_k and the vertical depth of trailing edge of craft below level of water d are found from the following equation:

$$L_k = \lambda_e b + \frac{b\ tan(\beta)}{2\pi \tan(\tau_e)} \tag{2.18}$$

$$d = L_k\ sin(\tau_e) \tag{2.19}$$

- If the equation of equilibrium does not equal to zero, a different trim angle (τ) must be assumed and the procedure repeated till two different values of moment are found (negative and positive) and then by interpolation the equilibrium trim angle (τ_e), D_f and λ can be found [53].

2.5.1.2 Morabito Method

In this method, it is assumed that the pressure at the stagnation point is far greater than the pressure at the other parts of the hull. Therefore, the problem becomes very complex and direct calculation methods cannot be applied to calculate the pressure distribution along the hull surface. As a result, the pressure can be calculated in length-wise and breadth-wise directions independently. It could then be extended to a three-dimensional distribution over the hull. Figure 41 shows the three-dimensional pressure distribution over the bottom of a planing surface [60].

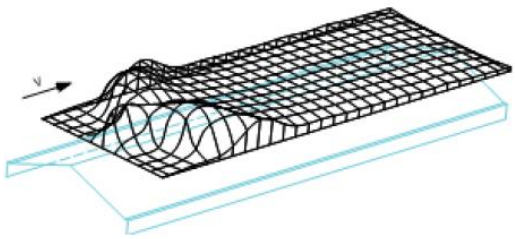

Figure 41. 3D pressure distribution over the bottom of a planing hull [61]

Iacono [61] studied Morabito method and stated that the dynamic pressure along the planing hull exhibits a maximum at the stagnation point. Eventually, the pressure deteriorates and reaches atmospheric pressure at the end of the hull. As explained in Figure 42, Morabito method focuses on the pressure distribution along the longitudinal keel line at the bottom of the hull. Also, it calculates the pressure at the transom and the longitudinal pressure distribution over other sections [61].

In the case of the keel line, Morabito [60] introduced the following equation to calculate the maximum pressure at the stagnation point:

$$\frac{P_{max}}{q} = sin^2\alpha \tag{2.20}$$

where α is the angle between the stagnation line and keel line shown in the next Figure, q is the pressure along the line which can be found from the following equation [52]:

$$q = \frac{1}{2}\rho V^2 \tag{2.21}$$

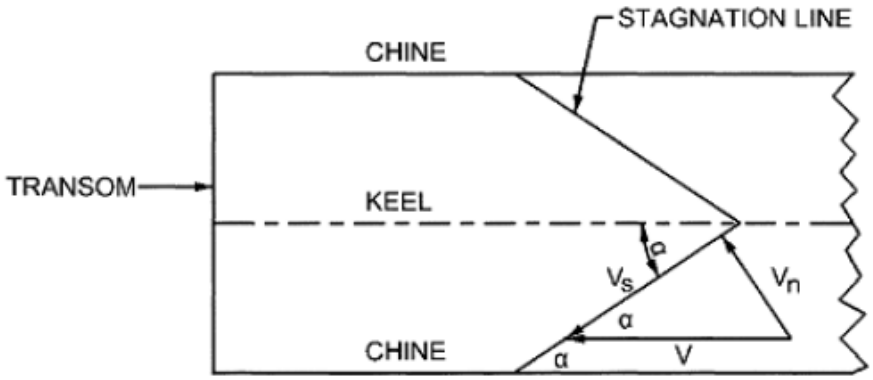

Figure 42. Components of planing hull explained by Morabito [61]

The pressure gradually decreases along the keel line till it becomes almost zero at the transom. The pressure reduction along the line can be calculated from the following equation:

$$\frac{P_L}{q} = 0.006\frac{\tau^{1/3}}{X^{2/3}} \tag{2.22}$$

where P_L is the pressure behind the stagnation point and X is the dimensionless distance from the stagnation and can be calculated from the following equation:

$$X = \frac{x}{b} \tag{2.23}$$

where b is the breadth of the hull. Then, Morabito modified the equation of reduced pressure along the keel line as follows:

$$\frac{P}{q} = \frac{0.006\tau^{\frac{1}{3}}X^{\frac{1}{3}}}{\left(X + \frac{\left(0.006\tau^{\frac{1}{3}}\right)^{1.5}}{2.588(\frac{P_{max}}{q})^{1.5}}\right)} \tag{2.24}$$

Morabito calculated the pressure at the transom by introducing the following equation:

$$P_T = \frac{\left(\lambda_y - X\right)^{1.4}}{\left(\lambda_y - X\right)^{1.4} + 0.05} \tag{2.25}$$

where λ_y is the dimensionless distance between the transom and the stagnation line as each longitudinal section and can be calculated from the following equation:

$$\lambda_y = \lambda - \frac{(Y - 0.25)}{\tan(\alpha)} \tag{2.26}$$

where $Y = \frac{y}{b}$ is the dimensionless transverse distance from the longitudinal symmetry (keel) line (the same as the previously defined X but in the transverse direction).

The previous equations of Morabito only measure the pressure distribution at the transom, at the stagnation point and along the symmetry line in between them. Morabito states that the pressure declines along the stagnation line and consequently, at each longitudinal section the maximum pressure is less than that on the longitudinal symmetry (keel) line. The latter has used the Swept Wing Theory to calculate the pressure reduction along the other sections [60].

As previously presented in Figure 42, Morabito [60] suggested that the fluid velocity is a combination of two components, velocity along the stagnation line and velocity normal to it. Using the normal component of velocity and resulting

pressure, the ratio of transverse pressure along the stagnation line is found as follows:

$$\frac{P_{YStag}}{P_R} = [1.02 - 0.25Y^{1.4}]\frac{0.5 - Y}{0.51 - Y} \tag{2.27}$$

By multiplying the previous equation by the maximum pressure, the pressure over the stagnation line at a desired longitudinal section is found as follows:

$$\frac{P_{max}}{q} = \frac{P_{YStag}}{P_R} sin^2(\alpha) \tag{2.28}$$

Morabito method is not able to define many terms needed in predicting the hydrodynamic performance of planing hulls. For example, it cannot define the porpoising stability limit. As a result, it cannot be used as the staple method for boat design.

2.5.1.3 CAHI Method

The CAHI method was proposed by Almeter [54]. This method is used to predict the performance of prismatic planing hulls. It is also known as Lyubomirov method or TSAGI method from the Central Aero-hydrodynamic Institute in Moscow. The CAHI method was initially developed by Perelmuter [62] who investigated the take-off characteristics of seaplanes.

Almeter [54] developed this method based on the same dynamic lift equations prepared by Sedov [49] that Savitsky [53] used to develop his method. In Savitsky method, the trim angle is corrected based on the constant dead-rise while in the CAHI method, the wetted area increases with dead-rise.

CAHI method concurs with the study of Chambliss and Boyd [63] as both conclude that in theory for a given lift coefficient, any increase in the dead-rise angle will increase the trim angle and wetted length of the planing hull. This means that the hydrodynamic resistance will increase. The procedure of CAHI method can be summarised as follows:

1. The variables defined in Savitsky's method are calculated and then the equation of moment should be solved to obtain the mean wetted length-beam ratio λ. Once an acceptable λ is obtained (almost 0.75*LCG) the trim angle τ and the dead-rise lift coefficient can be calculated. The equations for the aforementioned terms are as follows:

$$M = \frac{\frac{0.7\pi\lambda}{1+1.4\lambda}\left[0.75 + 0.08\frac{\lambda^{0.865}}{\sqrt{C_v}}\right] + \frac{(\lambda-0.8)\lambda^2}{(3\lambda+1.2)C_v^2}}{\frac{0.7\pi}{1+1.4\lambda} + \frac{(\lambda-0.4)\lambda}{(\lambda+0.4)C_v^2}} \tag{2.29}$$

$$C_{L\beta} = \frac{\Delta}{0.5\rho V^2 b^2} \tag{2.30}$$

$$\frac{C_{L\beta}}{\tau} = \frac{0.7\pi\lambda}{1+1.4\lambda} + \frac{(\lambda-0.4)\lambda^2}{(\lambda+0.4)C_v^2} \tag{2.31}$$

2. The mean wetted length-beam ratio and the trim angle can now be calculated for a dead-rise planing hull from the following equations:

$$\lambda_\beta = \frac{\lambda^{0.8}}{\cos(\beta)}[1 - 0.29(\sin(\beta))^{0.28}].\left[1 + 1.35(\sin(\beta))^{0.44}.\frac{M}{\sqrt{C_v}}\right] \tag{2.32}$$

$$\tau_\beta = \tau + \frac{0.15\left(sine(\beta)\right)^{0.8}}{C_v^{0.3}}.\frac{1 - 0.17\sqrt{\lambda_\beta\cos(\beta)}}{\sqrt{\lambda_\beta\cos(\beta)}} \tag{2.33}$$

3. After that, the wetted surface S, the average bottom velocity V_m and the drag of prismatic hull are calculated as follows:

$$S = \frac{b^2\lambda_\beta}{\cos(\beta)} \tag{2.34}$$

$$V_m = V\left[1 - \frac{\tau}{1+\lambda}\right] \tag{2.35}$$

$$D = \Delta\tan(\tau_\beta) + \frac{0.5C_f\rho S V_m^2}{\cos(\tau_\beta)} \tag{2.36}$$

where C_f can be calculated from the following equation which is the same equation proposed by Savitsky:

$$C_f = \frac{0.075}{(logR_e - 2)^2} \tag{2.37}$$

4. Finally, the wetted keel length and the wetted chine length are calculated as follows:

$$\lambda_\beta = \frac{L_m}{b} \tag{2.38}$$

$$L_m = \frac{L_k + L_c}{2} \tag{2.39}$$

$$L_k - L_c = \frac{b\tan(\beta)}{\pi\tan(\tau)} \tag{2.40}$$

2.5.1.4 Payne Method

In 1995, Payne [64] studied the planing theory. The latter has discussed the difference empirical equations used to predict the performance of flat and V-shaped planing hulls available at that time. As a result, a method to predict the resistance of planing hulls was proposed.

In his study, Payne [64] points out that Savitsky's equations are the most accurate equations developed in the last century for describing the total hydrodynamic drag and lift forces acting on a planing hull. Therefore, in order to validate his method, Payne compared his method to Savitsky's. Figure 43 presents a comparison between Payne's and Savitsky's results. The Figure shows the lift produced by a planing hull versus the wetted length-to-beam ratio. It can also be observed from Figure 43 that when the wetted length-to-beam ratio is low, Payne method overestimated the lift force. As the length-to-beam ratio increases, Payne method gives lower lift force estimations [56]. It is worth mentioning that Payne [64] states that the hydrostatic pressure acting on a planing hull is less than Archimedes force.

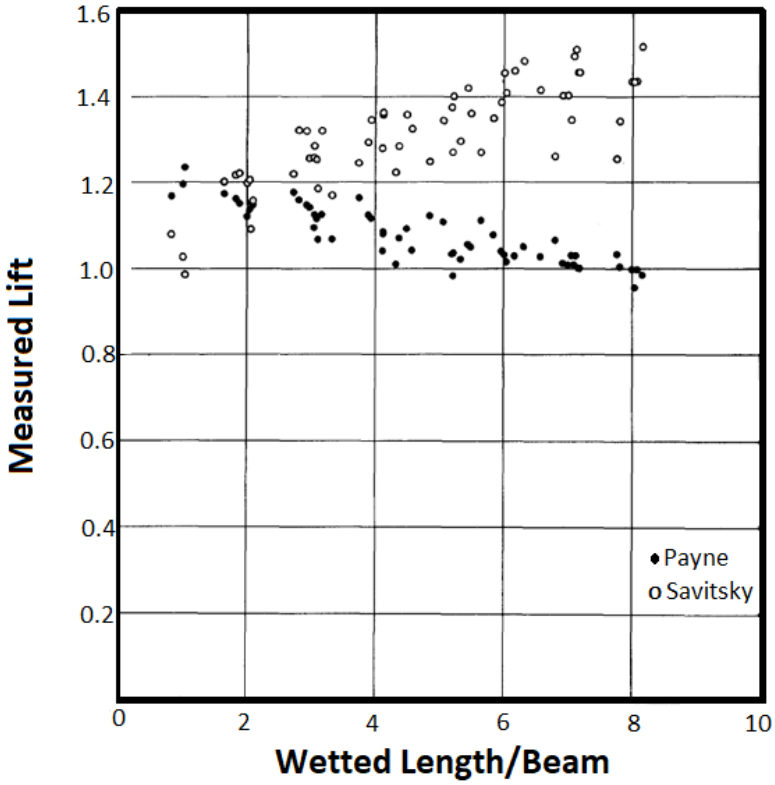

Figure 43. Comparison between Payne and Savitsky Methods [64]

Payne theory is based on two-dimensional flow analyses of a flat plate. It can be seen as an improved version of the resistance prediction methods available at its time. The latter modified the coefficients developed previously. Furthermore, Payne [64] made different assumptions based on the revision of the experimental data available. The latter states that the modifications are made to the coefficients used in the "added mass" equations for planing forces predicted formerly.

Table 1 summarises the different empirical equations of hydrodynamic lift of planing plates developed previously as provided by Payne [64].

Table 1. Equations of hydrodynamic lift of planing plates [64]

Author	Year	Equation	Geometrical Specifications
Perring and Johnson [65]	1935	$C_L = 0.9\tau A^{0.42}$	$\beta = 0°$
Sottorf [66]	1937	$C_L = 0.845\tau A^{0.5}$	$\tau \leq 10°$
Perelmuter [62]	1938	$C_L = \frac{2A\tau}{(1+A)}$	$5° \leq \tau \leq 8°$
Sedov from [64]	1939	$C_L = \frac{0.7\pi A\tau}{(1.4+A)}$	$\tau \leq 4°$
Siler [67]	1949	$C_L = \frac{\pi A\, sin\tau\, cos\tau}{(4+A)} + 0.88\, sin^2\tau\, cos\tau$	$\beta = 0°$
Korvin-Kroukovsky et al. [51]	1949	$C_L = 0.012\tau^{1.1}A^{0.5}$	$\tau \leq 4°$ $\beta = 0°$
Locke [50]	1948	$C_L = \frac{k}{2}\tau^n$ k and n are given in the reference as functions of the aspect ratio A	$\beta = 0°$
Korvin-Kroukovsky [68]	1950	$C_L = \frac{0.73\pi A\tau}{(2+A)} + 0.88\tau^2$	$0.25° \leq \tau \leq 10°$
Schnitzer [69]	1953	$C_L = \varphi\left(\frac{\pi^3 A}{16}\, sin\tau\, cos^2\tau + 0.88 sin^2\tau cos\tau\right)$ $\varphi = \frac{1}{\sqrt{1+\lambda^2}}\left(1 - \frac{0.485}{1+\frac{1}{\lambda}}\right)$	$0° \leq \tau \leq 45°$ $\beta = 0°$ $\beta = 30°$

Shufford [70]	1954	$C_L = \frac{\frac{\pi}{2}A\tau}{(1+A)} cos^2\tau + sin^2\tau cos\tau$	$\tau \leq 16°$ $\beta = 0°$
Brown from [64]	1954	$C_L = \frac{2\pi}{cot\frac{\tau}{2} + \pi + (2cot\frac{\tau}{2} - \pi)\frac{1}{A}}$	$A > 1$
Brown from [64]	1954	$C_L = (1.67sin\tau + 0.09).(1 - A)sin\tau\, cos\tau + \frac{2\pi A}{3cot\frac{\tau}{2}}$	$A < 1$
Farshing [71]	1955	$C^3 + [2.293 - 1.571A)\tau - 2.379 - A]C^3 + [2A + 4 + (6.283A - 4.584)\tau]C - 6.283A\tau = 0$ $C_L = \xi C$ $\xi = 1.359 - \tanh\left(\frac{1+A}{8A}\right) + \left(\frac{\tau° - 18°}{90.53}\right) tanh\frac{1}{A^2}$	$18° \leq \tau \leq 30°$
Farshing [71]	1955	$C^3 + [2.293 - 1.571A)\tau - 2.379 - A]C^3 + [2A + 4 + (6.283A - 4.584)\tau]C - 6.283A\tau = 0$ $C_L = \xi C$ $\xi = 1.359 - \tanh\left(\frac{1+A}{8A}\right)$	$2° \leq \tau \leq 18°$

Shufford [72]	1958	$C_L = \frac{\frac{\pi}{2}A\tau}{(1+A)} cos^2\tau + \frac{4}{3} sin^2\tau\, cos^3\tau$	$8° \leq \tau \leq 18°$ $\beta = 0°$ $\beta = 20°$ $\beta = 40°$

2.5.1.5 Shufford Method

This method was developed to predict the performance of deep-V planing hulls operating at high-speed regime where the buoyancy force is negligible. It does not discuss the effects of spray drag. It discusses the effects of the vertical spray rails on the performance of planing hulls. It has been modified several times to produce improved performance prediction methods. Brown [73] produced a version of this method that takes in consideration the buoyancy force which makes his method applicable to lower speeds (lower Froude number). This modified version is based on the same basis as Savitsky method [73]. The equations and procedure of this method are explained in [72].

2.5.1.6 Summary of Prediction Methods

The advantages, disadvantages and method of validation of each analytical method discussed previously are listed in Table 2.

Table 2. Summary of hydrodynamic prediction methods

Method/Author	Advantages	Disadvantages	Validated with
Savitsky	•It can predict the porpoising stability limit. •It can predict the performance of hulls with pure planing conditions which have similar performance characteristics as seaplanes. •It is the most common method used in speedboat design.	•Applicable to steady state conditions only. •Only hydrodynamic investigations. No other forces are considered. •Only applicable to trim angle $\tau < 10°$. At higher trim angle, the results starts to deviate from the results of the experiments. •The centre of dynamic pressure is assumed to be at 75% of the mean wetted length forward of the transom which is not accurate when analysing seaplanes. •It assumes that the thrust is always parallel to the axis thruster (prime mover axis) which may not be always true. •Spray drag (whisker spray) is not included or taken into account.	Previous analytical methods

		•It starts to behave irrationally when the dead-rise angle (β) is higher than 50° or when the dead-rise angle is not constant along the hull. •Only applicable to calm sea conditions, no wave is considered.	
Morabito	•It can be used to predict the performance of displacement and planing hulls. •Very simple and easy to use.	•It does not define the porpoising stability limit of planing hulls. •It is not applicable for high coefficient of speed C_v. •It only investigates the pressure distribution along the keel line and stagnation line of the planing hull. •It does not explain the relations between the different design variables of the planing hull (dead-rise and trim angles). •It cannot be mathematical combined with the aerodynamic effect because it only explains the hydrodynamic pressure on the hull.	CFD and experiments

		•It does not investigate the contribution of the hydrostatic force (Buoyancy). •Spray drag (whisker spray) is also not included or taken into account.	
CAHI	•Was initially developed to predict the characteristics of seaplanes. Thus, it can be modified to give more accurate results under different conditions.	•This method is based on Savitsky method. As a result, it has the same limitations. •It does not define the porpoising stability limit of planing hulls. •Only applicable to a certain hull geometry. •Only applicable under the same conditions and assumptions it is based on.	Experiments
Payne	•It can be used to predict the performance of displacement hulls.	•It does not define the porpoising stability limit of planing hulls. •It is not applicable for high coefficient of speed C_v.	Experiments and previous analytical methods

	•Very simple and easy to use.	•It only discusses the hydrodynamics of flat plates with no dead-rise angle. •It lacks the investigations of the aerodynamic forces acting on planing hulls.	
Shufford	•It can be applied to high speed-regime ($F_n > 1.0$). •Applicable to high trim angle $8° \leq \tau \leq 18°$. •Different dead-rise angles were tested in the development of this method.	•It is based on the same basis as Savitsky method. •Pure hydrodynamic conditions.	Experiments

CHAPTER 3

3. ANALYTICAL MECHANICS OF WATERBORNE AIRCRAFT

3.1 Introduction

The study of dynamics of GE vehicles can be split into two parts; kinematics and kinetics. Kinematics is the branch of science that treats geometrical aspects of motion without paying attention to the forces that cause the motion. On the other hand, kinetics is the study of forces that cause the motion. In order to analytically study the motion of waterborne aircraft, it is necessary to understand the kinetics of rigid bodies [24]. An equation of motion of a rigid body in any form can be defined as a mathematical formula that shows the relationship between accelerations, velocities and position co-ordinates.

In the analytical study of submarines, aircraft, spacecraft, planing hulls, GE vehicles and other aero and hydro-planes, the body that is in motion is referred to as a rigid body. A body can only be rigid if under any circumstances, the separation between its particles remain constant. In other words, a body is said to be rigid if the compressions and stresses that the body encounters while in motion do not cause any elastic deformation within the body which means that there will be no geometrical shape changes in the body [74].

Many terms are used to describe the different aspects of motion of WIG effect vehicles in a seaway. Similar to planing hulls and other displacement ships, the general field of WIG effect vehicle motion can be divided into two headings; manoeuvrability and seakeeping [74]. Both of these theories are concerned with the same issue which is the analytical study of motion. However, the separation

between the two approaches allows different assumptions to be made based on the case of study. In the next two sub-sections, the manoeuvring and seakeeping theories will be defined.

3.1.1 Manoeuvring Theory

Within the frame of manoeuvring theory, the study of a planing hull advancing at a constant forward speed in calm water is based on the assumption that the hydrodynamic coefficients do not depend on frequency which means that wave excitation is negligible.

The manoeuvring theory in its basic form is linear and derived using Newton's equation of motion. Application of the nonlinear form of the manoeuvring theory is possible if Taylor Series Expansions are used [64, 74, 75].

3.1.2 Seakeeping Theory

This theory deals with the motion of a planing hull resulting from external disturbing forces and moments of sea waves and wind. In this case, the hydrodynamic coefficients and wave excitation forces and moments are calculated as functions of wave excitation frequency using the geometry of the planing hull and mass distribution. Lagrangian mechanics are used to study the linear motion of planing hulls under the frame of seakeeping theory. However, according to Fossen [24], expanding this theory to a nonlinear form is a very important field of research. Hence, this theory of analysis is adopted in this research.

In this theory, the problem is considered as a system in which the planing hull is excited by external forces and moments which means that it responds to external effects such as sea wave effects. Figure 44 presents the logic of analysis in the seakeeping theory. The responses of the planing hull can be presented as motions in the different axes, porpoising or structural loads.

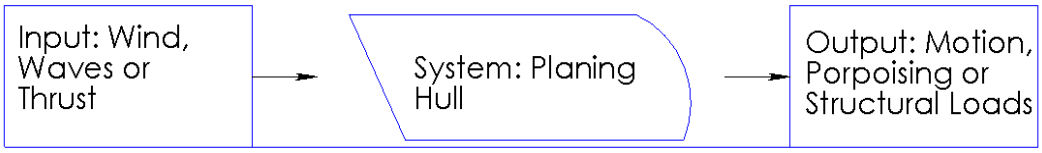

Figure 44. A schematic of the seakeeping theory

The system will be illustrated starting from the input which, in this research, is the sea wave effect. After that, the output of the system in form of motions will be discussed.

3.2 Wave Excitation Effect

Excitation forces and moments are generated by wind and sea waves. If the planing hull has a considerable surface area above the sea surface, the response to wind effect will be significant. Stability and manoeuvring in this case will be highly affected by the wind speed and direction [76]. However, in this research, the external excitation forces and moments are only considered to be produced by wave effect.

Waves are created by any form of energy supplied to the sea surface causing the water on the surface to make circular motions. The most common source of wave energy is the friction force between wind and sea-surface water. In fluid dynamics, wind-generated waves (also known as wind waves or gravity waves) are sea-surface waves generated by wind blowing over an area of fluid surface causing disturbance in the interaction between the fluid and any object moving through it [76]. Hence, the higher the speed of the planing hull, the larger the wave created by the interaction.

3.2.1 Linear Wave Theory

Linear wave theory is referred to waves with small amplitude. It is also known as harmonic wave theory. The wave spectrum is assumed to be linear and takes a sinusoidal wave shape. In theory, a sinusoid is a curve that describes smooth periodic oscillations. According to Young [76], nonlinearities in the linear wave

theory can be considered as perturbations to the linear solution. Nonlinearities in this problem have been ignored in the past. However, understanding the nonlinear behaviour of planing hulls traveling in sea waves is a very important field of research [76]. It is necessary at this point to define the terms used in sea wave calculations. Figure 45 shows the important parameters used to define a linear or harmonic wave.

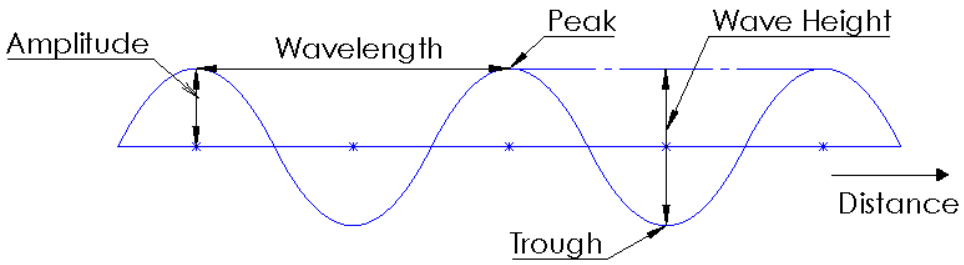

Figure 45. Harmonic wave spectrum

The definition of each term is listed below [76]:

- Amplitude: it is the maximum displacement of the sea wave.
- Wavelength: it is the distance between two successive peaks or troughs in the wave.
- Wave period: it is the time needed to travel one wavelength.
- Angular frequency: it is a measure of how the wave increases with time. In other words, it is the number of wave peaks (or successive identical points in the wave cycle) to pass a fixed point in one second.
- Wave height: it is the vertical distance between a trough and a peak.

In order to form a solution for the harmonic sea wave, the following assumptions are made [76]:

1. The water depth, the wavelength and wave period are assumed to be constant.
2. The wave motion is assumed to be two-dimensional as presented previously in Figure 45. This assumption leads to constant wave height. However, the height is small compared to the wavelength and water depth.
3. The wave shape do not change with time.

4. The sea water is incompressible which means the density is constant along the direction of motion.

In this research, the wave excitation forces and moments are assumed to be sinusoidal in nature to match the linear wave theory. Consequently, the excitation forces and moments can be expressed in the following general forms [6]:

$$F\ (t) = F_1 \cos(\omega_e t) + F_2 \sin(\omega_e t) = F_R \cos(\omega_e t + \sigma) \quad (3.1)$$

$$M\ (t) = M_1 \cos(\omega_e t) + M_2 \sin(\omega_e t) = M_R \cos(\omega_e t + \tau) \quad (3.2)$$

where F_R is the amplitude of the exciting force which is the resultant of the two amplitudes F_1 and F_2, M_R is the also the amplitude of the exciting moment which is again the resultant of the two components M_1 and M_2, σ is the phase lag of the exciting force relative to the wave motion, τ is the phase lag of the exciting moment relative to the wave motion and ω_e is the encounter frequency of the sea waves which will be discussed in details later in this chapter (section 3.4).

3.3 Simple Harmonic Motion

Simple harmonic motion (SHM) is characterised by the natural motion of a mass on a spring when it is subjected to a linear restoring force as shown in Figure 46. It is called the spring-mass-damper system of motion [77].

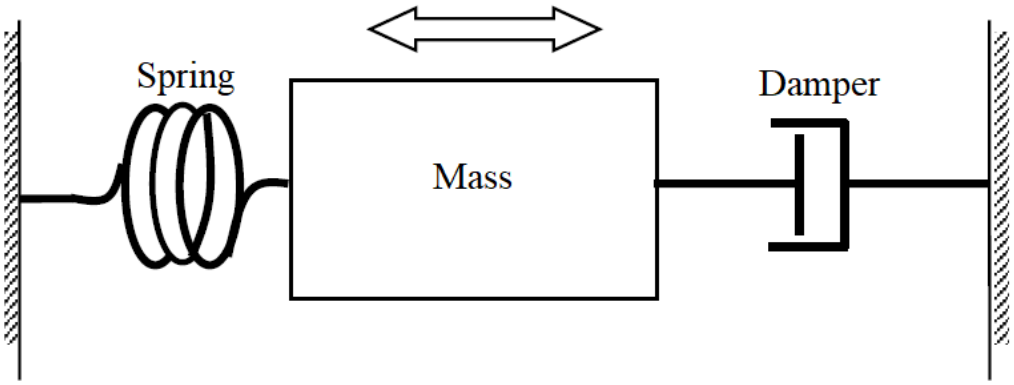

Figure 46. Spring-mass-damper system

Simple harmonic motion is essentially one type of the periodic motion where the restoring force is proportional to the displacement and acts in the direction opposite to that of displacement. The force must be proportional to the displacement of the mass of the object. This oscillatory motion is sinusoidal in time and presents a single resonant frequency. A system with a single-resonant frequency will take the form of a sine wave as a function of distance [77].

A seaplane is said to be in simple harmonic motion if some conditions are satisfied such as: it moves in a uniform path, a variable external force is acting on it, the motion is repetitive and always made in equal time periods. As shown in the Figure 47, the characteristics of such a system are similar to the characteristics of a harmonic wave.

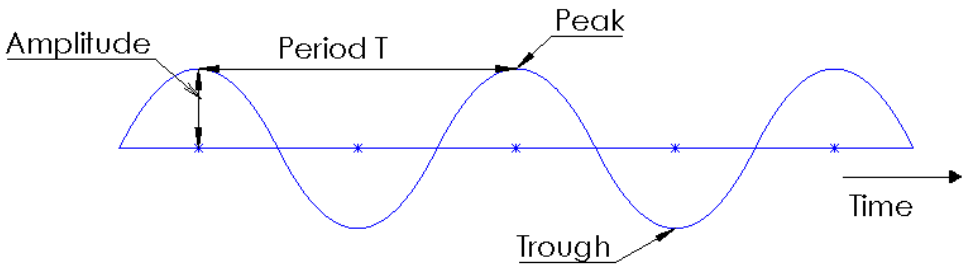

Figure 47. Sinusoidal motion of an object in SHM

The motion of such a system is mathematically presented by analytical equations developed by Lagrange. In the next sub-section, Lagrangian mechanics will be explained and compared to Newtonian mechanics. After that, the general Lagrangian equations of motion will be derived.

3.3.1 Lagrangian Mechanics

Newton's laws were proposed to study the motion of a single particle and can be extended to study systems of particles in motion. This approach of problem solving in mechanics is known as Vectorial Mechanics in which concepts such as force and momentum are used, both of those quantities are regarded as vector quantities. A different approach was proposed by Joseph-Louis Lagrange [78] to study the mechanics of an object moving through a fluid. This approach is known

as Analytical Mechanics in which the system is considered as a whole rather than studying the individual components. There are two fundamental quantities to consider when using Lagrange approach: kinetic energy and work, both of those quantities are scalar [78]. Lagrange approach is used in this research for the following reasons:

1. In Newton's approach, it is either the motion is given, solve for forces or the forces are given solve for motion which makes the approach suitable for solving simple systems in which the equations are linear. But when the system is complex and the equations are nonlinear then the terms in the equations will have magnitude and direction (vectors) which will be difficult to manage in Newton's approach. In Lagrange's approach the kinetic and potential energies and dissipation of energy functions are used to describe the motion. This approach solves for the motion in scalar form which avoids the complexity of Newton's approach [78].
2. The use of kinetic energy makes Lagrange's approach more interesting as the kinetic energy is a function of velocity and most of the coefficients that describe the motion of seaplanes are speed-dependent [79].
3. As the motion of seaplanes is described by a six DOF system, Newton's equations of motion will have acceleration terms in every direction which makes the problem more complicated to solve. In order to simplify the problem, researchers used to find the equilibrium point in which the speed of the craft is assumed to be constant so that the acceleration terms are eliminated. However, this approach leads to linearized unrealistic solutions [80].
4. The hydrodynamic and hydrostatic characteristics of seaplanes undergo continuous changes due to the varying underwater volume, varying pressure distribution on the hull of the craft and varying centre of buoyancy and gravity. As a result, solving the six DOF nonlinear equations of motion is very complicated using Newton's approach and may lead to undesired results that do not reflect the seaplane performance in real life situations. However, it is possible to develop the nonlinear equations of motion of seaplanes that take

the continuous changes of the characteristics into account by using Lagrange's approach [57].

5. If Newton's approach is followed, Taylor Series Expansions will then be used to determine the forces and moments on the hull of the craft which leads to physically unrealistic prediction of self-sustained oscillations (unsatisfactory or misleading results) unless certain relationships between the coefficients are satisfied which means that nonlinear analysis is needed to determine the relationships. On the other hand, if Lagrange's approach is followed, the nonlinear equations of motion of the craft are directly found from an energy formulation of the problem in which the sea and the craft are considered as a single dynamical system. This consideration assumes that the kinetic energy is positive definite for every motion and the potential energy is increasing with every displacement from the undisturbed position [80].
6. The angular motion of the craft in roll and pitch directions is coupled and can only be accurately described by nonlinear equations which is not applicable in Newton's approach [57].
7. When studying the wave effects on the motion of seaplanes, Newton's approach assumes linear relationship between the craft response frequency and the water wave frequency which is an approximation because the response depends on speed and geometry of the craft. The wave frequency has vital importance in the nonlinear problem [79].
8. In Newton's approach, the hydrodynamic coefficients in the equations of seaplane motion are assumed to be speed-independent. However, this assumption is only valid for added mass coefficients (section 3.4.2.1) because the restoring forces and moments coefficients (section 3.4.2.3) are speed-dependent [57].
9. Newton's approach necessitates the calculation of constraint forces resulting from kinematical relations although these forces may be of no interest because they play no particular role in the study of nonlinear motion of objects. Constraint forces can be defined as the forces that make the object obey to the geometrical configuration of the system [78]. For instance, skin

friction drag is not calculated when studying the motion of seaplanes using Lagrangian mechanic.

10. Lagrange's approach completely eliminates the dependence of the formulation on coordinate systems and also permits an efficient treatment of problems associated with multi-degree-of-freedom systems as well as problems involving curvilinear coordinates or various types of constraints [78].
11. As previously mentioned in section 3.2.1, Lagrangian mechanics have not been used to study the nonlinear motion of seaplanes. However, a large number of researchers have used Newton's approach to study the motion of seaplanes.

The Lagrangian equation of motion of an object moving in a fluid is derived from a variation principle called Hamilton's Principle [81]. It is also known as the principle of least action or stationary action because it is concerned with the minimisation of a quantity (minimising the action) in a manner that is identical to extremum problems solved using the calculus of variations [82]. In this formalism, every mechanical system is characterised by a definite function expressed as:

$$L(q, \dot{q}, t) \tag{3.3}$$

The motion of the system can be completely defined when a certain condition is satisfied. For instance, if at times t_1 and t_2, the position of an object is defined by two sets of coordinates q_1 and q_2. Then, the condition is that the object moves between the two coordinates in such a way that the following integral [81]:

$$S = \int_{t_1}^{t_2} L(q, \dot{q}, t)\, dt \tag{3.4}$$

takes the least possible value. Here, L is called the Lagrangian of the system, S is the action and q is a generalised coordinate that completely define the position of the mechanical system [81]. More details about the derivation of Lagrangian equation of motion can be found in [77, 78, 81, 82].

3.4 Hull Response

In this research, the planing hull response to wave effects is considered to be in form of motions. The response of the planing hull to sea waves highly depends on the frequency of the external excitation loads. However, the wave frequency is not the only frequency that the external excitation loads depend on. The frequency of the external loads is also influenced by the speed and direction of motion of the seaplane relative to the direction of the wave. This consideration is very important in the analytical prediction of seaplane motion. Hence, the frequency of the external excitation forces and moments is called the encounter frequency ω_e. It allows for the speed of the seaplane and its direction relative to the waves to be taken into account. The encounter frequency is calculated from the following equation [6]:

$$\omega_e = \omega_w - \frac{\omega_w^2 V cos(\mu)}{g} \tag{3.5}$$

where ω_w is the frequency of the sea wave, V is the seaplane speed, g is the acceleration of gravity and μ is the angle of seaplane direction of motion relative to the direction of the wave. It is known as the heading angle and it ranges from 0° to 180° [6]. Figure 48 illustrates how this angle is measured.

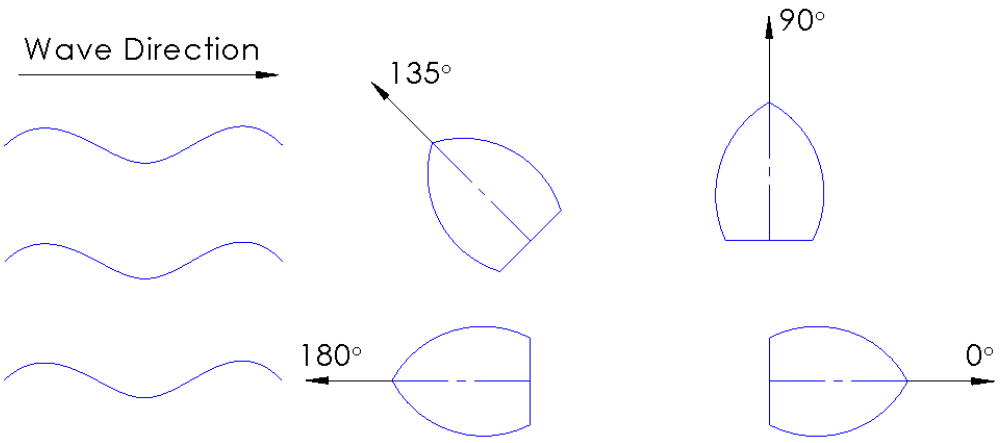

Figure 48. Illustration of the heading angle

It should be mentioned that maximum amplitude of oscillations will be encountered when the external excitation frequency is equal to the natural frequency of the system. For a seaplane, the natural frequency depends on its mass and stiffness [24]. This condition is called resonance. If the aim is to reduce motions, resonance should be avoided [77].

When the encounter frequency is known, it is then possible to predict the seaplane responses which, as previously mentioned, is considered to be in form of rigid body motions. The system of motion is explained in the next sub-section.

3.4.1 The Six-Degree-of-Freedom System of Motion

A WIG vehicle is considered a rigid body floating on surface of water which can experience motion in all six-degrees-of-freedom. The six motions are a set of independent displacements and rotations that completely define the displaced position and orientation of the vehicle. Therefore, WIG vehicles motion can be considered to be made of three translational (linear) components ($surge^1$, $sway^2$ and $heave^3$), and three rotational (angular) components ($roll^4$, $pitch^5$ and yaw^6). The six DOF system of a planing hull is represented in an orthogonal coordinate system having the centre of gravity as its origin as shown in Figure 49 [24]. The six motions are divided into two categories. The first one includes motions that are induced by waves which are heave, pitch and roll. In ship theory, these motions are referred to as oscillations with damping effect and they cannot change the position of the hull of the vehicle on the sea surface. A solution for each motion of this category can be obtained if the frequency of the wave is known [83]. The second category includes motions caused by propellers, rudders, currents and winds which are surge sway and yaw. Clearly, the forces coming from this category can move the planing hull to a new position. Full description of each motion is given below [83].

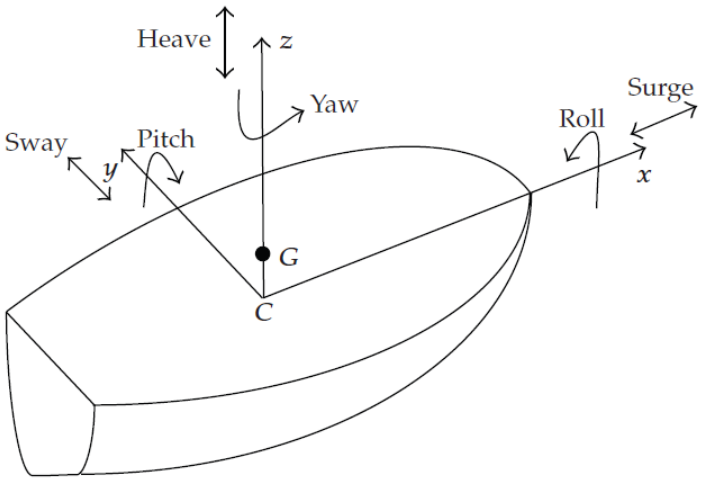

Figure 49. The six motions of a planing hull [57]

1. Surge: it is the forward and aft translational motion directed along the x-axis. This motion includes not only the movement caused by the propellers, but also the forward and backward movements on a wave peaks and troughs respectively. This planing hulls behaviour is known as surfing.
2. Sway: it is the transverse translational motion along the y-axis. The sideslip due to centripetal forces during tuning is also considered a sway motion.
3. Heave: it is the vertical bodily translational motion in the z-axis. It is caused by the change in buoyancy when waves pass underneath the hull. Heaving is periodic and coupled with pitching and rolling motions. The action of sea waves can cause the planing hull to move out of water or sink below its waterline. This affects the balance between the displacement and the buoyant force that creates a reaction force to restore the hull to its original waterline position. This restoring force is proportional to the distance displaced by the centre of gravity of the hull. This indicates that the heave motion has the same characteristics as the SHM. An explanation of heave force generation is shown in Figure 50.

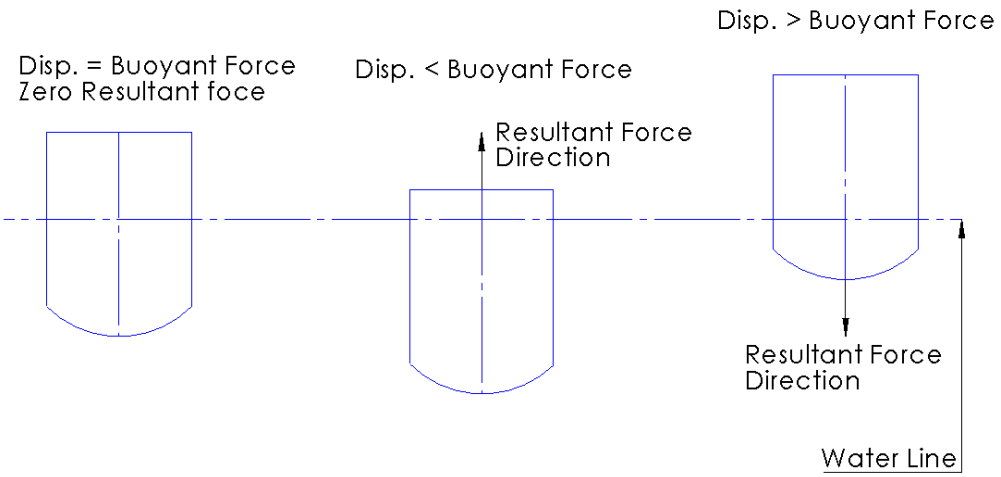

Figure 50. Heaving force generation

4. Roll: it is the rotational motion about the longitudinal x-axis and it is the motion that affects the comfortability of passengers. In contrast to pendulums, planing hulls have an instantaneous axis located near the centre of gravity of the craft not a fixed point of rotation. Therefore, a path in space passing through the centre of gravity is considered as the axis of rotation. This path remains constant with respect to the planing hull.
5. Pitch: it is the rotational motion about the transverse y-axis. Pitching is also known as the bow-down motion. This motion is very important for planing hulls operating in sea environment because of the high altitude waves due to the high risk of porpoising. When a planing hull is advancing in sea waves, the slope of the waterline changes the location of the centre of buoyancy. As a result, a righting moment is created to restore the vertical alignment between the two centres of gravity and buoyancy. Figure 51 explains this point.

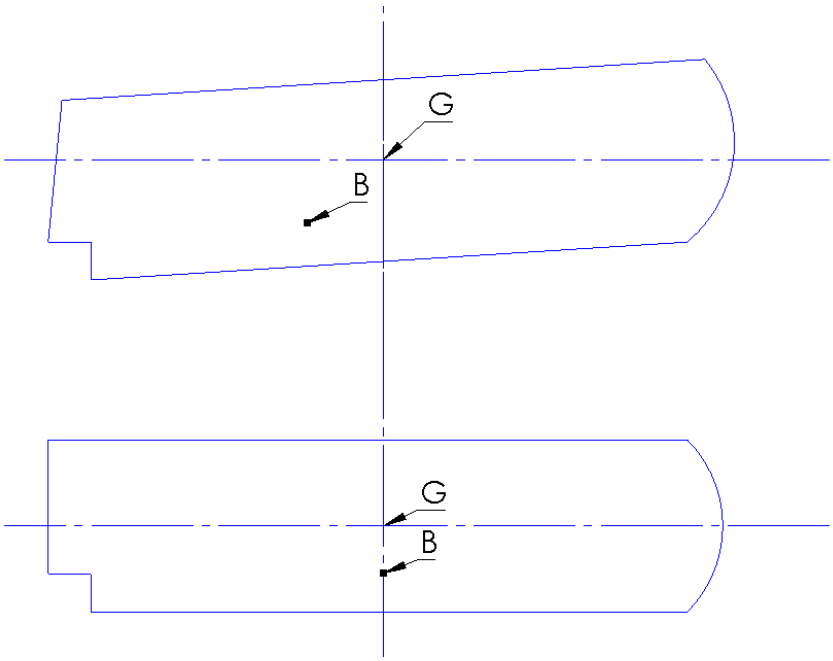

Figure 51. Pitching force generation

6. Yaw: it is the rotational motion about the vertical z-axis. It can also be defined as the tendency to veer off course. In contrast to pitching and rolling, this motion has no restorative moment. Therefore, external surfaces such as rudders should be used to control this motion.

The general equations of seaplane motion can be developed by either using Lagrangian mechanics [84, 85, 86] or by using Newtonian mechanics [87, 88, 89]. The hydrostatic and hydrodynamic forces and moments acting on a planing hull can be derived in two approaches. In the first approach, a mathematical development based on Taylor Series Expansions of force function is used. The second approach utilises the integration of hydrodynamic pressure acting on the wetted surface of the planing hull to obtain the forces and moments. The second approach is known as the "Strip Theory" and will be discussed in details later in this chapter (section 3.5). In the next sub-section, the Lagrangian equations of seaplane motion will be presented.

3.4.2 Lagrangian Equations of Seaplane Motion

The equations of motion of a seaplane advancing at a constant forward velocity with arbitrary heading in regular sinusoidal sea waves are presented in this section. As previously mentioned, a seaplane can experience motions in six directions. Hence, the performance of seaplanes is presented by a six DOF system. By taking into consideration that the responses are linear and harmonic, the six linear equations of motion can be written using subscript notation as follows [90]:

$$\sum_{k=1}^{6}\left[\left(M_{jk}+A_{jk}\right)\ddot{\eta}_k + B_{jk}\dot{\eta}_k + C_{jk}\eta_k\right] = F_j e^{i\omega t} \tag{3.6}$$

where:

- $j = 1 \ldots 6$
- M_{jk} is the component of the generalised mass matrix of the craft in the j^{th} direction due to k^{th} motion.
- A_{jk} is the added-mass coefficient in the j^{th} direction due to k^{th} motion.
- B_{jk} is the damping coefficient in the j^{th} direction due to k^{th} motion.
- C_{jk} is the hydrostatic restoring force coefficient in the j^{th} direction due to k^{th} motion.
- F_j are the complex amplitudes of the exciting forces and moments in the j^{th} direction.

In this research, focus will be given to the two coupled motions of heave and pitch for the following reasons:

1. For a planing hull with lateral symmetry, the six coupled equations of motion are reduced to two sets of equations, connecting respectively, the heave, pitch and surge, and the sway, roll and yaw. This means that the translational equations are not coupled with the angular equations. As long as the planing hull is assumed to be a slender body, the hydrodynamic forces associated with the surge motion are much smaller than the forces associated with the other

motions. As a result, the motion of the craft can be described by the two coupled equations of heave and pitch motions [5, 91].

2. The porpoising stability limit is studied from the equations of heave and pitch only because porpoising is a coupled oscillatory motion in those two direction as explained previously (see section 2.2.3).
3. Dynamic stability in take-off and landing, which is the subject of this research, is studied from heaving and pitching motions.

A heaving and pitching system of seaplane motion behaves like a two-degree-of-freedom spring-mass system. According to Ogilvie [90], this assumption is clear when a craft model is given heave or pitch displacements from its equilibrium position, it will rapidly oscillate several times before it comes to rest. Therefore, the resulting equations of heave and pitch motions of seaplanes are expressed as follows:

$$(m + A_{33})\ddot{\eta}_3 + A_{35}\ddot{\eta}_5 + B_{33}\dot{\eta}_3 + B_{35}\dot{\eta}_5 + C_{33}\eta_3 + C_{35}\eta_5 = F(t) \quad (3.7)$$

$$A_{53}\ddot{\eta}_3 + (A_{55} + I_{55})\ddot{\eta}_5 + B_{53}\dot{\eta}_3 + B_{55}\dot{\eta}_5 + C_{53}\eta_3 + C_{55}\eta_5 = M(t) \quad (3.8)$$

The subscript 3 stands to the heaving motion and 5 stands to the pitching motion. More details about the analytical investigations of heaving and pitching motions of planing hulls can be found in [5, 6, 90, 91, 92, 93, 94, 95].

The determination of the hydrodynamic coefficients and exciting forces and moments is a major problem in the analytical prediction of planing hulls motion. It depends on forces amplitude, harmonic motion of the planing hull and phase lag between the forces and moments. In order to simplify this problem, the craft can be divided into transverse strips or segments. The coefficients are then calculated by applying a two-dimensional hydrodynamic strip theory [6]. Before performing the strip theory calculations, it is necessary to understand the physical meaning of each coefficient.

3.4.2.1 Added Mass

In hydromechanics, additional effect must be considered when formulating the equations of unsteady motion of objects on water or when dealing with unsteady flow around objects. This effect is a result of the interaction between the fluid and the structure of the object. This added effect is known as added mass or virtual mass and it can be defined as the added inertia to the system due to the movement of fluid around the structure of the craft when it moves through it [96]. Lata and Thiagarajan [97] defined the added mass of an oscillating body as the pressure force per unit acceleration acting on a body floating on water. Thus, the added mass can be described as the increase in kinetic energy of fluid due to an object accelerating through it. Added mass effect should also be considered when studying the motion of fluid around a resting object [98].

Added mass can be explained by the viscosity difference between fluids. For example, the viscosity of air is less than the viscosity of water. As a result, an object moving through air will need less power to overcome the drag produced by air. On the other hand, the viscosity of honey is higher than the viscosity of water. Thus, an object moving through honey will need more power to overcome the drag. This indicates that the added mass effect is proportional to fluid density. Therefore, from a physical point of view, added mass is the weight added to an object moving unsteadily in a fluid due to the fact that the body has to move some volume of the surrounding fluid equal to its volume while it moves because the body and the fluid cannot simultaneously occupy this physical space [98].

3.4.2.2 Damping

Damping can be described as an influence within an oscillatory system that has the effect of reducing, restricting or preventing its oscillations. In terms of physics, damping is produced by processes that dissipate the energy stored in the oscillation [99]. According to Tongue [100], damping is any external effect on an oscillatory system that tends to reduce the amplitude of vibrations. In a mechanical

system, damping is caused by the internal friction. In this case, damping is proportional to the object velocity, fluid viscosity and roughness of the structure.

In ship theory, damping is only related to ocean waves propagating away from the ship body. The main difficulty in the analytical prediction of ship motion is the estimation of ship roll damping because damping has a major effect on the roll motion of a ship. Usually, ship dynamic analysis consider a ship in still water, and the ship roll damping coefficients are then determined by experiments of free oscillations of a model ship. However, it is very important to consider damping effects in wavy conditions because, under this condition, damping highly enhances comfortability as it reduces peak vibration amplitude to a considerable level. Moreover, it plays an important role in ship safety [101]. Thus, damping of a high-speed planing hull depends on many factors such as: hull shape, weight of the hull, wave encounter frequency, roll angle and the external excitation moment.

3.4.2.3 Restoring Forces and Moments

In physics, the restoring force is the force that supports the equilibrium of a system. In ship theory, hydrostatic restoring forces and moments support the ship to return to its static equilibrium position after a disturbance. The restoring forces and moments are in direct relationship with the displacement and rotations of the ship. These forces and moments are only experienced in the vertical plane (heave, roll and pitch motions only). In simple harmonic motion, restoring is referred to the force that is responsible of retrieving original size and shape [99]. An example of a restoring moment was given in section 3.4.1 when pitch motion was illustrated.

3.5 Strip Theory Calculations

The coefficients of the coupled heave and pitch equations of motion can be analytically obtained by a method known as the strip theory. The objective of this method is to calculate the coefficients of the heave and pitch equations of motion of ships or any type of planing hulls or high-speed boats when the frequency of oscillations is known. The two equations can then be solved by using complex

forms to obtain the values of heave and pitch motions. Strip theory is considered to be a very effective tool because of its ability to analytically determine the coefficients in the coupled heave and pitch equations of motion under any sea wave or speed conditions. In this section, the strip theory proposed by Bhattacharyya [6] will be explained and applied to obtain the values of the coefficients of the coupled heave and pitch equations for a planing hull so that further analytical investigations could be carried. Other strip theories were proposed by Salvesen et al. [91], Korvin-Kroukovsky [95] and Faltinsen [102]. All strip theories share the same basic principles such as the sea wave is periodic, the hull of the seaplane is symmetric in the transverse section and the heave and pitch motions are coupled. However, the differences between them are in the number of segments the ship is divided into and in the assumptions made when calculating the sectional added mass, sectional damping and sectional restoring force and moment coefficients.

In order to be compatible with the objectives of this research, a few assumptions are made in the mathematical formulation of the strip theory such as [6]:

1. The sea wave is periodic and linear (regular sea waves / sinusoidal).
2. The forces and moments generated by wind and propellers are neglected.
3. The seaplane is unrestrained, rigid and have a slender shape.
4. The seaplane is symmetric in the x-z plane.
5. The planing hull is assumed to be heading into the waves in a direction transverse to their peak line (heading angle is 180°).
6. The vertical motion is assumed to be composed of coupled pitching and heaving motions.

With these assumptions in mind, the planing hull structure is divided into four segments or strips which are rigidly connected to each other, and the flow around it is considered to be two-dimensional in nature [103]. Those considerations allow the problem to be reduced from three to two-dimensional with each segment treated as part of an infinite cylinder having two-dimensional flow around it. This implies that there is no interaction between flows at the adjacent segments [6]. After that, the

response of each segment is calculated separately and then the total response of the planing hull can be found by integrating the component reactions of all segments over the total length of the planing hull. Strip theory calculations are presented in Appendix A. In summary, the strip theory can be performed by the following steps:

1. The planing hull is divided into four sections to provide representation of the underwater hull shape.
2. The sectional added mass, damping and restoring force coefficients are then determined by using tables to facilitate the calculations.
3. Next, the hydrodynamic coefficients of the heave and pitch equations are calculated by performing integrations along the length of the hull.
4. Finally, the excitation forces and moments are calculated from given sea wave characteristics and hull shape.

CHAPTER 4

4. ANALYTICAL PREDICTION OF MOTION

4.1 Introduction

The key to solving modern physical problems is mathematical modelling. However, many physical problems facing engineers, physicists and mathematicians exhibit certain essential features such as nonlinearity that prevent exact analytical solutions. Most nonlinear phenomena are models of real-life problems. Nonlinear equations are widely used as models to describe complex physical phenomena in various fields of science especially in dynamic stability analysis. Thus, in order to obtain solutions to nonlinear equations, approximations or numerical methods are used. The most common approximation methods used are the perturbation methods. In this chapter, the nonlinear equations of heave and pitch motions are solved analytically by using a perturbation method. First, the equations are reduced to a system of coupled Duffing equations with cubic nonlinearity. Then, the perturbation method used is discussed and finally the analytical solutions to the nonlinear equations of motion are presented.

4.2 The Duffing Equation

In many engineering systems, oscillatory behaviour of dynamical systems due to periodic excitation is of great importance. There are two types of oscillatory responses; forced oscillations and parametric oscillations [2]. Forced oscillations appear when the system is excited by a periodic input. If the frequency of oscillations of the external excitation force is close to the natural frequency of the system, then the system will experience resonance (i.e. oscillations with large amplitude) [2]. On the other hand, parametric oscillations appear when the system has time-varying (periodic) parameters [104]. In this case, the system will

experience parametric resonance. It means that the system is oscillating with an external excitation frequency equal to twice the natural frequency of the system. The amplitude of the oscillations in the output of this system will also be large [104]. In this research, the dynamical system of motion is assumed to be driven by a forced oscillatory external excitation frequency. This is because the input of the system of motion is a pattern of sinusoidal sea wave that has a constant frequency of oscillations. In addition, the parameters of the two equations of heave and pitch motions are constant and can be calculated using a strip theory as described in section 3.5.

A very important example of nonlinear dynamical equations of motion driven by a periodic external excitation force is the Duffing equation. It was first developed by Georg Duffing in 1918 [105]. It is a second order nonlinear differential equation used to describe the motion of driven and damped oscillators. It is the first step in moving from a linear to a nonlinear system [105]. This type of equation is used to describe several nonlinear systems in a wide range of applications such as the motion of a pendulum with a small frequency of oscillations as well as the behaviour of some isolators and electric circuits. Although many physical systems cannot be accurately described using this equation, it is possible to use it as an approximate description so that their nonlinear behaviour can be studied qualitatively [105]. Therefore, the Duffing equation is used in this research to model the nonlinear motion of seaplanes advancing through harmonically excited head sea waves. The two equations of heave and pitch motions (equations 3.7 and 3.8) are reduced to two-dimensional Duffing equations with cubic nonlinearity by making the following assumptions:

1. The restoring forces behave according to Hooke's law but with nonlinear nature. It is demonstrated in [57, 106, 107] that cubic nonlinearity is sufficient to describe the coupled motion of ships and floating objects moving over linear sinusoidal sea waves. Hence, cubic nonlinearity is considered in this research.
2. The system is perturbed by a sinusoidal head sea wave.

3. The damping effect is negligible because the hydrodynamic coefficients associated with damping are much smaller than the added mass and restoring force coefficients. That is because damping coefficients are functions of frequency and speed, which are both small compared to the mass of the seaplane.
4. The pitch angular acceleration is zero in the heave equation and the heave translational acceleration is zero in the pitch equation (A_{35} and A_{53} are very small compared to other coefficients). The seaplane is then assumed to be advancing forward with a constant velocity.

With that taken into consideration, this two degree-of-freedom system can be modelled by two coupled, second order nonlinear differential equations of the following form:

$$\ddot{u} + {\omega_0}^2 u + a_1 v + a_2 u^3 = F_1 \cos(\omega t) \quad (4.1)$$

$$\ddot{v} + {\omega_0}^2 v + b_1 u + b_2 v^3 = M_1 \cos(\omega t) + M_2 \sin(\omega t) \quad (4.2)$$

where:

- a_1 is the pitch coupling term coefficient.
- a_2 is the heave nonlinear term coefficient.
- b_1 is the heave coupling term coefficient.
- b_2 is the pitch nonlinear term coefficient.
- F_1 is the heave amplitude.
- M_1 and M_2 are the pitch amplitudes.
- ω_0 is the natural frequency.
- ω is the external excitation frequency.
- u is the heave translational displacement.
- v is the pitch angular displacement.

Equations 4.1 and 4.2 are harmonically excited Duffing equations used in this research to describe the motion of seaplanes advancing through head sea waves. They are usually used to model the two-dimensional motion of a pendulum

oscillating with a small frequency which is very similar to the behaviour of seaplanes during take-off and landing [105]. More details about the Duffing equation can be found in [2, 104, 105, 107, 109].

Chaos theory is one of the most significant achievements of nonlinear science. The Duffing equation is associated with mathematical chaotic behaviour. This chaotic behaviour exists in many natural systems such as weather and climate [110]. It also occurs spontaneously in some systems with artificial components, such as road traffic. Chaos theory has applications in several other disciplines including meteorology, sociology and environmental sciences. Chaos is defined as a periodic long-term behaviour in a deterministic system that exhibits sensitive dependence on initial conditions [110]. There are three properties that must exist in a dynamical system to be classified as chaotic:

- It must have periodic long-term behaviour meaning that the solution of the system settles into an irregular patter as $t \to \infty$. The solution does not repeat or oscillate in a periodic manner.
- It is sensitive to initial conditions. This means that any small change in the initial condition can change the trajectory, which may give a significantly different long-term behaviour.
- It must be "deterministic" which means that the irregular behaviour of the system is due to the nonlinearity of the system, rather than outside forces.

Thus, Duffing oscillators find applications in Chaos theory, which is the field of study in mathematics that studies the behaviour of dynamical systems that are highly sensitive to initial conditions. Small difference in initial conditions (such as those of rounding errors in numerical computation) yields widely diverging outcomes for such dynamical systems, rendering long-term prediction impossible in general [110].

The analytical solution of the Duffing equation is essential due to its applicability in a wide range of engineering applications. Several approaches have been proposed to solve the nonlinear Duffing equation. The most commonly used

analytical methods to solve the Duffing equation in its various forms are the method of multiple scales [85], Bogolubov-Mitropolski method [111], He's energy balance method [112, 113], the Global Error Minimisation method [114], the Variational iteration method [115], the Jacobi elliptic functions method [109], the Homotopy perturbation method [116] and the Poincare-Lindstedt method [2]. These analytical methods are extended to solve a system of two coupled nonlinear differential equations describing the motion of a pendulum. The coefficients of the equations must be constants with varying external exciting force with time. In this work, the perturbation method used to solve the two nonlinear equations of heave and pitch is the Poincare-Lindstedt method.

4.3 The Poincare-Lindstedt Perturbation Method

Generally, perturbation methods can be defined as mathematical methods used to find approximate analytical solution of nonlinear differential equations by starting from an exact solution of a related but simpler problem which, in many cases, is the linear form of the equation [117]. Perturbation methods rely on there being a parameter in the equation that is relatively small. Such a situation is very common in engineering applications, and this is the reason why perturbation methods are the foundation of applied mathematics [118]. Nonlinear problems can be solved with very good accuracy using computers. However, computer solutions do not provide insight into the physics of the problem. In contrast, perturbation methods provide a reasonably accurate expression for the solution of nonlinear differential equations that can be used to explain the physics behind the problem [118]. The solution can then be used to explain the effect of each parameter in the differential equation describing the problem so that design enhancements can be carried out. Not only that, but also perturbation methods are capable of dealing with nonlinear, inhomogeneous and multidimensional problems [118].

The solution obtained using perturbation methods is presented by a form of convergent power series expansions with respect to a small, dimensionless parameter which is of the same order of the nonlinearity and amplitude of motion [119]. The use of this technique leads to an expression for the desired solution in

terms of a formal power series in small parameter (ε) known as perturbation series that quantifies the deviation from the exactly solvable problem [120]. Perturbation methods are classified into two types; regular and singular [119]. A basic feature of regular perturbation is that the exact solution for small but not zero (ε) smoothly approaches the unperturbed solution as (ε) $\rightarrow$ 0. On the other hand, singular perturbation problems are those which cannot be solved when (ε) = 0. Problems of this type feature a parameter for which the solution of the problem at a limiting value of the parameter are different in character from the limit of the solution of the general problem. The difference between the two types is explained in the following example: when a spring-mass system is affected by a small amount of damping, the system will oscillate and slowly damp. This small damping is a small correction (regular perturbation). However, when the same system has a small mass, then the system will be a highly damped system which will oscillate only when the mass is not equal to zero (singular perturbation) [119]. More details about perturbation methods can be found in [121, 122, 123, 124].

The Poincare-Lindstedt method is a technique used for uniformly approximating periodic solutions to ordinary differential equations. The structural design of a sea-craft requires the evaluation of its motions and wave induced pressure distributions over the hull in wavy sea conditions. Thus, a nonlinear seakeeping solution must simulate, with sufficient accuracy and efficiency, the seakeeping behaviour of a sea-craft in wave trains that may be several hours long in duration. With this goal in mind, the development of nonlinear periodic solution was initiated [125]. The Poincare-Lindstedt method eliminates the secular terms arising in the straightforward application of regular perturbation theory to weakly nonlinear equations [126]. Secular terms are the terms that grow without bound. Those terms have a singularity point at which a given mathematical object is not defined [126]. This method is adopted in this research because it is usually used to obtain periodic solution to nonlinear differential equations which presents the behaviour of seaplanes moving over sinusoidal waves. It describes the period of unstable motion of seaplanes so that porpoising can be predicted analytically.

Moreover, it can be applied to obtain a closed form solution without the use of any computer software.

4.4 The Analytical Solution to the System of Nonlinear Equations

In this section, an approximation to equations 4.1 and 4.2 for small but finite (ε) is determined by assuming an expansion that is non-uniform for large times. This is achieved by assuming that the nonlinearity, the coupling and the excitation force/moment appear at the same order in each equation (same order of strength for coupling, nonlinearity and amplitude of external force). Hence, an infinitesimal parameter (ε) is introduced and equations 4.1 and 4.2 are written as follows:

$$\ddot{u} + {\omega_0}^2 u + \varepsilon a_1 v + \varepsilon a_2 u^3 = \varepsilon F_1 \cos(\omega t) \tag{4.3}$$

$$\ddot{v} + {\omega_0}^2 v + \varepsilon b_1 u + \varepsilon b_2 v^3 = \varepsilon M_1 \cos(\omega t) + \varepsilon M_2 \sin(\omega t) \tag{4.4}$$

Here, it is assumed that the system undergoes resonant oscillations, that is (ω) is an integer multiple of the natural frequency of the system, and is initially assumed to be unknown. Thus, it possesses an (ε) expansion of the form:

$$\omega = n\omega_0 + \varepsilon\omega_1 + \varepsilon^2\omega_2 + O(\varepsilon^3) \tag{4.5}$$

where n is a positive integer. Similarly, the phase variables u and v are assumed to represent a perturbation of the harmonic oscillator (u_0, v_0) through the following equations:

$$u = u_0(\tau) + \varepsilon u_1(\tau) + \varepsilon^2 u_2(\tau) + O(\varepsilon^3) \tag{4.6}$$

$$v = v_0(\tau) + \varepsilon v_1(\tau) + \varepsilon^2 v_2(\tau) + O(\varepsilon^3) \tag{4.7}$$

In order to construct this perturbation, the time variable is first rescaled as:

$$\tau = \frac{\omega}{n\omega_0} t \tag{4.8}$$

Here, u_i and v_i are periodic functions of the rescaled time variable (τ) and ω_0 is the natural frequency of the system. By substituting this scheme into equations

4.3 and 4.4, each term defining the approximate periodic solution can be approximated in a recursive manner.

The frequency of the forcing term is initially assumed to be unknown, but close to a multiple of the natural frequency (ω_0). Hence, n is introduced to define the order of resonance so that the range of applicability of the solution can be extended to include different cases (i.e different orders of resonance). Then, using the chain rule, the equations become:

$$\omega^2 u'' + \omega_0^2 u + \varepsilon a_1 v + \varepsilon a_2 u^3 = \varepsilon F_1 \cos(\tau) \quad (4.9)$$

$$\omega^2 v'' + \omega_0^2 v + \varepsilon b_1 u + \varepsilon b_2 v^3 = \varepsilon M_1 \cos(\tau) + \varepsilon M_2 \sin(\tau) \quad (4.10)$$

where the prime indicates the derivative with respect to τ. The unknown frequency of the system now appears in the differential equations. Without loss of generality, we assume that the leading order frequency (ω_0) is unity (i.e it is the natural frequency of the system). The analytical solutions of the uncoupled and coupled system of equations obtained using the Poincare-Lindstedt perturbation method are presented in the next two sub-sections.

4.4.1 Uncoupled System

The approximate solution of the uncoupled equations is first discussed, that is the case where $a_1 = b_1 = 0$. The two equations can be solved independently by substituting 4.5, 4.6 and 4.7 into 4.9 and 4.10, and separating terms with the same order of the small parameter (ε) [119]. This leads to the following system of equations:

- Heave equation:

$$\varepsilon^0 : u_0'' + u_0 = 0 \quad (4.11)$$

$$\varepsilon^1 : \omega_0^2[u_1'' + u_1] + 2\omega_0\omega_1 u_0'' + a_2 u_0^3 = F_1 cos(\tau) \quad (4.12)$$

$$\varepsilon^2 : \omega_0^2[u_2'' + u_2] + 2\omega_0\omega_1 u_1'' + 2\omega_0\omega_2 u_0'' + \omega_1^2 u_0'' + 3a_2 u_0^2 u_1 = 0 \quad (4.13)$$

- Pitch equation:

$$\varepsilon^0: v_0'' + v_0 = 0 \tag{4.14}$$

$$\varepsilon^1: \omega_0^2[v_1'' + v_1] + 2\omega_0\omega_1 v_0'' + a_2 v_0^3 = M_1\cos(\tau) + M_2\sin(\tau) \tag{4.15}$$

$$\varepsilon^2: \omega_0^2[v_2'' + v_2] + 2\omega_0\omega_1 v_1'' + 2\omega_0\omega_2 v_0'' + \omega_1^2 v_0'' + 3a_2 v_0^2 v_1 = 0 \tag{4.16}$$

Solving equations 4.11, 4.12 and 4.13 gives the leading order, first order and second order solutions for the heave equation. Moreover, the first order and second order solutions of the heaving frequency can also be obtained. The solution obtained for the heave equation and heaving frequency of oscillations are as follows:

$$\begin{aligned} u\,(\mathrm{t}) &= \mathrm{A}\cos(\omega\mathrm{t}) + \varepsilon\frac{\mathrm{a}_2\mathrm{A}^3}{32\omega_0^2}\cos(3\omega t) \\ &+ \varepsilon^2\left[\frac{(36\mathrm{A}^2\mathrm{F}_1\mathrm{a}_2 - 21\mathrm{a}_2^2\mathrm{A}^5)\cos(3\omega\mathrm{t}) + \mathrm{a}_2^2\mathrm{A}^5\cos(5\omega\mathrm{t})}{1024\omega_0^4}\right] \end{aligned} \tag{4.17}$$

$$\begin{aligned} \omega\,(\text{Heave}) &= \omega_0 + \varepsilon\left[\frac{3\mathrm{a}_2\mathrm{A}^3 - 4\mathrm{F}_1}{8\mathrm{A}\omega_0}\right] \\ &+ \varepsilon^2\left[\frac{48\mathrm{A}^3\mathrm{a}_2\mathrm{F}_1 - 15\mathrm{A}^6\mathrm{a}_2^2 - 32\mathrm{F}_1^2}{256\omega_0^3\mathrm{A}^2}\right] \end{aligned} \tag{4.18}$$

Similarly, the leading order, first order and second order solutions of the pitch equation and its frequency can be obtained by solving equations 4.14, 4.15 and 4.16. The solutions obtained are as follows:

$$\begin{aligned} v\,(\mathrm{t}) &= \mathrm{A}\cos(\omega\mathrm{t}) \\ &+ \frac{AM_2}{M_1}\sin(\omega\mathrm{t}) \\ &+ \varepsilon\left[\frac{\mathrm{b}_2\mathrm{A}^3(M_1^2 - 3M_2^2)}{32\omega_0^2M_1^2}\cos(3\omega\mathrm{t}) + \frac{\mathrm{b}_2\mathrm{A}^3M_2(3M_1^2 - M_2^2)}{32\omega_0^2M_1^3}\sin(3\omega\mathrm{t})\right] \\ &+ \varepsilon^2\left[\frac{A^5b_2^2M_2(5M_1^4 - 10M_2^2M_1^2 + M_2^4)\sin(5\omega\mathrm{t})}{1024M_1^5\omega_0^4}\right. \\ &+ \frac{A^5b_2^2(M_1^4 - 10M_2^2M_1^2 + 5M_2^4)\cos(5\omega t)}{1024M_1^4\omega_0^4} \\ &+ \frac{3A^2b_2M_2(3M_1^2 - M_2^2)(-7A^3b_2M_1^2 - 7A^3b_2M_2^2 + 12M_1^3)\sin(3\omega t)}{1024M_1^5\omega_0^4} \\ &\left.+ \frac{3A^2b_2(M_1^2 - 3M_2^2)(-7A^3b_2M_1^2 - 7A^3b_2M_2^2 + 12M_1^3)\cos(3\omega t)}{1024M_1^4\omega_0^4}\right] \end{aligned} \tag{4.19}$$

$$\omega \text{ (Pitch)} = \omega_0 + \varepsilon\left[\frac{3M_1^2 b_2 \mathrm{A}^3 + 3b_2 A^3 M_2^2 - 4M_1^3}{8M_1^2 \mathrm{A}\omega_0}\right] + \varepsilon^2\left[\frac{-18\mathrm{A}^6 b_2^2 M_1^4 - 18\mathrm{A}^6 b_2^2 M_2^4 - 36A^6 b_2^2 M_1^2 M_2^2 + 48A^3 b_2 M_1^5 + 48A^3 b_2 M_1^3 M_2^2 - 32M_1^6}{256\mathrm{A}^2 M_1^4 \omega_0^3}\right] \quad (4.20)$$

These expressions are obtained by ensuring, at each order, that all terms entering the perturbation are periodic.

4.4.2 Coupled System

When a slender body floats on the free surface of water it will oscillate with a frequency equal to the natural frequency. This is known as the resonant case. However, due to incident waves, the oscillations will have strong effect on the coupling between heave and pitch motions. As a result, there is no guarantee that these two motions will take place independently. Therefore, a coupling term is considered in each equation. The process of obtaining the solution is similar to that adopted in section 4.4.1 but this time the two equations are solved simultaneously. The analytical solution of the coupled system is obtained up to the first order. Hence, the following system of equations is obtained after substituting equations 4.5, 4.6 and 4.7 into 4.9 and 4.10, and separating terms with the same order of the small parameter (ε) as follows:

- Heave equation:

$$\varepsilon^0: u_0'' + u_0 = 0 \quad (4.21)$$

$$\varepsilon^1: \omega_0^2[u_1'' + u_1] + 2\omega_0\omega_1 u_0'' + a_1 v_0 + a_2 u_0^3 = F_1\, cos(\tau) \quad (4.22)$$

- Pitch equation:

$$\varepsilon^0: v_0'' + v_0 = 0 \quad (4.23)$$

$$\varepsilon^1: \omega_0^2[v_1'' + v_1] + 2\omega_0\omega_1 v_0'' + b_1 u_0 + a_2 v_0^3 = M_1 \cos(\tau) + M_2 \sin(\tau) \quad (4.24)$$

In order to obtain a closed form solution to the system of equations, the leading order solutions of both equations are assumed to have the following forms:

$$u_0 = Acos(\tau) \tag{4.25}$$

$$v_0 = Bcos(\tau) + Csin(\tau) \tag{4.26}$$

The corrections to the linear solution are determined in the course of the analysis by requiring the expansion of u and v to be uniform for all τ. However, the particular solution of the first order terms of u and v contain secular terms which make the expansion non-uniform. In order to have uniform expansions, the secular terms in u_1 and v_1 have to be eliminated. To this end, the coefficients of the secular terms are set to zero in order to find expressions for the first order frequency (ω_1). By doing so, only inhomogeneous terms in equations 4.22 and 4.24 governing u_1 and $v_1$are to be inspected. This will result in the expansions being uniform for all first order solutions because secular terms do not appear in them. Removing all secular terms up to the first order requires that the following system of equations to be satisfied:

$$a_1 B - F_1 = 0 \tag{4.27}$$

$$3a_2 A^3 + 4a_1 C - 8A\omega_0\omega_1 = 0 \tag{4.28}$$

$$3b_2 B^3 + 3b_2 C^2 B - 8B\omega_0\omega_1 - 4M_1 = 0 \tag{4.29}$$

$$4Ab_1 + 3b_2 C^3 + 3b_2 B^2 C - 8C\omega_0\omega_1 - 4M_2 = 0 \tag{4.30}$$

The solution of this system can be expressed as:

$$B = \frac{F_1}{a_1} \tag{4.31}$$

$$C = \frac{F_1(M_2 - Ab_1)}{a_1 M_1} \tag{4.32}$$

$$\omega_1 = \frac{3a_2 A^3 M_1 - 4Ab_1 F_1 + 4F_1 M_2}{8AM_1\omega_0} \tag{4.33}$$

while A satisfies the following cubic polynomial:

$$3F_1(b_1^2 b_2 F_1^2 - a_1^2 a_2 M_1^2)A^3 - 6b_1 b_2 F_1^3 M_2 A^2 + (4a_1^2 b_1 F_1^2 M_1 - 4a_1^3 M_1^3 + 3b_2 F_1^3 M_1^2 + 3b_2 F_1^3 M_2^2)A - (4a_1^2 F_1^2 M_1 M_2) = 0 \quad (4.34)$$

The quantity A represents the amplitude of the external force which is the amplitude of the sea wave. The nonlinear coefficients a_2 and b_2 are found from the polynomial assuming in first approximation that both coefficients are equal. The other terms are found from the following equations:

$$a_1 = \frac{C_{35}}{m + A_{33}} \quad (4.35)$$

$$b_1 = \frac{C_{53}}{A_{55} + I_{55}} \quad (4.36)$$

$$F_1 = \frac{F_a}{m + A_{33}} \quad (4.37)$$

$$M_1 = \frac{M_a}{A_{55} + I_{55}} \quad (4.38)$$

$$M_2 = \frac{M_b}{A_{55} + I_{55}} \quad (4.39)$$

$$\omega_0 = \sqrt{\frac{C_{33}}{m + A_{33}}} = \sqrt{\frac{C_{55}}{I_{55} + A_{55}}} \quad (4.40)$$

where the terms of the equations are found from the strip theory. Equations 4.22 and 4.24 then become:

$$u_1'' + u_1 = \frac{a_2 A^3}{4\omega_0^2} \sin(3\tau) \quad (4.41)$$

$$v_1'' + v_1 = -\frac{b_2 F_1^3 (6Ab_1 M_2 - 3A^2 b_1^2 + M_1^2 - 3M_2^2)}{4a_1^3 M_1^2 \omega_0^2} \cos(3\tau) - \frac{b_2 F_1^3 (M_2 - Ab_1)(2Ab_1 M_2 - A^2 b_1^2 + 3M_1^2 - M_2^2)}{4a_1^3 M_1^3 \omega_0^2} \sin(3\tau) \quad (4.42)$$

Without loss of generality, the analytical solutions obtained for the coupled heave and pitch motions as well as the frequency of oscillations are as follows:

$$u\,(\mathrm{t}) = \mathrm{A}\sin(\omega\mathrm{t}) - \varepsilon\left[\frac{a_2A^3}{32\omega_0^2}\cos(3\omega t)\right] \tag{4.43}$$

$$\begin{aligned} v\,(t) &= \frac{F_1}{a_1}\cos(\omega t) + \frac{F_1(M_2 - Ab_1)}{a_1M_1}\sin(\omega t) \\ &+ \varepsilon\left[\frac{b_2F_1^3(Ab_1 - M_2)(M_2^2 - 2Ab_1M_2 + A^2b_1^2 - 3M_1^2)}{32a_1^3M_1^3\omega_0^2}\sin(3\omega t)\right. \\ &\left. - \frac{b_2F_1^3(3M_2^2 - 6Ab_1M_2 + 3A^2b_1^2 - M_1^2)}{32a_1^3M_1^2\omega_0^2}\cos\,(3\omega t)\right] \end{aligned} \tag{4.44}$$

$$\omega = \omega_0 + \varepsilon\left[\frac{3a_2A^3M_1 - 4Ab_1F_1 + 4F_1M_2}{8AM_1\omega_0}\right] \tag{4.45}$$

CHAPTER 5

5. CFD SIMULATION OF MOTION

5.1 Introduction

Computational fluid dynamics (CFD) is a comprehensive field covering a broad range of fluid dynamics problems. It provides an effective means of simulating real fluid flows by the numerical solution of governing equations [127]. It can be defined as the science that produces quantitative predictions of fluid flow phenomena based on the conservation laws (conservation of mass, momentum and energy) with the help of digital computers as illustrated in Figure 52 [128]. The predictions obtained through CFD normally occur under the conditions defining the flow geometry, the physical properties of the fluid and the boundary conditions of the flow field. Generally, those predictions include a set of values of flow variables such as velocity, pressure or temperature at chosen locations in the domain. The hydrodynamic forces acting on an object and the consequent motions may also be predicted using CFD. Therefore, CFD is used in a wide range of research and engineering applications in many fields of study and industries such as aerodynamics, aerospace, weather simulation, hydrodynamics, environmental engineering and engine combustion analysis. It is often used alongside experimental or analytical results in automotive and aerospace research [127]. During the past three decades, several other numerical methods are developed to simulate fluid flow like finite difference, finite element, finite volume and spectral methods [128].

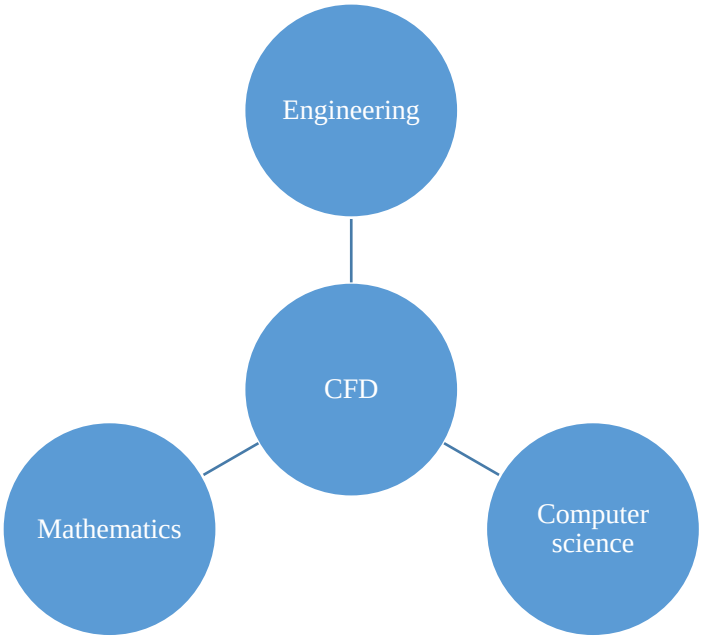

Figure 52. The different disciplines contained within CFD

Recently, CFD has gained a lot of importance and significantly enhanced in terms of accuracy and computational time. However, due to many potential sources of errors involved, such as incorrectly defined boundary conditions, inaccurate input data and irrelevant modelling, the predictions are never completely exact [128]. Nevertheless, assumptions and approximations are also required during the production of CFD models. Therefore, in order to correctly perform CFD simulations, it is very important to understand the limitations and the applicability range of the CFD tools.

As a research tool, CFD is used as a validation or verification method to experimental or theoretical fluid dynamics (see Figure 53). Validation is the comparison between numerical predictions and actual physical flow data from a wind tunnel [129, 130]. Verification, on the other hand, is the term used in reference to the establishment of the level of agreement between numerical predictions and the specific mathematical model [130, 131]. This is because CFD has a large number of advantages such as:

- Results can be produced inexpensively without the need for extraordinary amount of training. However, interpreting the results often requires experience.
- It permits input parameters to be changed. Hence, validating design optimisation. These changes are usually prohibitively expensive or time consuming in experimental investigations [132].
- It has the ability to simulate realistic and unrealistic conditions. Unlike experiments, CFD can simulate fluid flow directly under practical conditions. For instance, CFD allows unwanted events to be investigated such as nuclear power plant failure [128]. However, large scale models may be impractical to investigate experimentally.

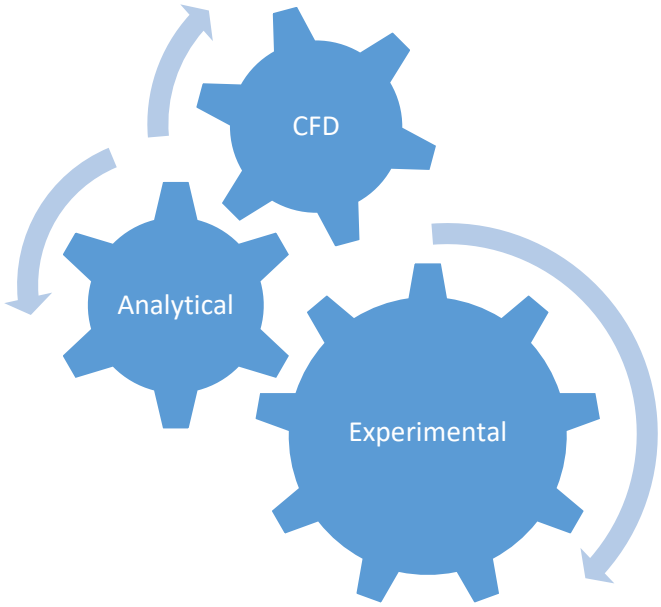

Figure 53. The three methods used to study fluid dynamics

However, the accuracy of the CFD results is limited by numerical errors which are inherent to digital computation such as:

- Round-off error: this is due to finite word size available on the computer [133].

- Truncation error: this is due to approximations in the numerical models. Mesh refinement may reduce the truncation error [134].

Further information about CFD can be found in [135, 136, 137]. In this research, the analytical results are verified with Ansys Fluent CFD simulation results [138, 139]. In addition, the results are verified with results obtained from Ansys AQWA [140].

5.2 Fluent Simulation of Motion of 2D Hulls

5.2.1 Introduction

Ansys Fluent is a computational fluid dynamics software package that is written in the C language. It contains the broad, physical modelling capabilities needed to model flow, turbulence, heat transfer and reactions for industrial applications [138]. This software is used because it has the following advantages:

- It has the ability to simulate 2D planar flows, axisymmetric flows and 3D flows which allows the researcher to further extend the research.
- It has the ability to simulate multiphase flows, which is exactly the case of this research.
- It offers a highly scalable, high performance computing to help solve complex computational fluid dynamics problems quickly and cost-effectively [138].
- It is widely used for academic and also commercial purposes [139].

The process of performing simulations on Ansys Fluent is described in the following Figure:

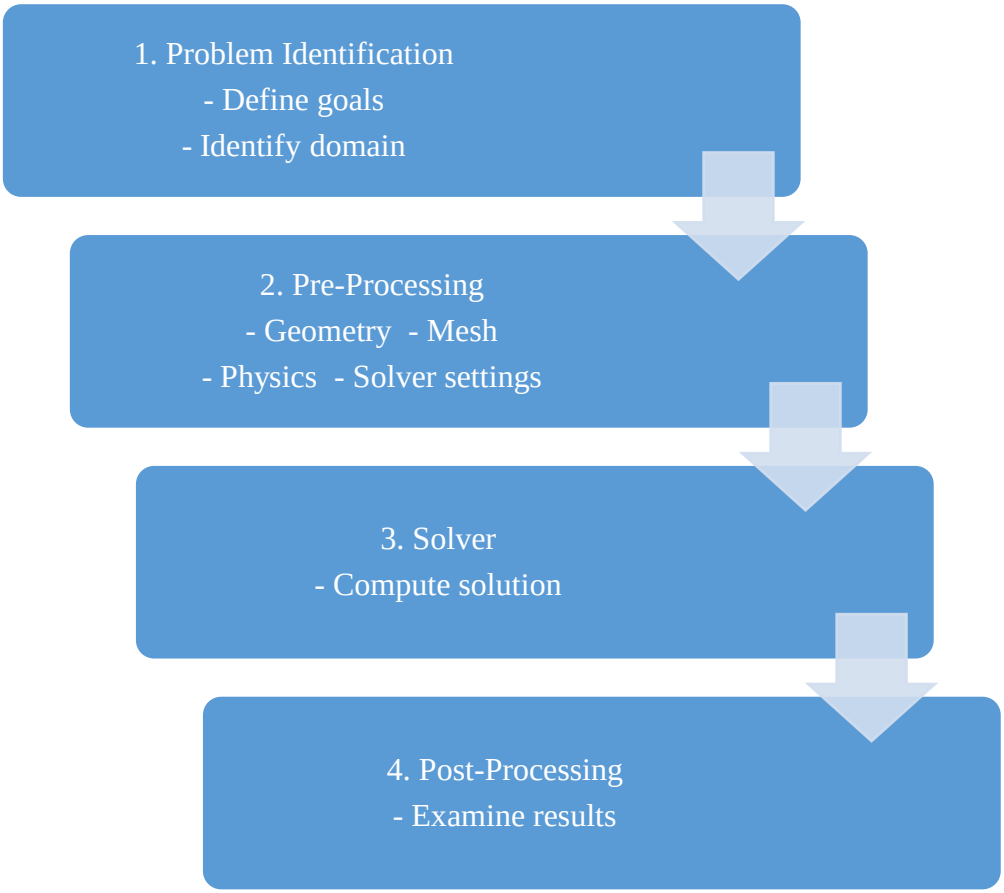

Figure 54. Process of performing simulations on Fluent

5.2.2 Governing Equations

The CFD solver used is Ansys Fluent R19.2 which is based on the incompressible unsteady Reynolds Averaged Navier-Stokes equations (RANSE) [141]. This solver decomposes the solution variables of the exact Navier-Stokes equations into the mean (time-averaged) and fluctuating components. Hence, the velocity components are:

$$u_i = \bar{u}_i + u_i' \tag{5.1}$$

where $\bar{u}_i$ and u_i' are the mean and fluctuating velocity components in the direction of the Cartesian coordinate x_i. Likewise, the expression used to calculate the pressure and other scalar quantities is the following:

$$\varphi_i = \bar{\varphi} + \varphi' \tag{5.2}$$

where φ refers to a scalar quantity such as pressure or energy. By substituting equations 5.1 and 5.2 for the flow variables in the instantaneous continuity and momentum equations and taking a time derivative, the RANSE will have a Cartesian tensor form as follows:

$$\frac{\partial \rho}{\partial t} + \frac{\partial}{\partial x_i}(\rho u_i) = 0 \tag{5.3}$$

$$\frac{\partial}{\partial t}(\rho u_i) + \frac{\partial}{\partial x_j}(\rho u_i u_j) = \frac{\partial p}{\partial x_i} + \frac{\partial}{\partial x_j}\left[\mu\left(\frac{\partial u_i}{\partial x_j} + \frac{\partial u_j}{\partial x_i} - \frac{2}{3}\delta_{ij}\frac{\partial u_l}{\partial u_l}\right)\right] + \frac{\partial}{\partial x_j}(-\rho\overline{u_i' u_j'}) \tag{5.4}$$

Equations 5.3 and 5.4 are the RANSE continuity and momentum equations respectively. In the two equations, ρ is the density of fluid, p is the mean pressure and μ is the dynamic viscosity. The final term in equation 5.4 represents the Reynolds stress tensor. It is a three symmetrical tensor representing six unknowns which must be solved so that turbulence effect can be modelled. This is done by using the Boussinesq approach in Fluent which assumes that these unknowns can be linked to the mean velocities of the fluid through turbulence viscosity which is the constant μ_t [142]. Thus, the Reynolds stress can be related to the mean velocity gradient as follows:

$$-\rho\overline{u_i' u_j'} = \mu_t\left(\frac{\partial u_i}{\partial x_j} + \frac{\partial u_j}{\partial x_i}\right) - \frac{2}{3}\left(\rho k + \mu_t\frac{\partial u_i}{\partial x_i}\right)\delta_{ij} \tag{5.5}$$

where k is the turbulence kinetic energy.

5.2.3 The Viscous Model

The turbulence model used is the two-equation k – ω SST model. This model includes two additional transport equations to represent turbulent properties of flow

in order to account for history effects like convection and diffusion of turbulent energy. The transport variable k determines the energy in turbulence while ω determines the scale of turbulence. It is widely used to simulate aerodynamic flow for aeronautical applications and known for its ability to handle a variety of turbulent flows such as the rapid length scale changes [143]. This turbulent model was developed by Menter in 1992 and is an extension to the standard k- ω model. It is a hybrid model combining the standard k-ω and the k-ε models such that the k-ω is used in the inner region of the boundary layer close to the wall and k-ε in the freestream flow [144]. It accounts for the transport of the turbulent shear stress and offers improved prediction of flow separation. In addition, the SST model exhibit less sensitivity to freestream conditions away from the boundary layer. The two transport equations used in this model are as follows:

$$\frac{\partial \rho k}{\partial t} + u_i \frac{\partial \rho k}{\partial x_j} = P - \beta^* \rho \omega k + \frac{\partial}{\partial x_j}\left[(\mu + \sigma_k \mu_t)\frac{\partial k}{\partial x_j}\right] \tag{5.6}$$

$$\frac{\partial \rho \omega}{\partial t} + u_j \frac{\partial \rho \omega}{\partial x_j} = \frac{\gamma}{v_t} P - \beta \rho \omega^2 + \frac{\partial}{\partial x_j}\left[(\mu + \sigma_\omega \mu_t)\frac{\partial \omega}{\partial x_j}\right] + 2(1 - F_1)\frac{\rho \sigma_{\omega^2}}{\omega}\frac{\partial k}{\partial x_j}\frac{\partial \omega}{\partial x_j} \tag{5.7}$$

5.2.4 The Computational Domain

5.2.4.1 Geometry

The two geometries used in this research are the 2D hulls presented in [6] and [95] which will be later referred to as model 1 and model 2 respectively. The computational geometry is created using Ansys Designmodeler. As the aim is to investigate the dynamic stability in take-off and landing, only the hull of the seaplane is considered in the simulations. During take-off and landing, hydrodynamic stability prediction is of great importance in the design of seaplanes as it provides information about the water drag resistance and porpoising [20]. The geometry of the 2D simulations performed is shown in Figure 55. The computational domain is divided into three zones; moving zone, re-meshing zone and stationary zone. This is because the area around the hull of the seaplane has to

oscillate in accordance to the structural response the hull to the sea waves. The re-meshing zone does not oscillate but the mesh in this zone responds to the motion of the moving zone and constantly re-construct the elements of the mesh. This is done to reduce the computational time as only the re-meshing and moving zones have high-definition mesh.

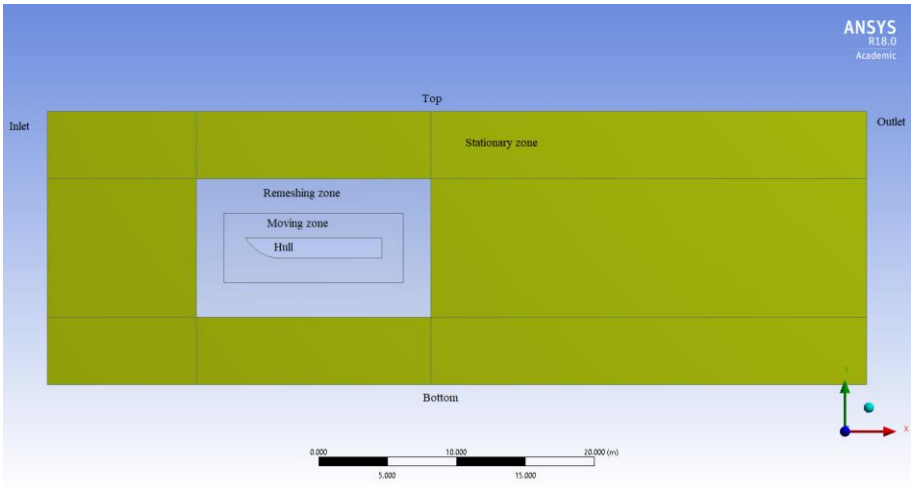

Figure 55. Geometry used

The distance from the free surface (sea water level) to the top of the domain is assumed to be equal to the hull length. The depth of the domain is also equal to the hull length. Moreover, the distance from the centre of gravity of the hull to the outlet is assumed to be 4 times the length of the hull. Nevertheless, the distance from the CG of the hull to the inlet is twice the length of the hull. This agrees with the International Towing Tank Conference (ITTC) practical guidelines for ship CFD applications [140]. The body-fixed reference frame axes are chosen to coincide with the principal axes of inertia and the origin is taken coincident with the centre of gravity of the hull.

5.2.4.2 Mesh

In order to solve the governing equations of fluid flow, the fluid domain has to be discretized into geometrically simple elements of cells. This process in known as meshing and it plays a significant role in CFD as the accuracy of the solution is in direct relation to size and shape of the mesh elements [127]. Generally, meshes

can be generated in a wide range of forms, but they are usually identified as being structured or unstructured. As the name suggest, structured meshes require a systematic scheme of elements. This type is the most common in CFD applications as it recues the computer memory requirements and hence reduces computer processing time. However, the main disadvantage of structured mesh is that it can be difficult to create and hence it cannot be used to simulate complex geometries [61]. On the other hand, unstructured mesh is complex process of segmenting a CFD domain into regions. The elements of this mesh type are not ordered in any regular fashion. The computation time of this mesh type is very high compared to the structured mesh. However, this type can be used to model complex geometries [61].

Ansys Meshing has been used to produce the mesh which can be generated after creating the geometry on Designmodeler. In this case, any update to the geometry in Designmodeler is automatically applied to mesh. The mesh generated is a hybrid mesh that combines structured (hexahedral) elements in the stationary zone and unstructured (tetrahedral) elements in the re-meshing and moving zones. This is done to reduce the computation time as the stationary zone does not necessitate any need for a high-definition mesh as it is just a freestream region. The mesh generated is shown in Figure 56 which shows the hexahedral mesh zone (structured mesh generated for the freestream). The tetrahedral mesh is shown in Figure 57. Edge sizing has been introduced to the edges of the re-meshing and moving zones for mesh refinement.

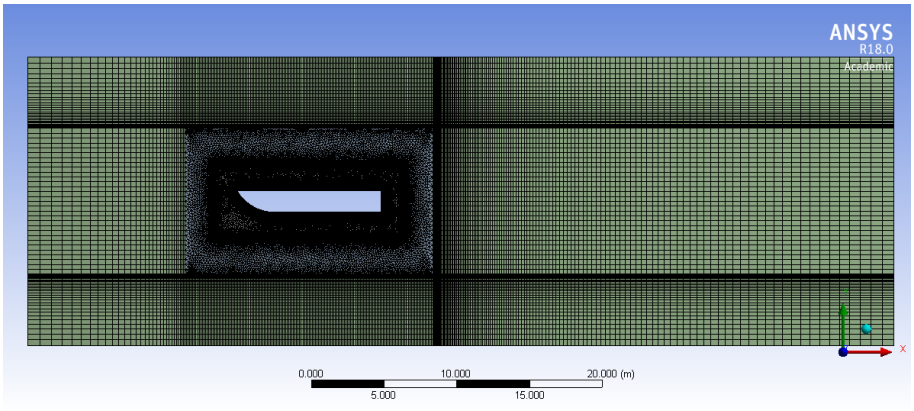

Figure 56. Mesh generated

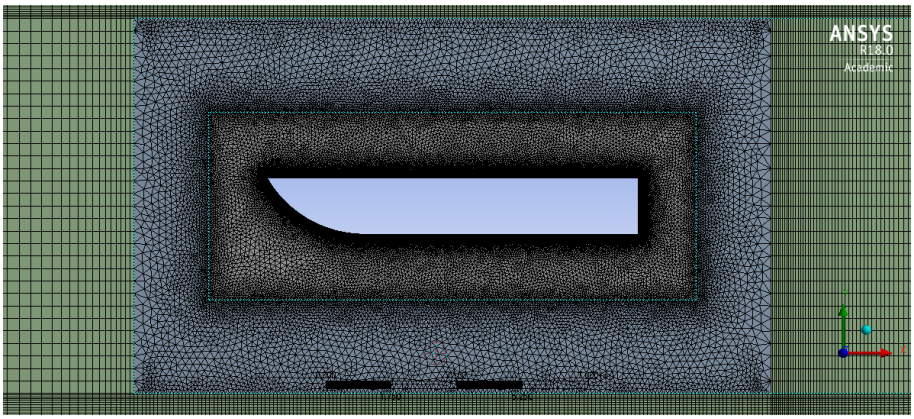

Figure 57. Tetrahedral mesh zone

5.2.4.3 Mesh Sensitivity Study

Mesh sensitivity is defined as the influence of the size of the mesh on the results obtained from CFD [146]. Therefore, in order to obtain accurate CFD results, it is very important to conduct a grid independence study. The grid is measured from its density, which can be presented in form of the total number of elements of the mesh, or in form of the size of the elements around the boundary layer. The higher the density of the mesh, the larger the number of mesh elements. This means that the density increases with the decrease of each element size around the boundary layer. Since each grid point represents a point at which the flow will be calculated, the density is taken as a measure of the accuracy of the CFD results [130, 146]. Hence, the density of the mesh should be high enough to capture all the

features of the fluid flow. However, the effect of computational errors and the associated cost in time necessitates the use of as few mesh elements as possible. Therefore, it is significant to specify the grid areas where the flow is very important such as the leading edge, boundary layer and wake region, and the less important areas of flow such as the freestream. In this research, a mesh sensitivity study is conducted to establish the accuracy of the CFD solution, to ensure grid independence and to keep the computational time as low as possible. The influence of mesh density is defined through examining the effect of the size of the edge of the hull (see Figure 58). This edge represents the location of the boundary layer and the region of wakes where the characteristics of fluid flow is of great importance.

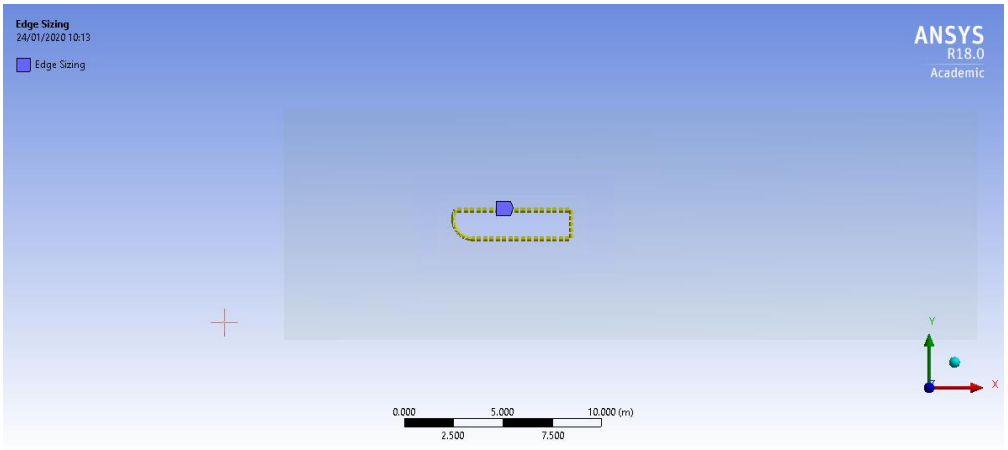

Figure 58. Edge of the hull

The size of the mesh elements around this edge plays a significant role in CFD simulation. Any change in the edge size will have a significant effect on the number of elements of the mesh. The elements developed at the boundary layer are shown in Figure 59.

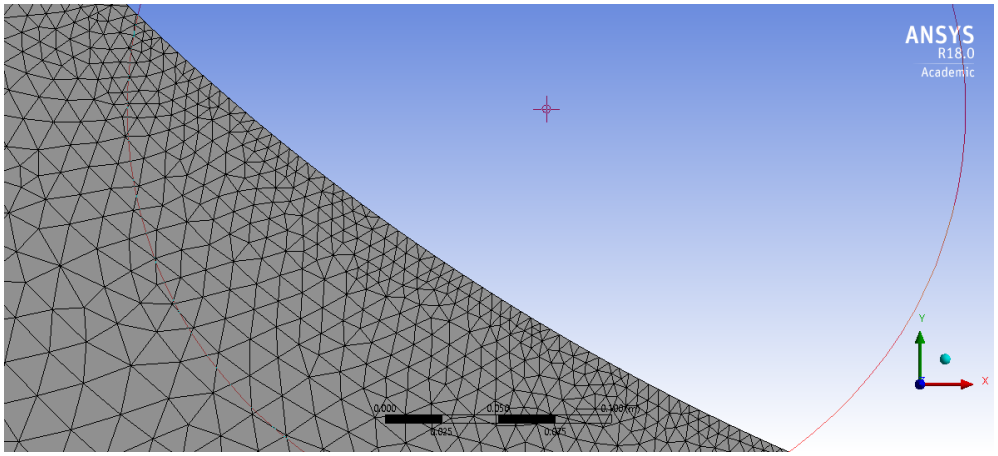

Figure 59. Elements at the location of the boundary layer

Mesh density was evaluated for 7 different boundary layer edge sizes and plotted against the coefficient of drag of the hull as shown in Figure 60. Each edge size produces a total number of mesh elements. Predictions of the coefficient of drag of the seaplane hull were very sensitive to the change of mesh density. For example, for a hull edge size of 0.02 m, the coefficient of drag was predicted to be 1.41 (see Figure 60). However, it is significantly changed when the edge size is reduced. The number of mesh elements that corresponds to each edge size examined along with the computation time needed to obtain the results are highlighted in Table 3. The optimum edge size of the hull was found to be 0.0025 m. This is the point where the solution starts to converge in which the difference in the coefficient of drag produced by any smaller size is negligible. Also, this edge size produces around 165,000 mesh elements which can be simulated using a high specification PC in an acceptable time.

It should be mentioned that the coefficient of drag is chosen to study the mesh sensitivity because in the case of seaplane motion, the boundary layer will be developed around the hull from the bottom (water side) and from the top (air side). If the coefficient of lift is chosen as the criterion to study the influence of mesh density, only the boundary layer developed at the bottom of the hull will be considered which will reduce the effect of mesh density on the results.

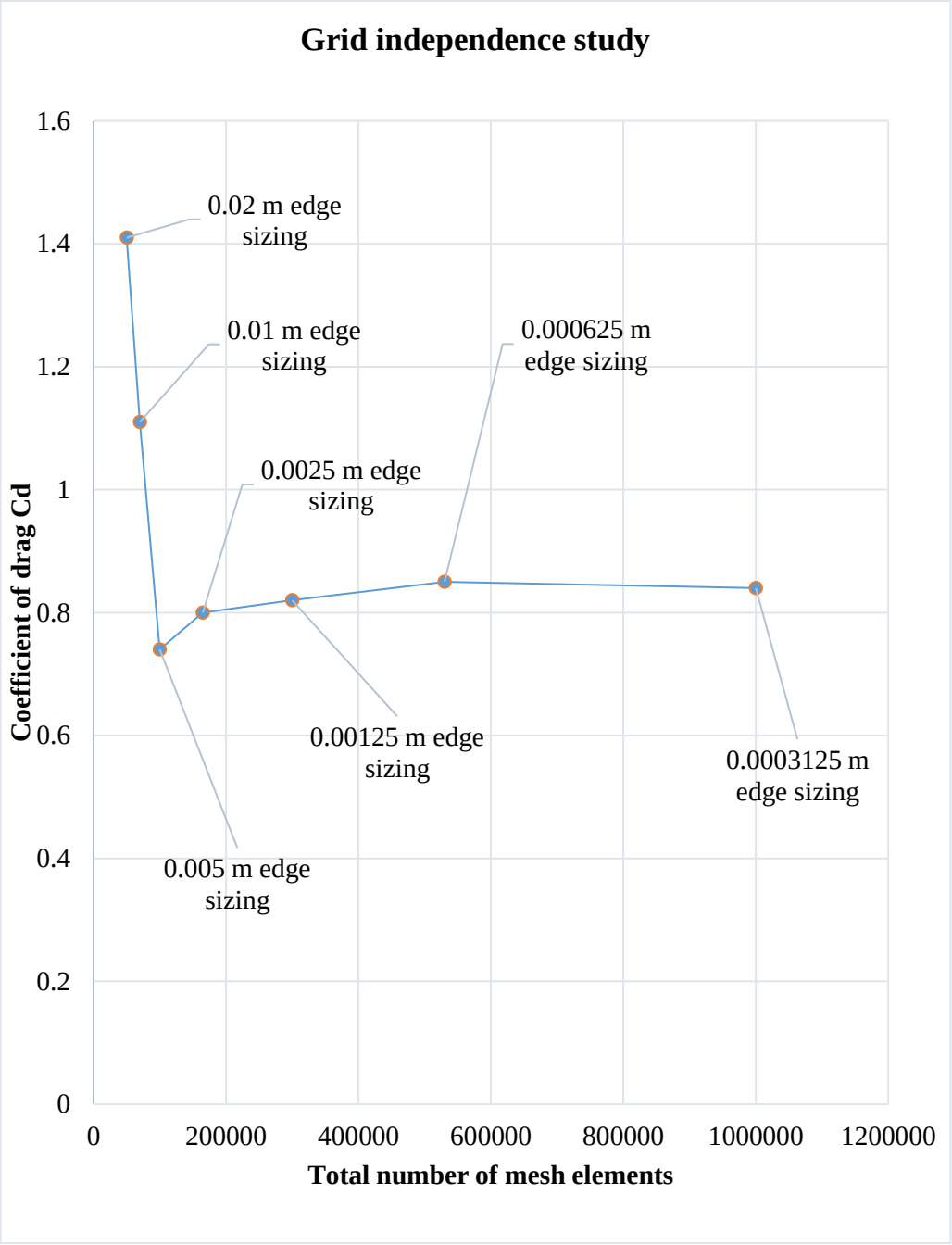

Figure 60. Grid independence graph

Table 3. Grid independence data

Boundary layer edge size (m)	Number of mesh elements	Computation time (hours)
0.0003125	1M	~480
0.000625	530K	~360
0.00125	300K	~240
0.0025	165K	160
0.005	100K	70
0.01	70K	40
0.02	50K	15

5.2.5 The Boundary Conditions

The boundary conditions applied in this CFD investigations are illustrated below. The location of each boundary is shown in Figure 55:

- Inlet: velocity-inlet type is selected at the inlet. Open channel wave BC is enabled so that wave details and location of free surface can be defined.
- Outlet: pressure-outlet is selected for this boundary. Open channel is enabled to define the bottom level of the computational domain that is filled with water.
- Top: pressure-outlet is selected at the top. This is to let air flow freely in the zone above the hull so that no pressure is created in the air region. The phase in this boundary should only be defined as air (volume fraction should be given a value of zero).

- Bottom: pressure-outlet is selected here. The phase in this boundary should only be defined as water (volume fraction should be given a value of one). This is to let water flow underneath the hull freely so that no pressure is developed.

5.2.6 The Numerical Model

5.2.6.1 Multiphase Flow

Volume of fluid (VOF) is selected in the multiphase flow tab under models. This is to define the computational domain as a two-phase flow domain with air as the primary fluid and water as the secondary fluid (see Figure 61). VOF is a surface-tracking technique designed for two or more immiscible fluids where the position of the interface between the fluids is of interest. In the VOF model, a single set of momentum equations is shared by the fluids, and the volume fraction of each of the fluids in each computational cell is tracked throughout the domain. It is widely used to model the flow of ships and seaplanes [147]. Open channel flow and open channel wave BC should be enabled in order to define the head-sea wave. Numerical beach should be enabled in the stationary zone to account for wave damping at the outlet.

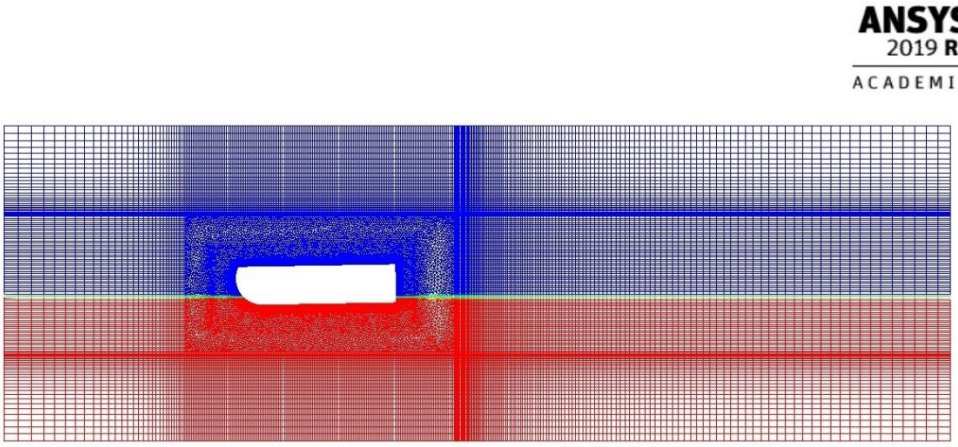

Figure 61. Numerical domain

5.2.6.2 Dynamic Mesh Setup

Dynamic mesh is used in this research. This is to allow the hull to respond to sea waves in form of motions in only two degrees-of-freedom. The motion is restricted by the use of a user defined function (UDF) [148]. The UDF generated is presented in Appendix B. The UDF is used to record the heave and pitch motions, define the mass and mass moment of inertia of the hull [145]. Smoothing and re-meshing are enabled to allow the mesh to reconstruct the moving cells. Ansys Fluent six DOF solver computes external forces and moments such as aerodynamic and gravitational forces and moments [148]. However, Additional information about the dynamic zones are needed. Therefore, the following are defined:

- Hull: it is defined as a rigid body so that forces on it can be calculated and hence, motions of its centre of gravity are recorded.
- Moving zone: it is also defined as a rigid body but with passive option enabled so that the zone moves with the hull without calculating the forces on it.
- Re-meshing zone: this is defined as a deforming zone as the tetrahedral cells in this zone are re-constructed subject to the motion of the hull.
- Stationary zone: as its name suggests, this is defined as a stationary zone.

5.2.6.3 Choice of the Time Step

The Courant number (CFL) is used to define the simulation time step. It is defined as the ratio of time step (Δt) to the mesh convection time scale [149]. It is used to relate the mesh minimum cell dimension (Δx) to the mesh flow velocity (U) as given in the following equation:

$$CFL = \frac{U\Delta t}{\Delta x} \tag{5.8}$$

As moving mesh characteristics are used in this research, this quantity is considered to have a value of 1 for numerical stability [150]. Moreover, as implicit simulation method is used, which require more computational effort in each solution step, this will allow the use of larger time step without sacrificing accuracy.

5.2.6.4 The Discretization Methods

The phasic momentum equations, the shared pressure, and the phasic volume fraction equations are highly coupled in multiphase flow. Hence, these equations are solved in a segregated fashion using some variation of the SIMPLE algorithm to couple the shared pressure with the momentum equations. This is attained by effectively transforming the total continuity into a shared pressure [151]. In this research, the space discretization method implemented is Ansys Fluent Phase Coupled SIMPLE algorithm which solves a wide range of multiphase flows [148].

In regards to time discretization, first-order implicit discretization method is usually used to accurately model most multiphase flow. This is because the explicit formulation is used to capture the transient behaviour of moving waves, such as shocks. Moreover, because the time step is chosen based on the speed of the hull and the size of the mesh, which results in a time step that ranges between 0.0002 to 0.04, the first-order scheme is found to be sufficient [151].

5.3 AQWA Simulation of Motion

The mathematical model is also verified using Ansys AQWA [152]. This is an engineering analysis suite of tools that can be used to investigate the effect of wave, wind and current on floating objects and fixed offshore and marine structures. AQWA is a comprehensive tool that can solve several hydrodynamic problems such as the determination of free height of floating bodies, the calculation of body membrane effects of fixed and floating platforms in marine environment, the calculation of forces on floating structures and the discharge of boat from main ship [152]. Nevertheless, dynamic analysis and structural response of ships and seaplanes moving through sea waves can be performed using AQWA Hydrodynamic Diffraction tool. The results obtained from this tool are suitable for stationary or low speed applications as this software generates pressure and inertial loading for use in a structural analysis as part of the vessel hull design process. Slow drift effects and extreme wave conditions may also be investigated. The results are presented in form of time-series data such as motion history over time using AQWA

Hydrodynamic Response tool [152]. The process of performing AQWA simulations is illustrated in Figure 62.

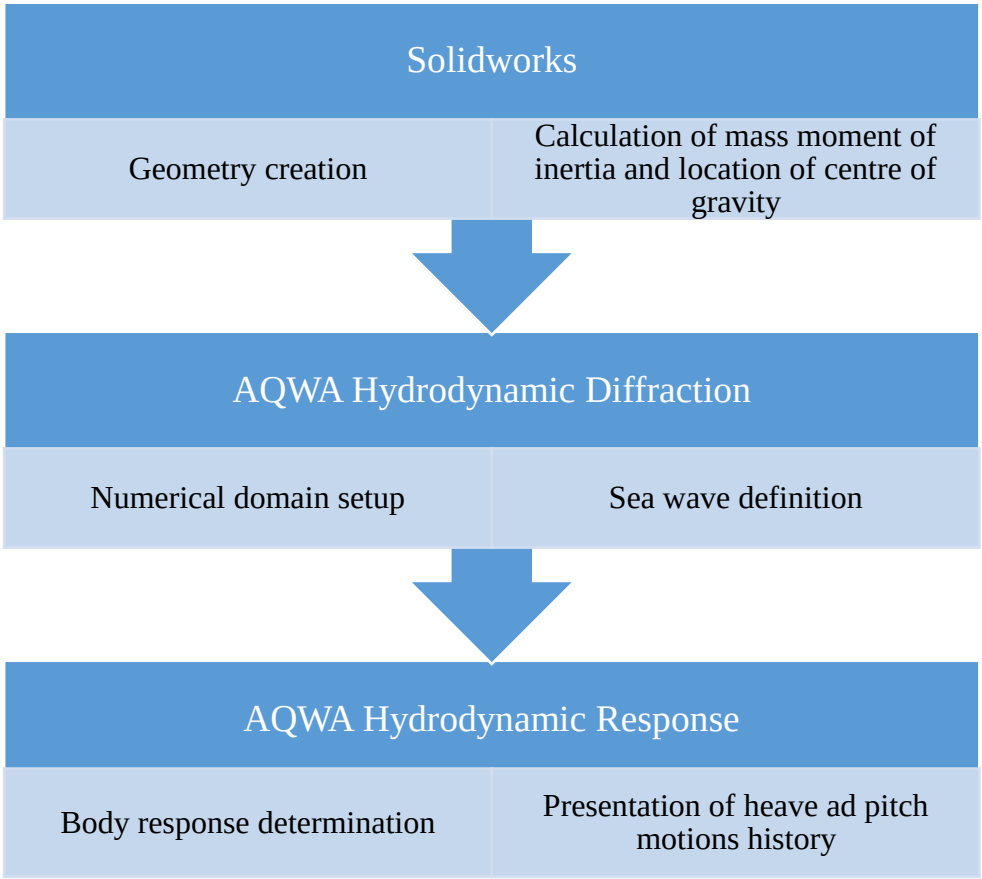

Figure 62. Process of simulation in AQWA

5.3.1 Geometry

The hull geometry used in this research is shown in Figure 63. It is the hull used in [153] to numerically investigate the hydrodynamic drag associated with motion through head sea waves. The centre of gravity (CG) of the hull is assumed to coincide with the centre of mass and centre of rotation.

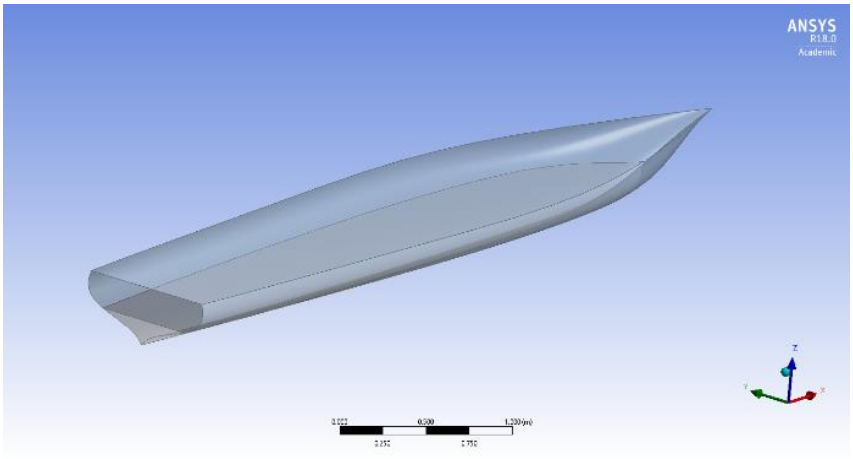

Figure 63. Hull used in AQWA

5.3.2 Numerical Setup

In AQWA Hydrodynamic Diffraction, an integrated domain is provided to apply the analysis of complex motion and response of structures. Hydrodynamic conditions such as sea water depth, water density, wave frequency of oscillations, wave amplitude, incident wave height, wave velocity, centre of mass and mass moment of inertia are defined. In addition, meshing to the structure of the object and marine environment are automatically applied. This means that there is no user control on meshing which means that no mesh sensitivity study is required. Nevertheless, boundary conditions such as kinematics and dynamics of the oscillating body and seabed conditions are automatically defined in AQWA. These properties of AQWA reduce the computational time significantly. The domain created in this research is shown in Figure 64. The wave is assumed to be a single wave with direction opposite to the direction of motion (i.e. head sea wave).

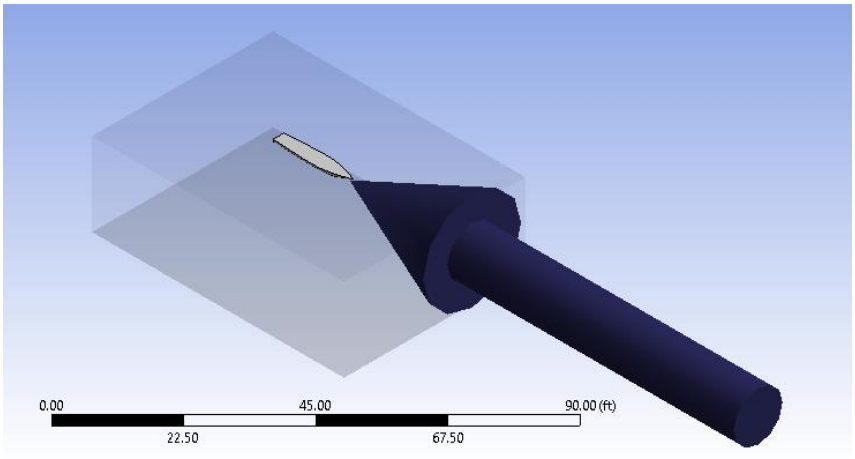

Figure 64. Numerical domain and wave direction

The seaplane is assumed to be driven by a pattern of regular Stokes' second order waves that have the linear form presented in Figure 65 [154].

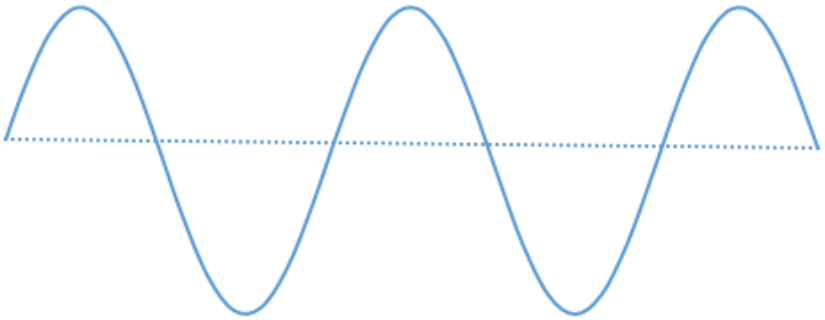

Figure 65. Stokes' linear second order regular wave form

The Stokes' second order linear wave can be expressed in the following form [155]:

$$n(x,t) = \text{acos}(\omega t - kx) + ka^2 \frac{\cosh(kd)}{4sinh^3(kd)}[2 + \cosh(2kd)][\cos[2(\omega t - kx)] \quad (5.9)$$

where a, k, ω, x and d stand for wave amplitude, wave number, wave frequency, wave phase and water depth respectively. The first term on the right-hand side of the aforementioned equation is the Airy wave of the linear wave theory and the

second term is the second-order Stokes' correction [155]. The amplitude of motion in this theory is assumed to be constant and the phase speeds are assumed to be equal. This implies that the surface profile does not evolve time or space (which means it is constant). No time or space discretization is then needed [155].

The wave is defined by its length, amplitude and frequency of oscillations. The length of the wave is assumed to be equal to the length of the hull. It is worth mentioning that the depth of the numerical domain is assumed to be equal to wavelength. In addition, the centre of gravity of the hull is assumed to be at a distance equal to twice the wavelength from the inlet and outlet.

CHAPTER 6

6. RESULTS AND DISCUSSION

6.1 Introduction

In this chapter, the results obtained from the nonlinear analytical solutions of the coupled and uncoupled equations of heave and pitch are presented. First of all, the analytical solution of the coupled equations is compared to the CFD results obtained from Ansys Fluent. Secondly, the analytical results are compared to simulation results obtained from Ansys AQWA. After that, the effect of nonlinearity and coupling on frequency of oscillations and amplitude of motion is examined. Finally, the analytical solution to the nonlinear equations is used to extend the analytical method of Savitsky to predict the porpoising stability limit of planing hulls.

6.2 Verification with Fluent

The heave and pitch history of motion is predicted for two different seaplane hulls analytically and using Fluent. As mentioned earlier, the two hulls used are the 2D hulls presented in [6] and [95]. In this section, the hulls are referred to as model 1 and model 2 respectively. The geometrical properties of the two hull models used in this research along with the wave characteristics are listed in Table 4. The centre of gravity (CG) of the hulls is assumed to coincide with the centre of mass and centre of rotation and it is defined using Solidworks. In addition, the wavelength is assumed to be equal to the hull length.

Table 4. The geometrical characteristics of the hull models and the wave amplitude used

Parameter	Model 1		Model 2	
	In SI units	In Imperial units	In SI units	In Imperial units
Overall length L_{oa}	5.850 m	19.200 ft	1.524 m	5.000 ft
Beam length	0.800 m	2.592 ft	0.203 m	0.666 ft
Draft	0.350 m	1.144 ft	0.025 m	0.081 ft
Mass	1296.000 kg	2837.760 lb	15.050 kg	33.200 lb
Radius of gyration	1.400 m	4.588 ft	0.381 m	1.250 ft
Moment of Inertia	3455.070 $kg.m^2$	1780.200 $lb.sec^2.ft$	2.790 $kg.m^2$	1.611 $lb.sec^2.ft$
Wave amplitude	0.060 m	0.200 ft	0.030 m	0.100 ft

Both models are assumed to have prismatic, axisymmetric two-dimensional hulls. This means that the results only depend on the weight, length, wave amplitude and speed of motion. The other geometrical characteristics such as the chine, dead-rise angle and beam length are not considered. This decreases the geometrical constraints of the research and allows for the application of the strip theory. The extension of the research to study the three-dimensional motion of seaplanes necessitates the inclusion of all geometrical characteristics of the hull because in 3D, the drag and lift are generated from every part of the fuselage of the seaplane.

The strip theory can now be applied so that the coefficients of the heave and pitch equations can be determined. In order to study the stability in take-off and landing, investigations have been carried out on two Froude numbers (F_n); 0.1 and 0.2. According to [24], this is the take-off or landing regime where the hull is supported by hydrodynamic forces. As discussed in chapter 2, this is the regime of max hydrodynamic resistance where porpoising prediction becomes of great importance. By following the steps of the strip theory method explained previously

in section 3.5, the values of the coefficients of the heave and pitch equations of the two models are found (see Table 5). An excel sheet is created to calculate the coefficients of the general equations of heave and pitch (equations 3.7 and 3.8).

Table 5. Results of the strip theory for the two models

Coefficient	Model 1		Model 2	
	$F_n = 0.1$	$F_n = 0.2$	$F_n = 0.1$	$F_n = 0.2$
A_{33} (lb.sec^2/ft)	75.600	75.600	0.939	0.939
A_{55} (lb.sec^2.ft)	1368.500	1368.500	1.399	1.399
C_{33} (lb/ft)	2588.500	2588.500	160.200	160.200
C_{35} (lb)	1115.000	1753.200	-7.500	-8.000
C_{53} (lb)	1242.500	1242.500	5.200	5.200
C_{55} (lb.ft/rad)	49610.068	49501.600	226.600	226.100
F_a (lb)	7.866	9.906	0.540	0.680
M_a (lb.ft)	355.217	372.600	3.135	3.270
M_b (lb.ft)	-222.642	-231.790	2.200	2.270

The coefficients of heave and pitch equations (equations 4.3 and 4.4) can now be calculated using equations 4.35 – 4.40. A Visual Basic code is created to perform the calculations. The code is presented in Appendix C. The values obtained for the coefficients of equations 4.3 and 4.4 are listed in Table 6.

Table 6. Values obtained for the coefficients of heave and pitch equations

Coefficient	Model 1		Model 2	
	$F_n = 0.1$	$F_n = 0.2$	$F_n = 0.1$	$F_n = 0.2$
a_1	6.811	10.664	-3.805	-4.059
b_1	0.394	0.394	1.727	1.727
ω_0	3.976	4.110	9.015	9.517
F_1	0.048	0.060	0.273	0.345
M_1	0.112	0.118	0.996	1.086
M_2	-0.070	-0.073	0.664	0.754

The non-dimensional parameter (ε) in the coupled system is assumed to have a value of 0.01 in all cases. This is to have the nonlinearity, coupling and external excitation force/moment in the same strength. Not only that, but also this allows the motion to be mainly excited by the harmonic part of the equation. The analytical and CFD results obtained using Fluent for model 1 are presented in Figures 66, 67, 68 and 69. The time history of motion obtained from the analytical solution of the nonlinear equations (equations 4.43, 4.44 and 4.45) is acquired using MATLAB. The code generated is shown in Appendix D. The heave motion results are presented in Imperial units to better quantify the discrepancy between the analytical and CFD results.

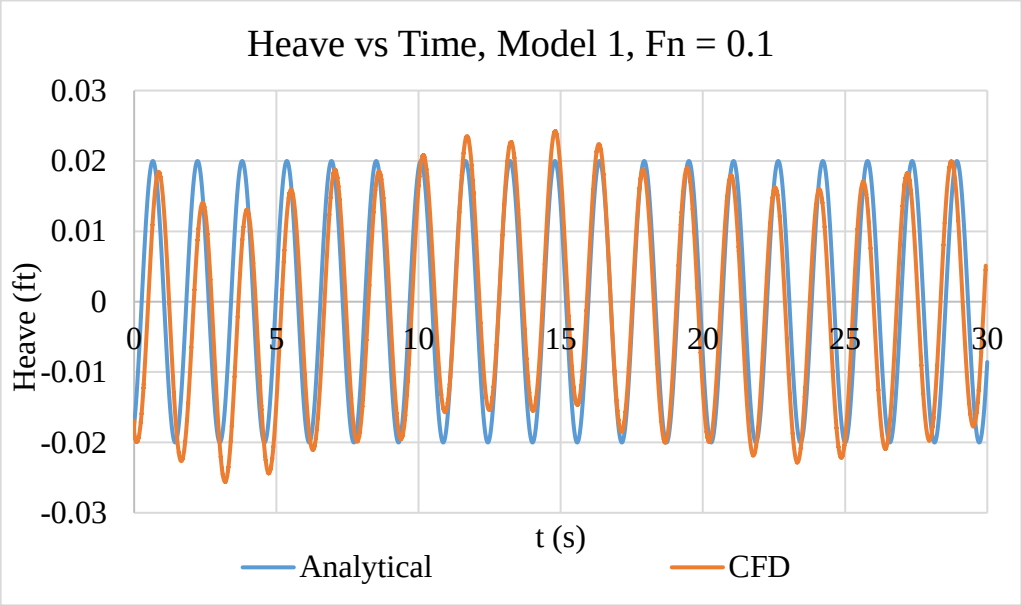

Figure 66. Time history of heave motion for model 1 at $F_n = 0.1$

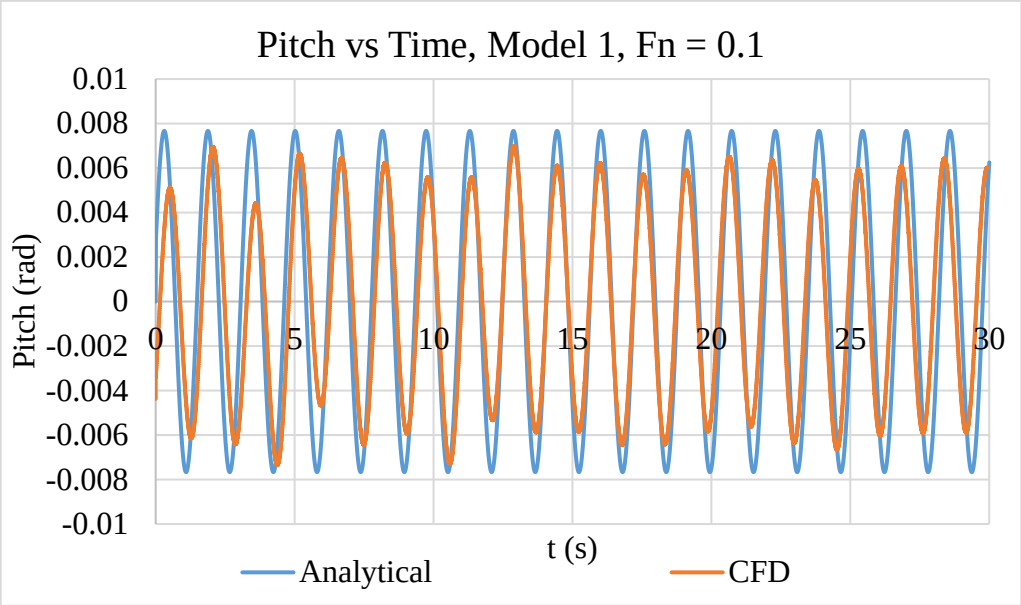

Figure 67. Time history of pitch motion for model 1 at $F_n = 0.1$

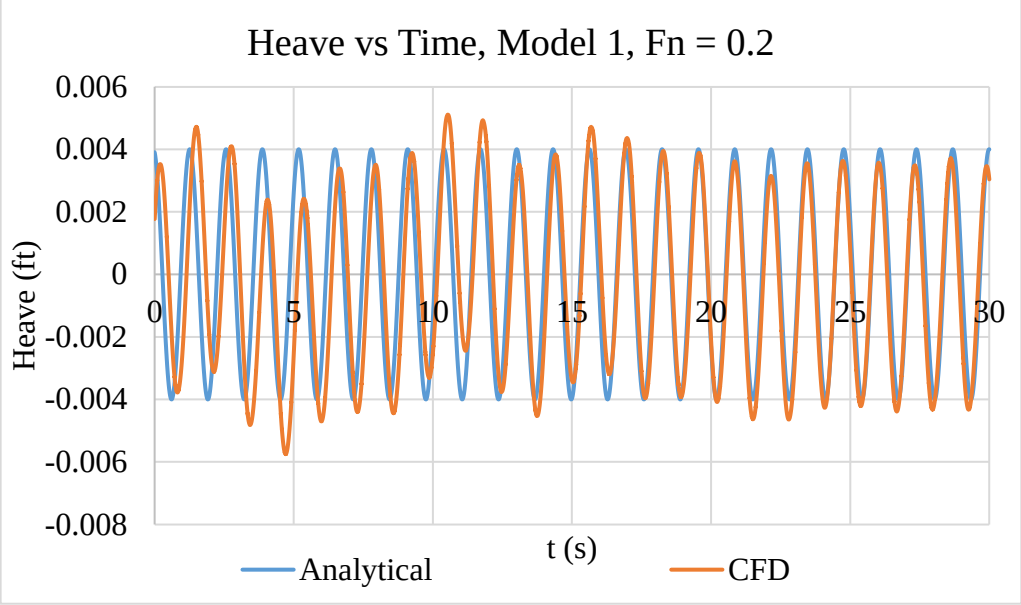

Figure 68. Time history of heave motion for model 1 at $F_n = 0.2$

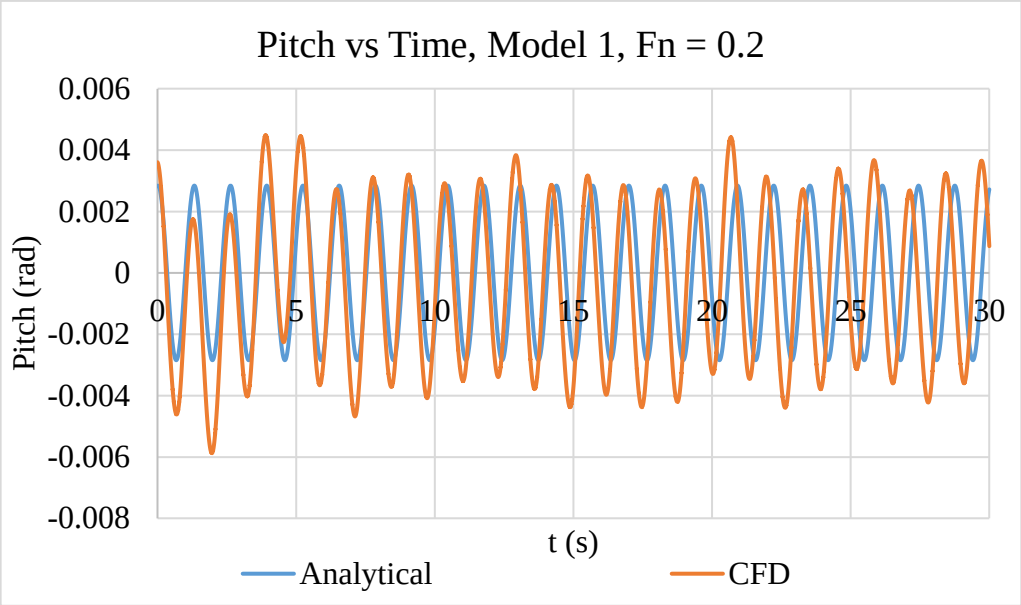

Figure 69. Time history of pitch motion for model 1 at $F_n = 0.2$

The CFD solution predicted the motion to be oscillating with an unsteady frequency while the analytical solution only produces constant frequency of oscillations. This is because in 2D simulations, the water is restricted to only flow underneath the hull whereas in reality a significant amount of water will be diverted around the sides of the hull. This will lead to the motion response of the hull being greater than expected as less energy will be dissipated from the hull to the water. This is due to the lower damping rate experienced in the two-dimensional hulls compared to the three-dimensional. This explains the high heaving amplitude of motion and lower pitch amplitude produced in the CFD solution. The lower pitch amplitude can be explained by the fact that pitching is restricted as it is a 2D hull and the buoyancy force is greater when the centre of buoyancy changes in reaction to the increase in pitching. There is a slight discrepancy between the results of the two methods in the first 5 seconds. This is due to the location of the free surface being defined based on the length-to-draft ratio of 10. However, this depends on weight, location of the CG and speed of the hull and takes a few seconds until it stabilises. When Froude number (F_n) is increased to 0.2, the amplitude of motion of the model is reduced while the frequency of oscillations is increased. Hence, the amplitude of motion is predicted with very good accuracy while pitching frequency

produced in the CFD solution has increased slightly with time. It is due to the greater motion response of the 2D hull as explained earlier. Finally, the discrepancy in the results can also be attributed to that in Fluent, aerodynamic and hydrodynamic effects are considered from the use of multiphase flow. However, the analytical solution only considers hydrodynamic effects. This is because the parameters of the two equations of heave and pitch are calculated from the strip theory which only considers hydrodynamics. The results obtained for model 2 are presented in Figures 70, 71, 72 and 73.

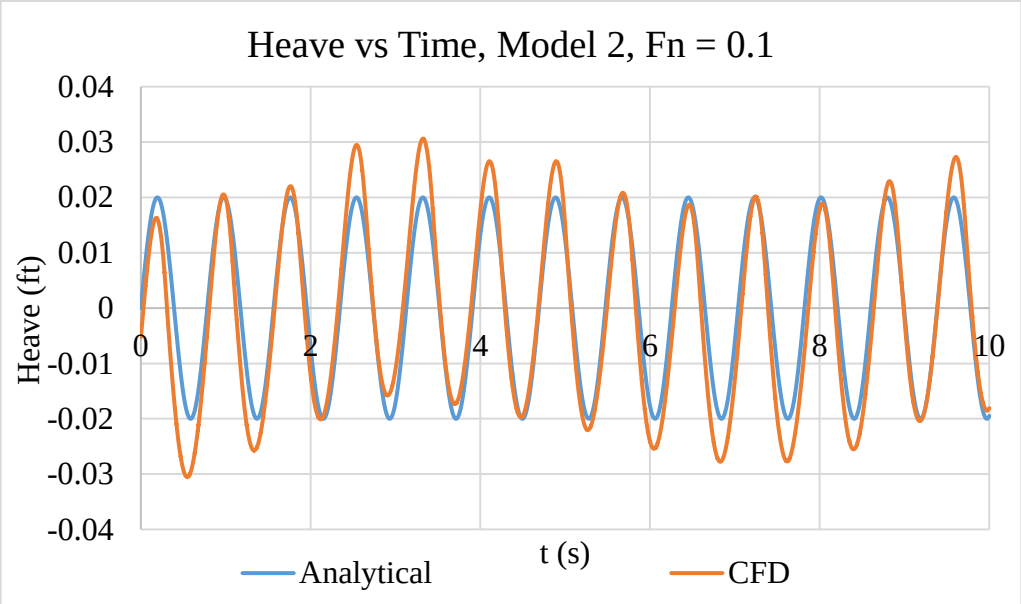

Figure 70. Time history of heave motion for model 2 at $F_n = 0.1$

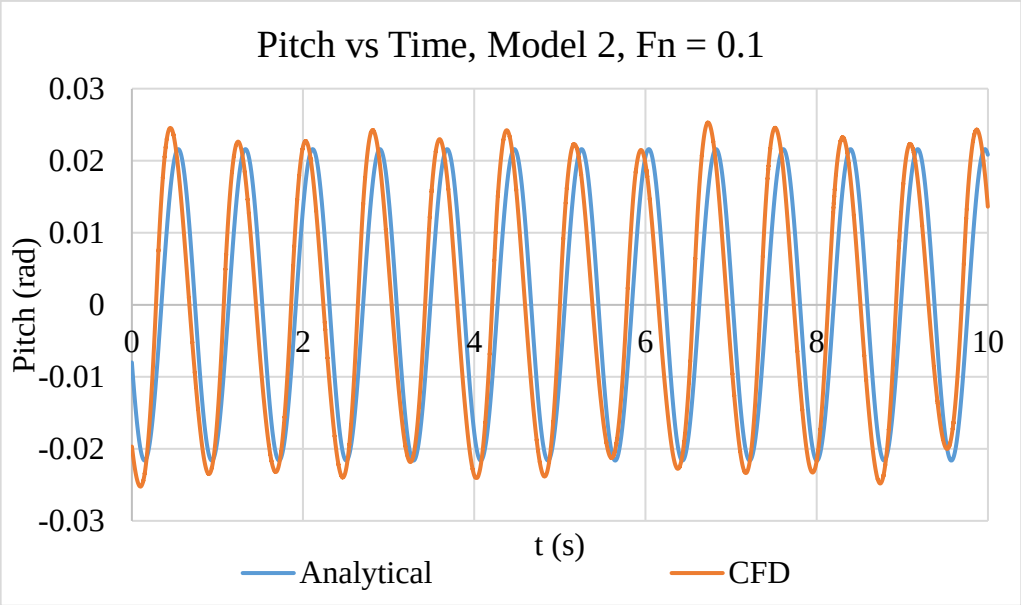

Figure 71. Time history of pitch motion for model 2 at $F_n = 0.1$

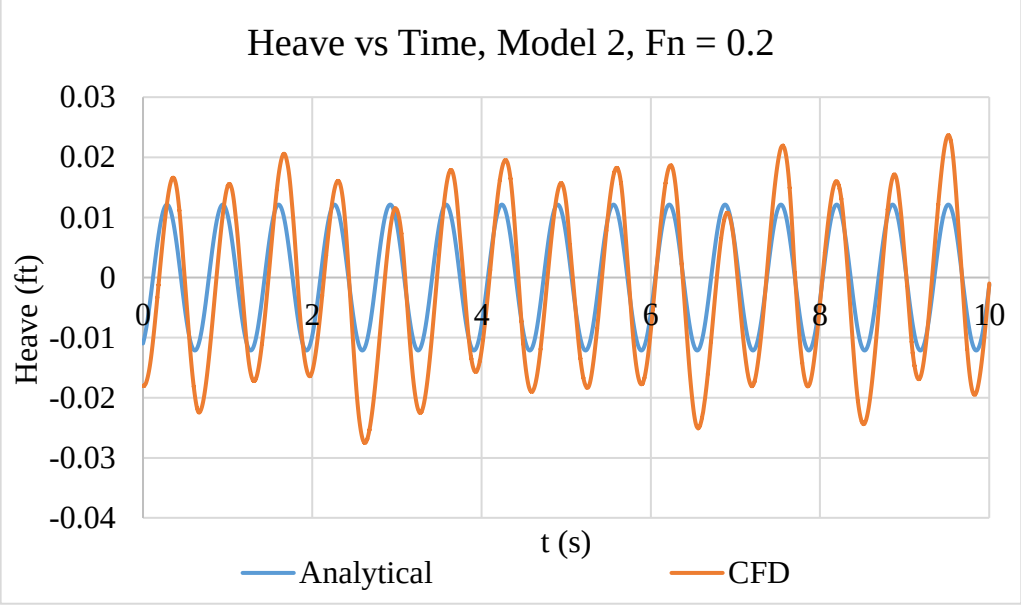

Figure 72. Time history of heave motion for model 2 at $F_n = 0.2$

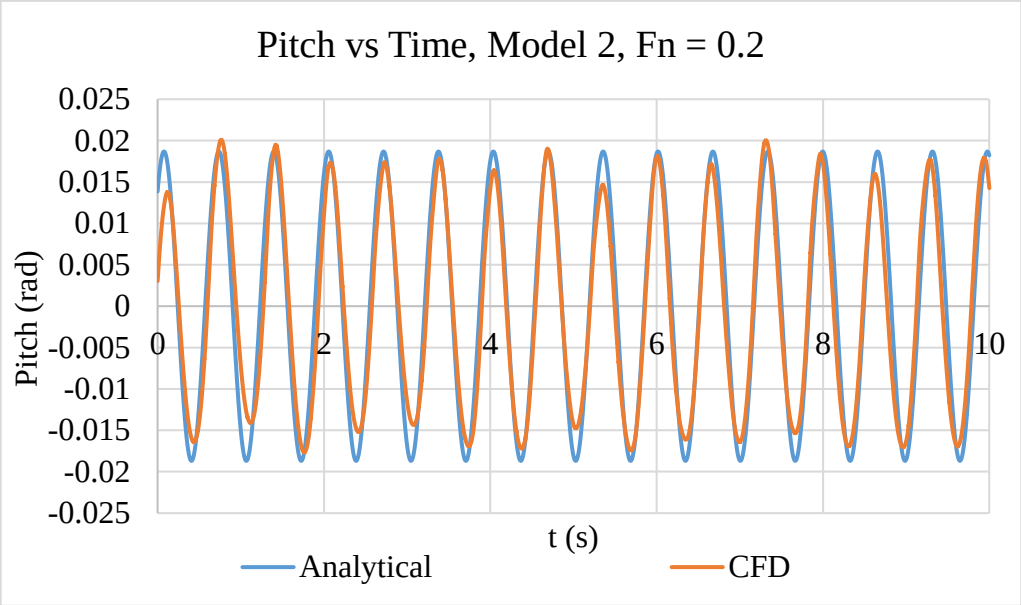

Figure 73. Time history of pitch motion for model 2 at $F_n = 0.2$

The results are presented for 10 seconds only because this model oscillates with much higher frequency than the previous one. This is caused by its much lower overall length and weight. The results of this model demonstrate that the amplitude of heaving and pitching obtained from both methods are in very good agreement. The slight discrepancy in the heave amplitude is due to the characteristics of the 2D simulation as explained earlier. Due to the less distance the centre of buoyancy travels compared to model 1, the pitching amplitude obtained from both methods is in very good agreement. As the hull of this case has much less weight, it takes very little time to stabilise after launching the simulation. Hence, the results obtained are in very good agreement in terms of amplitude and frequency. When the speed is increased, the results for this model becomes more stable as the frequency of oscillations of the CFD solution is almost constant. The heaving amplitude obtained from the CFD solution is still a little higher than the amplitude predicted analytically. However, the pitch amplitude and frequency of this case are in very good agreement.

6.3 Verification with AQWA

The heave and pitch history of motion is predicted for the seaplane hull presented in [153] analytically and using Ansys AQWA. The hull will be referred to as model 3. The results are also obtained for two different Froude Numbers; 0.1 and 0.2. Similar to the analytical analysis, AQWA only considers hydrodynamic effects. The geometrical properties of the hull used in this research along with sea wave conditions are listed in Table 7 [153]. The wavelength is also assumed to be equal to the hull length.

Table 7. The geometrical characteristics of model 3 and wave amplitude used

Parameter	Value	
	In SI units	In Imperial units
Overall length L_{oa}	5.517 m	18.100 ft
Beam length	0.999 m	3.280 ft
Draft	0.358 m	1.176 ft
Mass	1596.645 kg	3520.000 lb
Wave amplitude	0.076 m	0.246 ft

Similar to model 1 and 2, the strip theory is applied so that the coefficients of the heave and pitch equations for model 3 can be determined. The analytical and AQWA simulation results of heaving and pitching obtained for model 3 are shown in Figures 74, 75, 76 and 77.

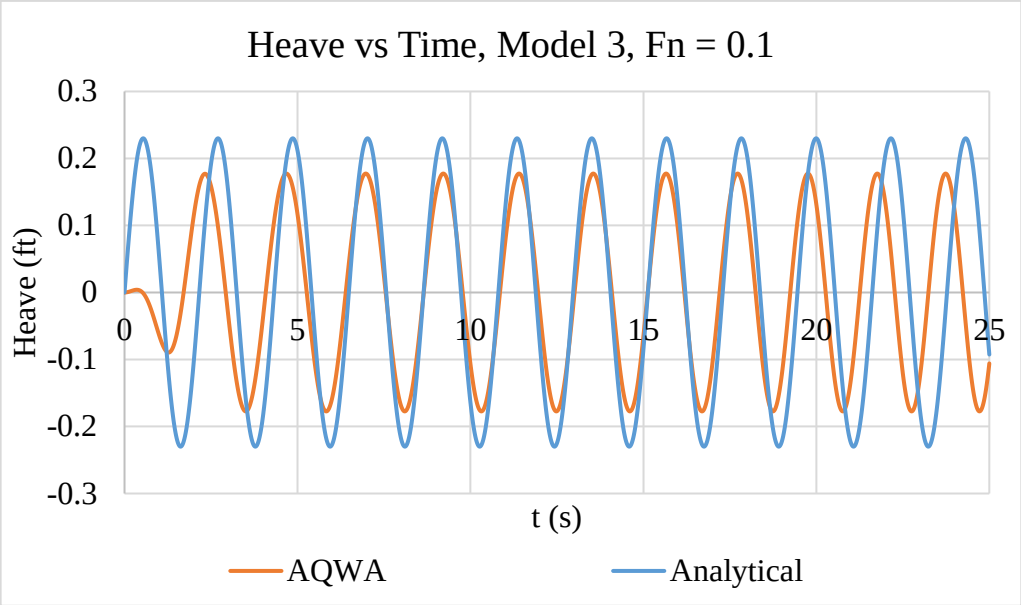

Figure 74. Time History of heave motion for model 3 at $F_n = 0.1$

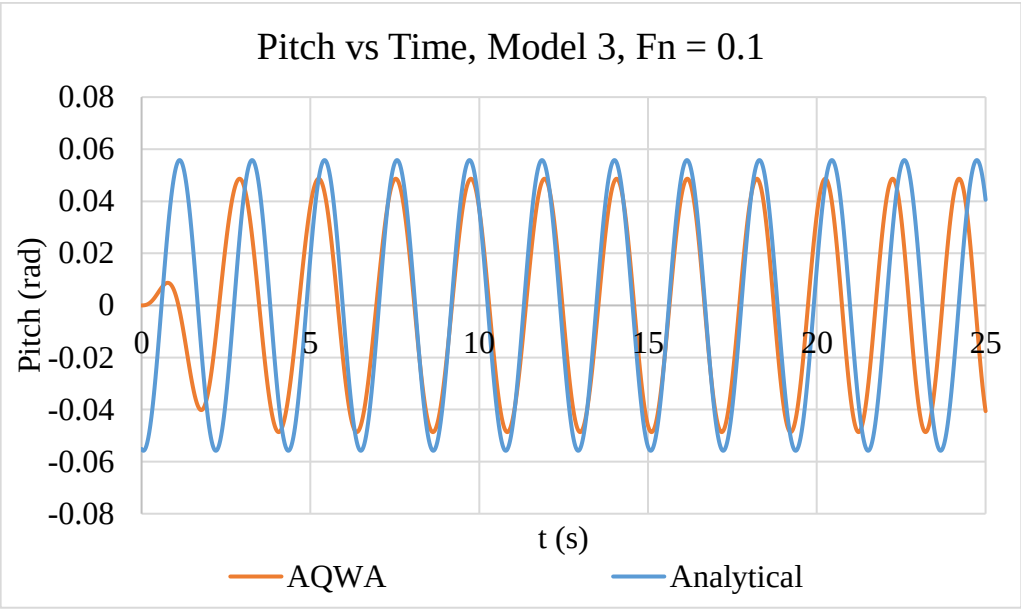

Figure 75. Time history of pitch motion for model 3 at $F_n = 0.1$

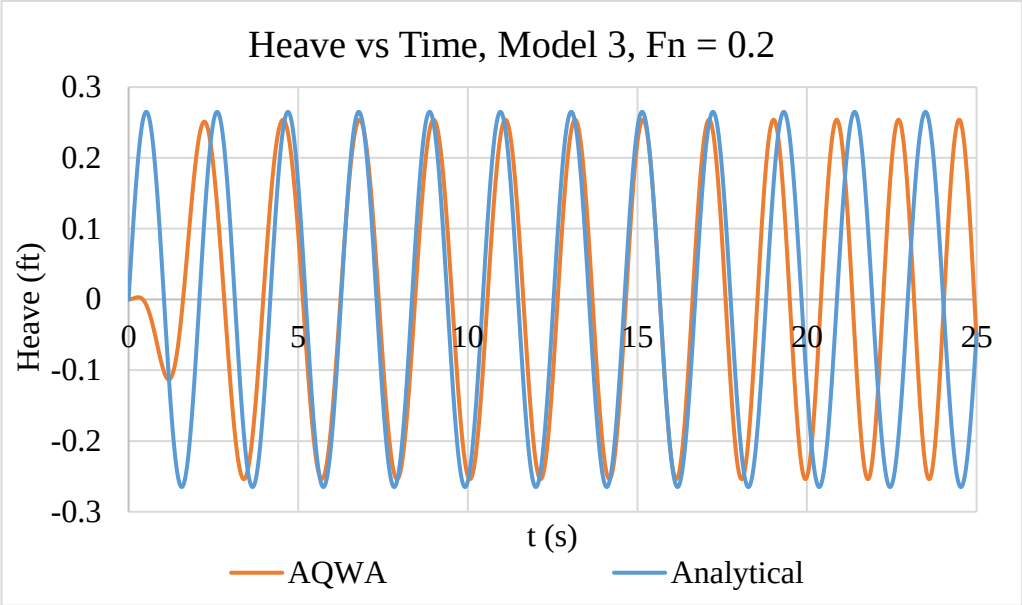

Figure 76. Time history of heave motion for model 3 at $F_n = 0.2$

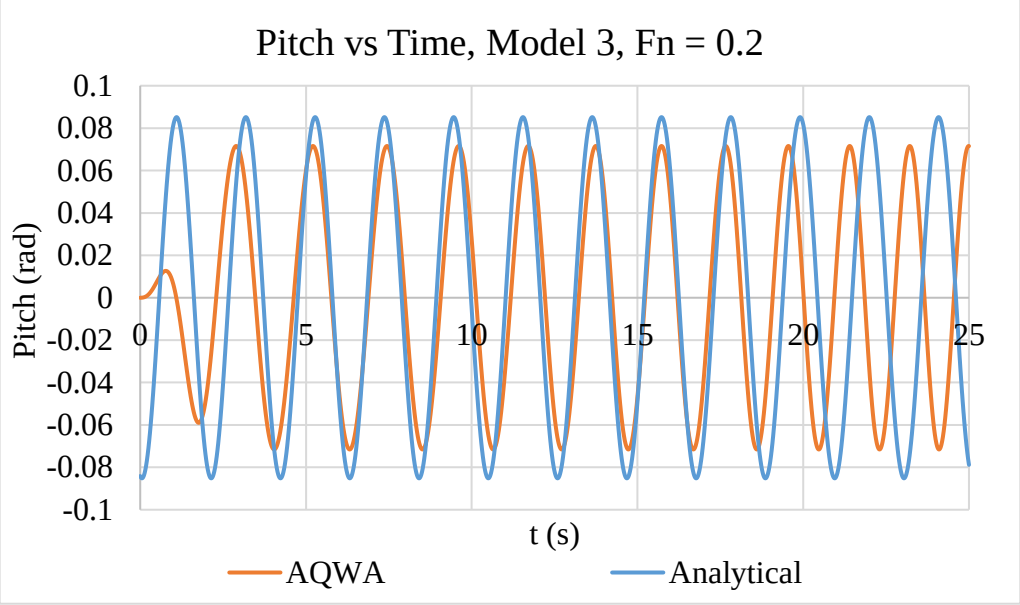

Figure 77. Time history of pitch motion for model 3 at $F_n = 0.2$

The results obtained are in very good agreement. However, as the analytical results are based on the data of the strip theory, which is two-dimensional, there is a slight discrepancy in the amplitude of motion. The numerical solution obtained from AQWA, which uses a 3D hull, takes in consideration that water will flow around the sides of the hull. This will increase the energy dissipated from the hull

to the water and enhance damping. However, the two-dimensional strip theory assumes that the water will only pass underneath the hull which will increase the structural response and reduce damping. At the higher speed regime ($F_n = 0.2$), the amplitude of motion is predicted with better accuracy. However, the nonlinearity of the frequency of oscillations becomes more evident after 20 seconds of motion. The frequency of oscillations obtained in AQWA increases with time while in the analytical approach, the frequency of oscillations can only be assumed to be constant for the whole period of motion. The increment in the oscillations indicates that porpoising is taking place. Hence, the parameters associated with the frequency of oscillations could be used to control porpoising. Nevertheless, AQWA predicted porpoising to take place after 20 seconds of motion because it is fundamentally a software used for stationary or low speed applications [140]. In a standstill, seaplanes will encounter porpoising if sea conditions are rough. Finally, in the analytical investigations, the hull is assumed to have its bow slightly directed upwards. This comes from the strip theory that assumes that pitching motion does not start when the hull is perfectly horizontal. It depends on the incident wave amplitude. This explains why pitching starts from a value of -0.05 rad in the lower speed simulations and -0.07 rad in the higher speed simulations.

6.4 Effect of Nonlinearity

In order to better quantify the effect of nonlinearity, the uncoupled form of the equations is examined. In this case, the coupling terms are assumed to be zero. Hence, their effect is eliminated. The results obtained from the nonlinear analytical models will be compared to the leading order solutions (which represent the linear solution of each equation) and to numerical results obtained from MATLAB using ODE45 solver. The code is shown in Appendix E. It should be noted at this point that the nonlinear terms (a_2 and b_2) are introduced to the equations and their value is assumed so that their effect on the frequency of oscillation is illustrated. The values used for the other parameters in the equations along with their physical meaning are listed in Table 8.

Table 8. Values of the parameters used in the examination of the uncoupled system

Parameter	Physical meaning	Value
ε	Non-dimensional parameter used to correct the solution for higher order terms	0.01
A	Initial amplitude (incident wave amplitude)	0.2 ft
F_1	Heave motion amplitude	5 ft
M_1	Component one of pitch motion amplitude	5 ft
M_2	Component two of pitch motion amplitude	0.5 ft
ω_0	Natural frequency of the system	1 rad/s

Nevertheless, in this analysis, the initial conditions used to obtain the numerical solution are as follows: $u_0(0) = 0.2,\ v_0(0) = 0.2,\ \dot{u}_0(0) = 0$ and $\dot{v}_0(0) = 0$. This means that the initial amplitude (incident wave amplitude) is equal to 0.2 ft and that the sea-craft is initially at rest. In order to understand the effect of the nonlinear coefficient on the heaving and pitching motions, three cases will be investigated in the next sub-sections.

6.4.1 Small Nonlinearity Parameters

In this case, the nonlinear coefficients a_2 and b_2 are assumed to be -670 and -659 respectively. This is because the aforementioned values will reduce the frequency of oscillations which is calculated from equations 4.18 and 4.20 by 25%

compared to the natural frequency of the system. This is the case when the nonlinearity in the system comes in form of external excitation force/moment. The results of this case are presented in Figures 78 and 79.

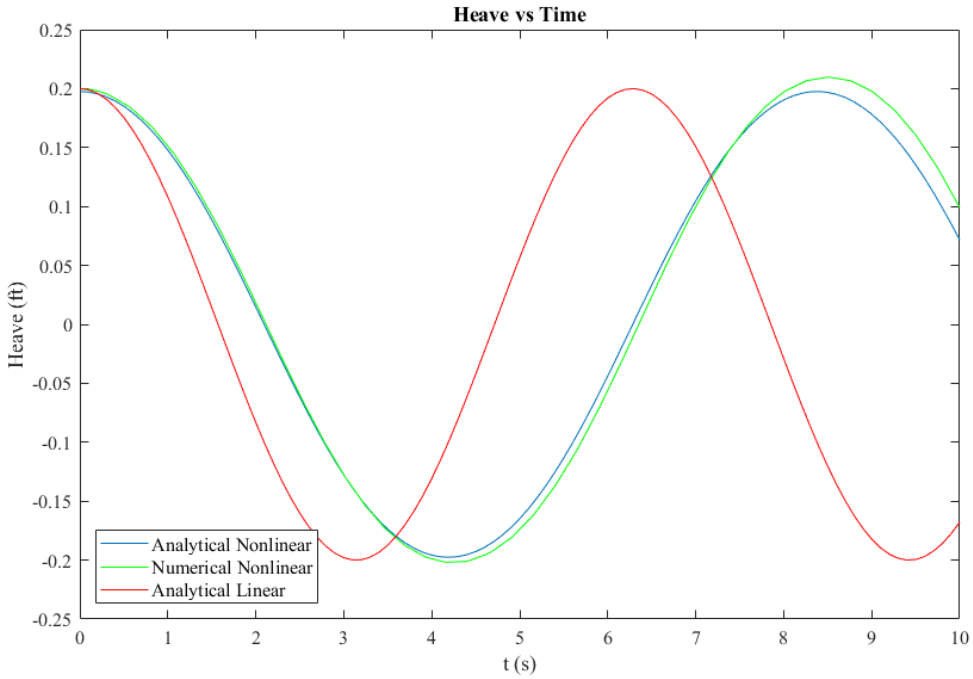

Figure 78. Effect of negative nonlinearity on heave motion

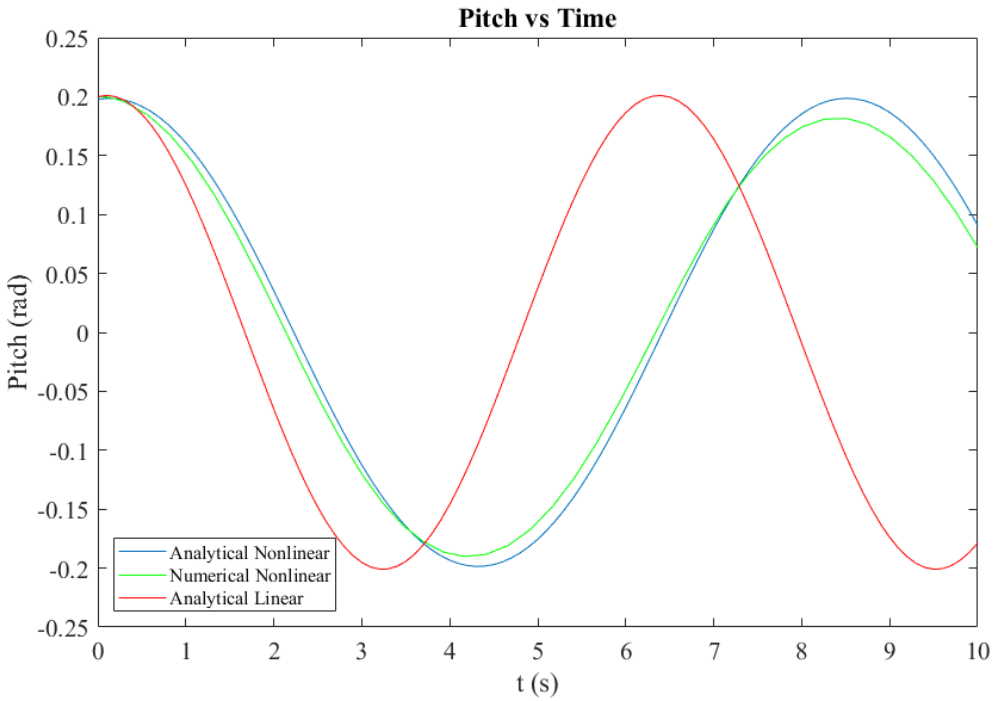

Figure 79. Effect of negative nonlinearity on pitch motion

The results of this case show that when the system is under high external excitation loads in form of negative nonlinear restoring force/moment, the frequency of oscillations tend to be reduced. It can also be seen that the results obtained from the perturbation theory match very well with the numerical results obtained from MATLAB. The linear solution does not account for any change in the nonlinearity and only predicts the motion with a frequency equal to the natural frequency.

6.4.2 Medium Nonlinearity Parameters

In this case, the nonlinear coefficients are changed so that the system oscillates with the same frequency as the natural frequency. The two coefficients a_2 and b_2 are both assumed to be equal to 825 so that the external excitation frequency becomes equal to the natural frequency of the system. The results obtained show that this is the pure resonance case because the system oscillates with a frequency equal to the natural frequency. The results of the nonlinear

analytical model are in a very good agreement with the linear model results and also with the numerical results (see Figures 80 and 81).

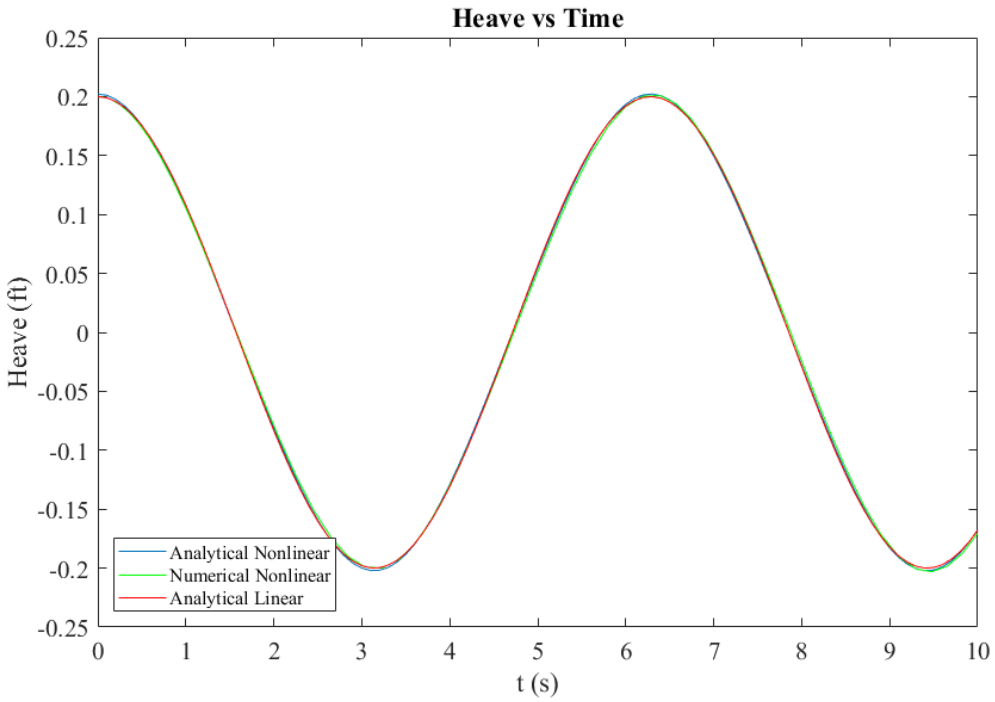

Figure 80. Effect of positive nonlinearity on heave motion

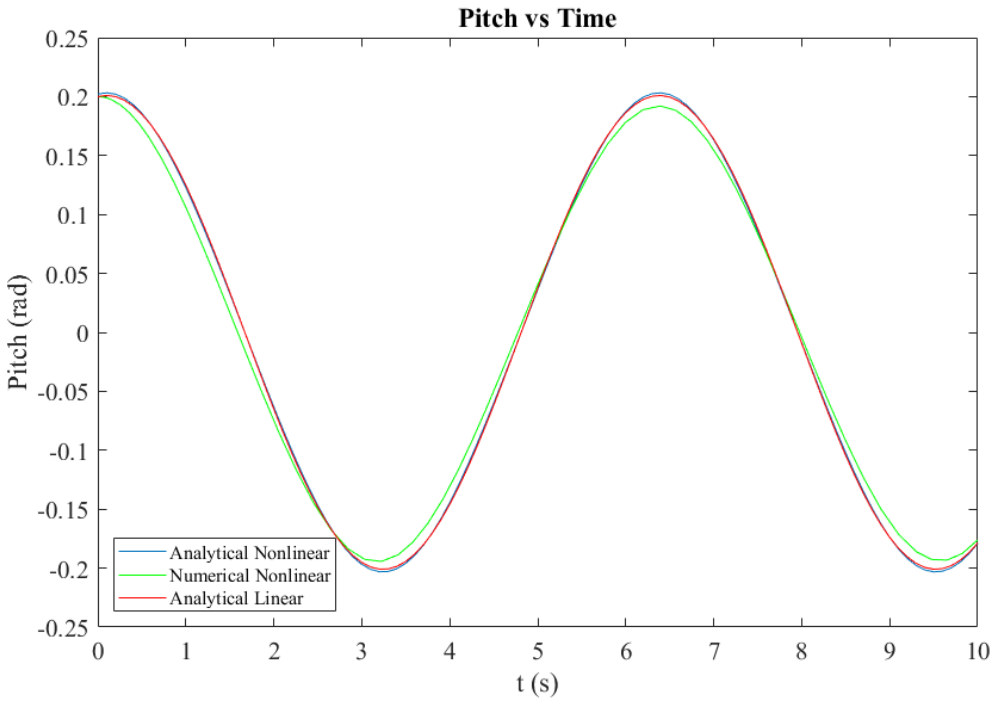

Figure 81. Effect of positive nonlinearity on pitch motion

The results in this case show that the nonlinear analytical, linear analytical and numerical results match very well in both heave and pitch. This is because the system is assumed to be oscillating with a frequency that is equal to the natural frequency. This case is the pure resonance case in which the leading order solution is sufficient to predict the behaviour.

6.4.3 Large Nonlinearity Parameters

This is the case when the system is under the effect of nonlinear restoring loads as the nonlinear coefficients have a very large value compared to the previous two cases. This will increase the frequency of oscillations by 25% compared to the natural frequency of the system. Hence, the heave nonlinear coefficient a_2 is assumed to have a value of 2662 and the pitch nonlinear coefficient b_2 is assumed to be 2758. Those are the values that increase the frequency of oscillations of the system by 25% compared to the natural frequency of the system. The results obtained are presented in Figures 82 and 83.

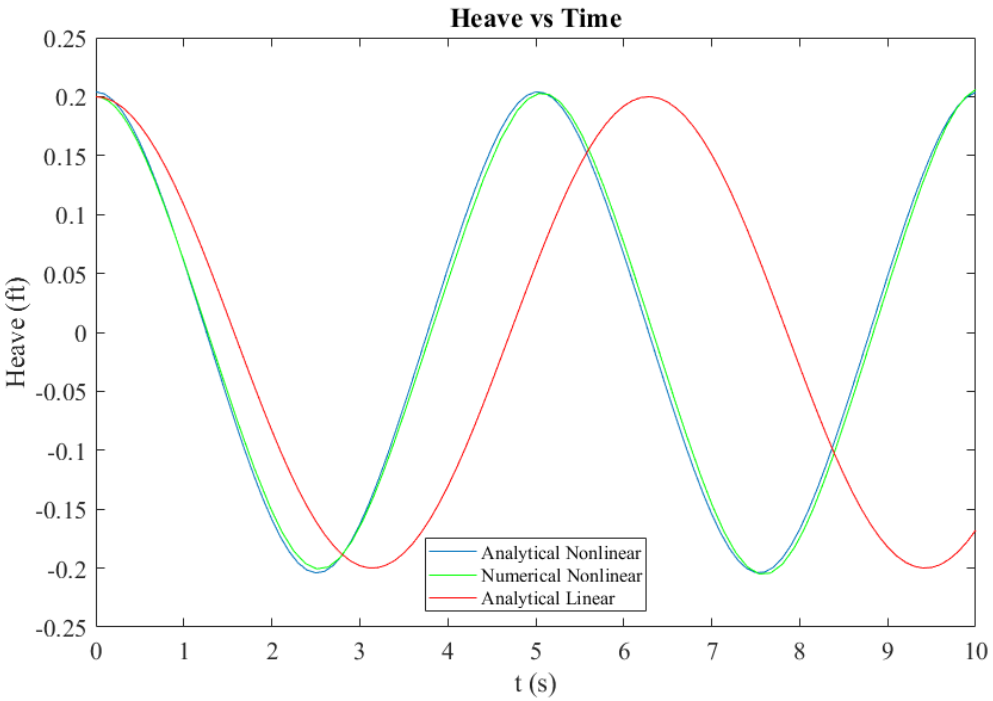

Figure 82. Effect of large nonlinearity on heave motion

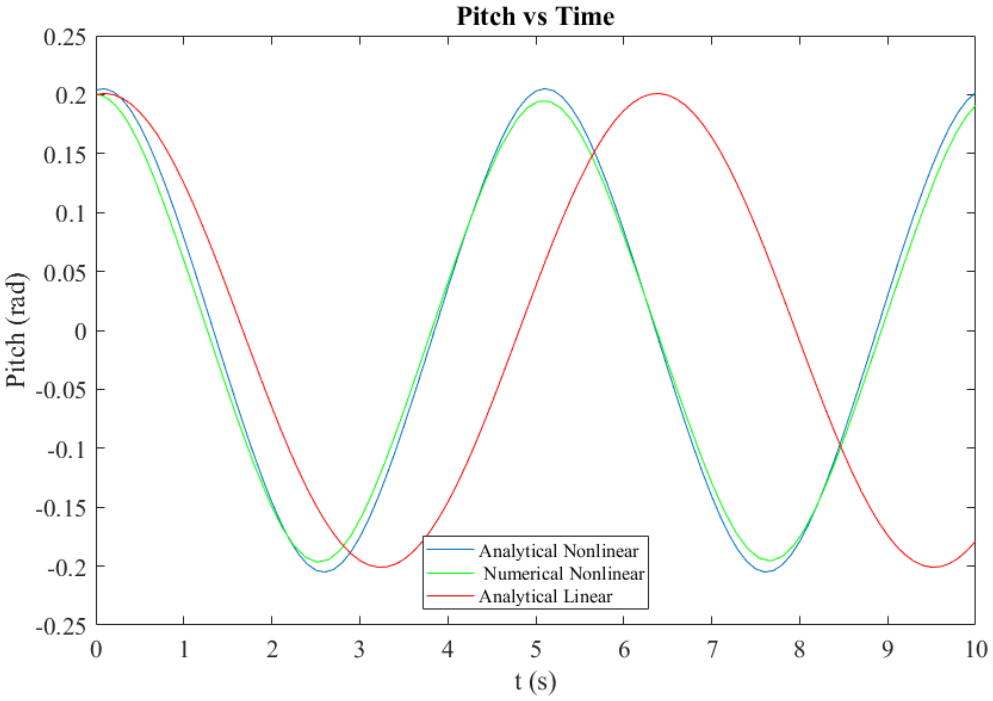

Figure 83. Effect of large nonlinearity on pitch motion

The results show that the frequency of oscillations increases with the increase of the restoring force resulted from the positive nonlinear coefficients. Also, it can be seen that the linear solution is unable to predict the motion in this case.

6.5 Effect of Coupling

The coupling between heave and pitch is very important when it comes to understanding the performance of sea-crafts during take-off and landing. Coupling effect will be explained from the results presented previously in section 6.2. The higher speed case of Froude Number (F_n) = 0.2 will be examined. For model 1, as the nonlinear coefficients in both equations are assumed to have a value equal to 100, the ratio of nonlinearity to model displacement becomes very small and equal to 0.035. Both quantities are regarded as forces opposite to each other. The nonlinear coefficient is a hydrostatic restoring force that is supposed to maintain the hull of the craft on water. Hence, very low amplitude of motion is encountered as the nonlinear effect is very small (see Figures 68 and 69). The amplitude and frequency response are small due to the coupling effect being larger than the nonlinear effect as the nonlinearity-to-displacement ratio is very small. This demonstrates that as the nonlinearity increases, the amplitude and frequency increases. For model 2, the ratio of nonlinear coefficient to model displacement is 3 which explains the higher amplitude and frequency obtained. The amplitude in this case is significantly greater than the previous case due to the higher pitch nonlinearity-to-displacement ratio and much higher heave coupling term. The frequency of oscillations is higher than the previous case because of the higher nonlinearity-to-displacement ratio (see Figures 72 and 73).

6.6 Summary of the Impact of Coupling and Nonlinearity

To summarise the effect of coupling and nonlinearity on frequency and amplitude of motion of the coupled system, equations 4.34 and 4.45 are used. A, which is represented by equation 4.34, is the amplitude of motion and it is a function of coupling, nonlinearity and frequency of oscillations (ω) which is represented by equation 4.45. Figure 84 illustrates the effect of coupling and nonlinearity on the

amplitude of motion. In addition, Figure 85 explains the impact of coupling and nonlinearity on the frequency of oscillations. In order to clearly see the effect of each term, the value of each term is increased from 0 to 90 while all other terms are given a constant value of 1 to minimise their impact.

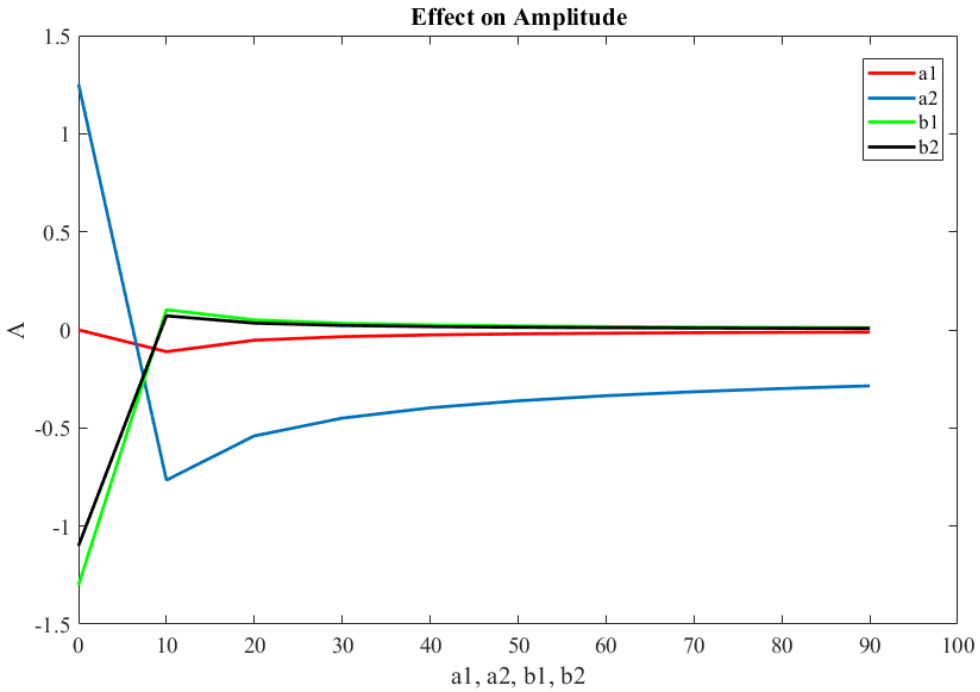

Figure 84. Amplitude against coupling and nonlinearity

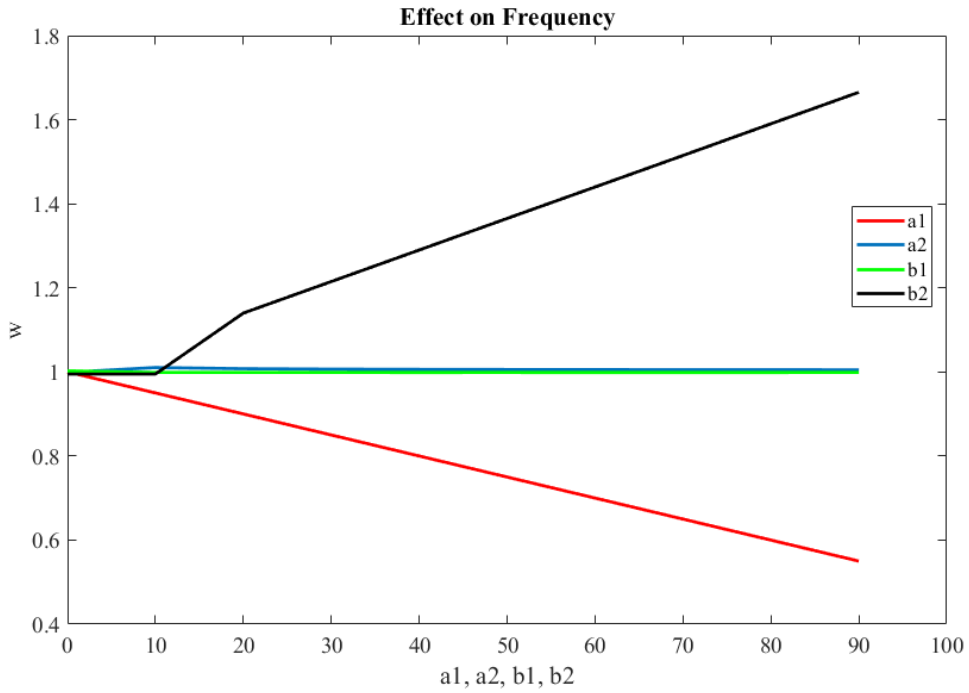

Figure 85. Frequency against coupling and nonlinearity

The pitch coupling term (a_1) has almost no effect on the amplitude of motion. However, the nonlinear term of heaving (a_2) reduces the amplitude of motion as it increases until it becomes much larger than other terms, then its effect deteriorates significantly. On the other hand, the heave coupling and pitch nonlinear terms (b_1 and b_2) of equation 4.4 increase the amplitude up to the point when they become much larger than other terms (the same point when heave nonlinear term stops reducing the amplitude). The point when the effect of terms become much less significant is when each term becomes almost 10 times more than the other terms. The amplitude of motion can be reduced by keeping pitch motion terms as minimum as possible and by increasing the heaving equation terms. This means that the amplitude of motion is influenced by the terms of the pitch equation of motion while the terms of the heave equation of motion have less impact on amplitude. Furthermore, the frequency of oscillations is only affected by terms related to pitching as it is significantly reduced by the increase of pitch coupling term (a_1) and it increases as pitching nonlinear term (b_2) increases. The effect of those two terms on frequency has no limit. However, the terms related to heaving have almost

no impact on the frequency of oscillations. Hence, the amplitude of motion can be controlled by the heave coupling term and the nonlinear terms of both motions. However, the frequency of oscillations is a function of pitching terms only. The frequency and amplitude responses of a seaplane hull are illustrated in Figure 86.

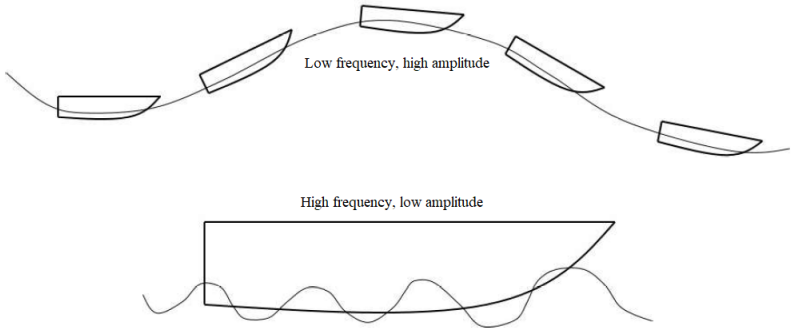

Figure 86. Seaplane hull response profile

6.7 Extension of Savitsky's Method

Planing crafts are high-speed marine vehicles that derive their support from hydrodynamic pressures acting on their bottom surfaces [22]. Savitsky [53] proposed an analytical method to predict the porpoising stability limit of this type of vehicles. This method was previously discussed in section 2.5.1.1 and its limitations were stated in Table 2. The analytical solution to the coupled, nonlinear heave and pitch equations obtained in this research will be used to extend this method in order to predict the porpoising stability limit of seaplanes. The extension presented in this section has the following advantages over Savitsky's method:

1. The seaplane hull is assumed to be affected by a pattern of sea waves (not calm sea conditions).
2. No geometry constraints as the hydrodynamic coefficients are calculated from a strip theory that can be applied to any geometry.
3. Nonlinear effects arising from restoring force/moment are taken into consideration.
4. The centre of gravity is assumed to be centre of rotation and centre of mass of the hull which is the case for many seaplanes.

5. No dependence on location or direction of thrust force.

As stated previously, porpoising is longitudinal instability that cause self-induced heave and pitch oscillations (see Figure 87). It causes submergence of the bow of the hull which leads to structural damage [20].

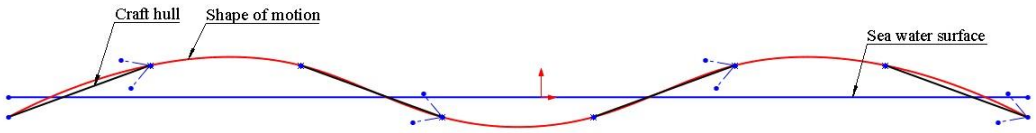

Figure 87. Profile of porpoising motion

Savitsky [53] studied the porpoising from the pitch angle and the coefficient of lift for a given speed. If the combination of the lift coefficient and the pitch angle is above the predicted line, then the hull will tend to porpoise. However, the combinations of pitch angle and lift coefficient which fall below the limit curve indicate stable operation [53]. According to Savitsky [53], there is a relation between the pitch angle and the lift coefficient which defines the inception of porpoising. Thus, equation 4.44 is used to obtain the pitch angle for 11 values of Froude Number (F_n); 0.1 to 1.1. This is the regime of speed that hydrodynamics play a significant role and the overall risk level of porpoising is high [24]. The coefficients of the equation are calculated from the strip theory explained in [6]. The coefficient of lift is calculated from equation 2.6. The hull examined has the geometrical characteristics presented in Table 9.

Table 9. Geometrical specifications of the hull used to examine porpoising

Parameter	Value	
	In SI units	In Imperial units
Overall length L_{oa}	22.860 m	75.000 ft
Beam length	4.267 m	14.000 ft
Draft	0.683 m	2.240 ft
Mass	27215.542 kg	60,000 lb

The wavelength is assumed to be equal to the hull length. In addition, the wave amplitude is assumed to be 0.5 m (1.64 ft) which corresponds to slight sea state characteristics [155]. The process of analytically obtaining the stability limit can be explained as follows:

- First, the coefficient of lift is calculated from equation 2.6 for the range of speeds examined.
- Then, the coefficients of equation 4.44 are calculated from the strip theory for each speed independently.
- After that, the pitch angle is calculated for the speeds examined. The seaplane is assumed to be initially at rest.
- Finally, the lift coefficient and pitch angle are now functions of speed and can be plotted against each other.

Figure 88 shows a comparison between the porpoising stability lines obtained by the solution of the coupled, nonlinear pitch equation of motion and Savitsky.

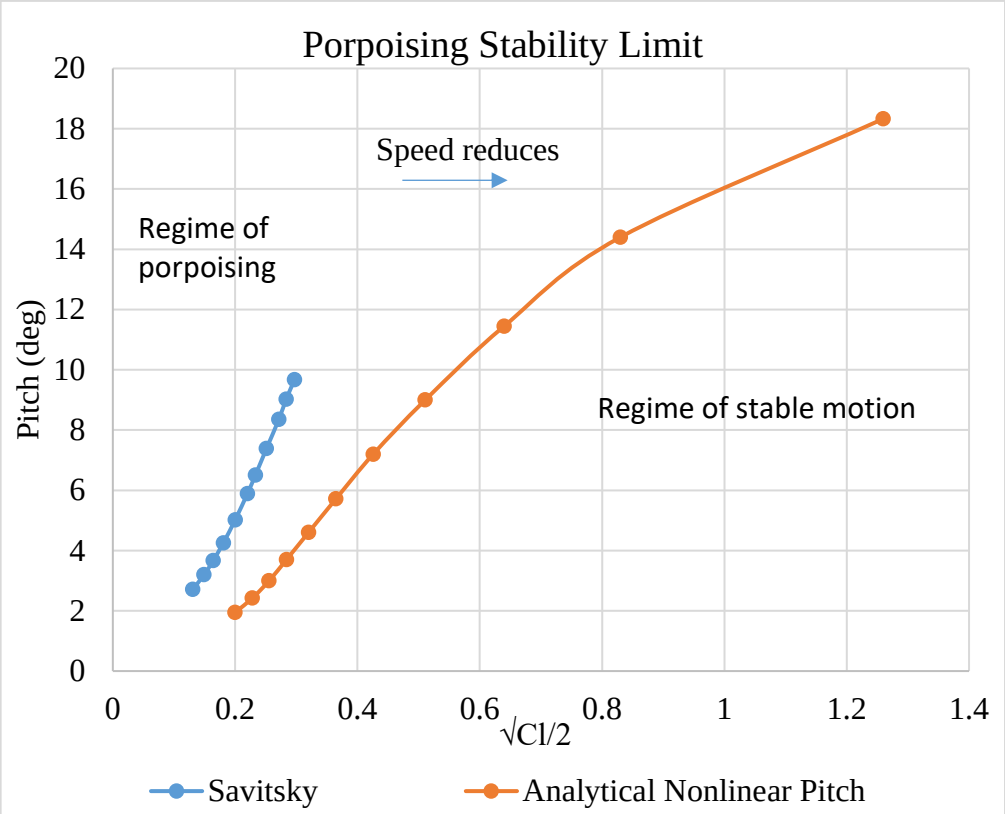

Figure 88. Porpoising stability limit predicted

As the lift coefficient is decreased, indicating a light hull and/or a high speed operation, the pitch limit for stability is decreased. Hence, if the hull is porpoising at a given speed and load, the rule is to lower the pitch angle to avoid porpoising. This can be achieved by moving the longitudinal centre of gravity forward (towards the bow). The results of Savitsky show that the pitch angle should be less than 10° to achieve stable motion when moving at a speed of 43 ft/s (13.1 m/s) or less. However, the nonlinear model proposed in this research show otherwise. The model proposed here show that if pitch angle is kept at 10°, stability is achieved if the hull is moving at a speed of 23 ft/s (7 m/s) or less. Increasing speed requires the pitch angle to be reduced to avoid porpoising. The porpoising line obtained by the nonlinear solution of pitch equation allows for higher loads stability prediction. The results obtained are for higher pitch angle as well. The difference in the results is due to the limitations of Savitsky's method as it can only predict the stability limit when the pitch angle is less than 10°. In addition, no wave effects are taken into consideration in Savitsky's approach.

CHAPTER 7

7. CONCLUSIONS AND RECOMMENDATIONS

7.1 Introduction

Seaplanes can be a very interesting alternative to current transport technologies as they combine the characteristics of ships and airplanes. This configuration uses the high-pressure region created underneath the hull as its flying medium because of the enhanced lift-to-drag ratio experienced in this region. This is known as the ground effect and can significantly reduce the fuel consumption and increase the number of passengers per flight. Nevertheless, this configuration is very interesting due to its ability to cover a wide range of applications as well as its ability to produce high lift-to-drag ratio. The stability in take-off and landing is a major problem that slows down the development of this type of crafts. Low speed stability is studied from heave and pitch motions as this type of crafts uses the open sea water surface as take-off and landing pathways. Hence, the hydrodynamic parameters associated with heaving and pitching motions on a wavy sea surface are much higher than the parameters of motion in other directions. This configuration is also called waterborne aircraft, Ekranoplan, ground effect vehicle or wing-in-ground effect vehicle. The study of nonlinear motion of this type of vehicles that takes in consideration the sea wave effect is of great importance. Previous analytical studies lack the ability to describe the nonlinear motion of seaplanes in head sea waves using Lagrangian mechanics and limited to certain geometrical characteristics. Hence, the goal of this research is to develop a mathematical tool that can be used to predict the dynamic stability of seaplanes on take-off and landing. Thus, the nonlinear heaving and pitching Lagrangian equations of motions driven by sinusoidal head sea waves are analytically investigated to find a solution that can be used to investigate porpoising (see section 1.2). The next section of this chapter will summarise the outcomes of this research with respect to its objectives

(see section 1.3). This is followed by a summary of the novel contributions of this study (see section 1.4). Finally, the last section discusses the limitations of the study and gives recommendations for future work based on the findings of this research.

7.2 Conclusions

An analytical tool that can be used to predict the performance of seaplanes advancing through head sea waves in take-off and landing is presented. The two nonlinear equations of heave and pitch motions are solved analytically by using the Poincare-Lindstedt perturbation method. The solution is verified with CFD simulations performed using Ansys Fluent and AQWA. Two different hull models are examined, and each is simulated at two different speeds using Ansys Fluent. The results obtained analytically and from Ansys Fluent are in very good agreement. However, as the CFD simulations are performed on 2D hulls, the amplitude of the heaving motion is slightly over predicted. This is due to the fact that in 2D simulations, the sea water is restricted to only pass underneath the hull, which will increase the vertical response of the craft. Moreover, in 2D simulations, less damping is experienced. In addition, the pitch amplitude produced by the CFD solution is less than the amplitude obtained using the analytical tool for model 1 which has a long hull of 19.2 ft. (5.85 m). This is attributable to the restricted 2D motion as the buoyancy force will be higher and thus the pitching motion will be reduced but not considerably. However, the less the distance that the centre of buoyancy moves away from the centre of gravity, the more accurate the pitch amplitude. The frequency of oscillations obtained from the CFD simulations is unsteady and moderately greater than the frequency of oscillations obtained analytically. As mentioned earlier, this is because of the characteristics of the 2D simulation that predicts higher hull motion response to sea water passing underneath it. The longer the distance the centre of buoyancy travels away from the centre of gravity, the higher the unsteadiness in frequency. Finally, considering that the simulations carried out are two-dimensional and that the strip theory only accounts for hydrodynamic forces, the results of the analytical tool presented are in very good agreement with the CFD results. The solution is also verified with

numerical simulations performed on Ansys AQWA. This software addresses the vast majority of analysis requirements associated with hydrodynamic assessment of all types of offshore and marine structures. It provides an integrated facility for developing primary hydrodynamic parameters required to undertake complex motions and structure response analysis. The results obtained from AQWA are in very good agreement with the analytical results. However, in the analytical solution, the amplitude of the heaving motion is slightly over predicted. This is because AQWA is a 3D platform in which damping is enhanced and amplitude response is reduced. The frequency of oscillations obtained analytically is constant while the frequency of oscillations obtained from AQWA increases with time. This increment in the frequency becomes clearer as the speed increases. This is due to the fact that AQWA is a low speed numerical simulation software. It predicts porpoising to take place after some patterns of head sea waves.

The Poincare-Lindstedt perturbation method was applied to obtain solution to the uncoupled and coupled equations of motion. In the uncoupled system, the effect of nonlinear on frequency of oscillations was investigated. It was shown that when the nonlinearity is an external driving force to the system, it reduces the frequency of oscillations. However, when the nonlinearity is an internal force that acts against the external exciting force, the system will oscillate with a frequency very close to the natural frequency of the system (pure resonance). The frequency of oscillations is increased by 25% when the nonlinearity is increased by almost 4 times the nonlinearity of the resonance case. In the study of the coupled system, two different methods of the strip theory were used to obtain the hydrodynamic parameters of the equations of the system for the same craft models used to verify the mathematical tool using Fluent. Model 1 has very low ratio of nonlinearity to model displacement. However, for model 2, the ratio of nonlinearity to model displacement is 3. It was found that the smaller the nonlinear effect, the less the amplitude of motion. It was also shown that the effect of nonlinearity is more significant when the system is uncoupled as coupling reduces the influence of nonlinearity. When the nonlinear coefficients are less significant than the coupling coefficients, the frequency of oscillations seems to be decreased. It can be concluded that the frequency of

oscillations is controlled by pitching terms only while the amplitude is increased with the increase of heaving terms and pitch nonlinear term.

Savitsky's method to study the porpoising of planing hulls is extended to include the effects of nonlinear restoring forces and sea waves. The results show that porpoising will be experienced at a lower speed than what Savitsky has predicted. The results are shown for a wider range of pitch angles. Also, the results show that porpoising can be controlled by moving the centre of gravity towards the bow of the hull. This will increase the speed at which porpoising starts for a given hull.

7.3 Novel Contributions

Several novel contributions have been made to the research field of nonlinear analytical motion of seaplanes and high-speed planing hulls. These can be summarised as:

- This study is the first of its kind to use the coupled nonlinear Duffing equation to describe the motion of seaplanes through head sea waves. Most studies in the field of analytical prediction of motion are based on linear Newtonian mechanics. This study used Lagrangian mechanics to develop the most general form of equations of motion in order to overcome the limitations of other methods.
- In this research, the Poincare-Lindstedt perturbation technique is used to obtain analytical solution to the nonlinear equations of motion describing the motion of seaplanes. The solution is then used to describe the effect of nonlinearity and coupling on the frequency and amplitude of motion.
- The method of Savitsky to study the dynamic stability of planing hulls is extended using the analytical solution of the coupled pitch equation. The solution obtained can be applied to any hull without any geometrical limitations. In addition, the porpoising can be predicted for a wider range of pitching angle.

- The motion of seaplanes is simulated in 2D in Fluent in which multiphase flow is used to consider the aerodynamic and hydrodynamic effects.
- The conventional analytical methods used to study the performance of planing hulls are reviewed in detail in this research. The limitations of each method are presented and the gap in the literature is clearly identified.

7.4 Limitations and Future Directions

The current research presents an initial analytical study of seaplanes motion through head sea waves. Hence, it was restricted by some limitations such as:

- As the investigations were carried out analytically, only 2^{nd} order nonlinear terms are calculated. In some cases, 3^{rd} order (or higher) terms are necessary to show the nonlinear effects.
- Only one type of linear sea wave theory is considered.
- The parameters of the nonlinear heave and pitch are determined using a strip theory, which is limited to speeds corresponding to the regime of maximum hydrodynamic support. The strip theory is also a 2D theory (see section 3.5).
- The coupling is limited to be cubic arising from heaving in the heave equations and from pitching in the pitch equation.

The research is restricted to the previously mentioned objectives. Thus, the following points present further areas of investigation for future research:

- Nonlinear analysis in the case of roll motion has been carried out by many researchers based on matching method and convolution integral formulation. However, perturbation analysis have not been used to analytically study the nonlinear roll motion [57]. This approach could be used to study the nonlinear roll motion because, similar to heave and pitch, the nonlinearity comes from damping and restoring moments. Moreover, the nonlinearity increases with the increase of roll angle which will also significantly increase the nonlinear damping. The results can be very helpful in the enhancement of dynamic stability of seaplanes during cruising and stationary.

- Nonlinearity could be applied from the calculations of the hydrodynamic coefficients which could result in a nonlinear strip theory. This allows for more accurate nonlinear analytical prediction of motion.
- Nonlinear wave theories such as Cnoidal wave theory [156] and nonlinear Stokes wave theory [157] could be used to study the nonlinear motion of seaplanes. In addition, irregular sea waves can be considered.
- This research only considered head sea waves. However, waves coming from other directions could be studied. Combination of waves coming from different directions is also possible.
- This research was limited to 2D analysis. However, it can be extended to study the motion in 3D. This means that other axes could be included such as rolling.
- Other types of coupling can be considered. For example, cross coupling between heaving and pitching. However, this is a more complicated type of coupled motion.
- Only periodic sea wave is considered. However, other external excitation types of forces/moments can be considered.
- This research focused on the motion of seaplanes in the maximum hydrodynamic support regime. This could be extended to predict the motion of seaplanes at higher speeds in which aerodynamic and hydrodynamic forces are encountered.
- The research can also be validated with experimental investigations using a towing tank in the first stage to study the motion in the low speed regime. Then, at higher speeds, the aerodynamic effect can be studied from a wind tunnel.

REFERENCES

[1] L. Yun, A. Bliault and J. Doo, *WIG craft and ekranoplan*. New York: Springer, 2010.

[2] V. Marinca and N. Herisanu, *Nonlinear Dynamical Systems in Engineering*. Berlin: Springer Berlin, 2011.

[3] H. Poincare, *Les méthodes nouvelles de la mécanique celeste*, Paris: Gauthier-Villars et fils, 1892.

[4] A. Lyapunov, *The general problem of stability of motion*. Kharkov: Izd. Kharkov University, 1893. (In Russian)

[5] M. Milton, "Theoretical prediction of motions of high-speed planing boats in waves," *Journal of Ship Research*, vol. 22, no. 3, pp. 140-169, 1978.

[6] R. Bhattacharyya, *Dynamics of marine vehicles*. New York: Wiley, 1978.

[7] K. Rozhdestvensky, "Wing-in-ground effect vehicles," *Progress in Aerospace Sciences*, vol. 42, no. 3, pp. 211-283, 2006.

[8] T. Hahn, W. Drewelow, D. Dewitz, B. Kolewe and B. Lampe, "Analysis of wing-in-ground-effect vehicle with regard to safety ensuring control," *IFAC Proceedings Volumes*, vol. 47, no. 3, pp. 863-868, 2014.

[9] R. Ollila, "Historical review of WIG vehicles," *Journal of Hydronautics*, vol. 14, no. 3, pp. 65-76, 1980.

[10] A. Ford, "Captured air bubble over-water vehicle concept," *Naval Engineers Journal*, vol. 76, no. 2, pp. 223-230, 1964.

[11] J. Bagley, "Pressure distribution on two-dimensional wings near the ground," Aeronautical Research Council, London, R&M no. 3238, 1960.

[12] A. Carter, "Effect of ground proximity on the aerodynamic characteristics of aspect-ratio-l aerofoils with and without end plates," NASA Langley Research Center, Langley, NASA-TN-D-970, 1961.

[13] J. Bate, "*Performance analysis and prediction of high-speed planing craft*," Ph.D. Thesis, Institute of Marine Studies, University of Plymouth, 1994.

[14] A. Maimun, S. Jamei, A. Priyanto and N. Azwadi, "Aerodynamic characteristics of wing of wig catamaran vehicle during ground effect," *WSEAS Transactions on Fluid Mechanics*, vol. 5, no. 3, pp. 196-205, 2010.

[15] C. Hiemcke, "*Design of a wing section in ground effect: application to high speed ground transportation*," Ph.D. Thesis, Iowa State University, 1994.

[16] M. Collu, "*Dynamics of marine vehicles with aerodynamic surfaces*," Ph.D. Thesis, School of Engineering, Cranfield University, Cranfield, 2008.

[17] Hydrodynamic Manual, Naval Air Test Center, Patuxent River, Md., USA, May 1958.

[18] R. Nangia, "Aerodynamic and hydrodynamic aspects of high-speed water surface craft," *The Aeronautical Journal*, vol. 91, no. 906, pp. 241-268, 1987.

[19] O. M. Faltinsen, *Hydrodynamics of high-speed marine vehicles*. Cambridge: Cambridge University Press, 2006.

[20] L. Dala, "Dynamic stability of a seaplane in takeoff," *Journal of Aircraft*, vol. 52, no. 3, pp. 964-971, 2015.

[21] K. Ito, T. Dhaene, Y. Hirakawa, T. Hirayama and T. Sakurai, "Longitudinal stability augmentation of seaplanes in planing," *Journal of Aircraft*, vol. 53, no. 5, pp. 1332-1342, 2016.

[22] Y. Ikeda and T. Katayama, "Porpoising oscillations of very-high-speed marine craft," *Philosophical Transactions of the Royal Society of London. Series A:*

Mathematical, Physical and Engineering Sciences, vol. 358, no. 1771, pp. 1905-1915, 2000.

[23] P. Payne, "Coupled pitch and heave porpoising instability in hydrodynamic planing", *Journal of Hydronautics*, vol. 8, no. 2, pp. 58-71, 1974.

[24] T. Fossen, *Handbook of marine craft hydrodynamics and motion control*, 1st ed. Chichester: John Wiley & Sons, 2011.

[25] H. Borst, "Analysis of vehicles with wings operating in ground effect," in *Advanced Marine Vehicles Conference*, Baltimore, MD, U.S.A, 1979.

[26] H. Hameed, "The design of a four-seat reverse delta WIG craft," *The Maldives National Journal of Research*, vol. 6, no. 1, pp. 7-28, 2018.

[27] S. Komissarov, *Russia's ekranoplans*. Hinckley: Midland, 2002.

[28] L. Yun, R. Datla and X. Yang, *Performance, technology and application of high performance marine vessels*, 1st ed. Newcastle upon Tyne: Cambridge Scholars Publishing, 2018.

[29] L. Yun and A. Bliault, *High performance marine vessels*. Boston, MA: Springer, 2012.

[30] L. Yun and P. Gui-Hua, "Dynamic air cushion wing in ground effect craft (DACWIG) - the prospect of high speed water transportation tool in the 21st century," in *25th International Conference on Air Cushion Technology*, Montreal, 1998.

[31] A. Nebylov and P. Wilson, *Ekranoplanes*. Southampton: WIT Press, 2002.

[32] R. Blockley and W. Shyy, *Encyclopedia of aerospace engineering*. Chichester: Wiley, 2010.

[33] M. Mashud, D. Mondal and M. Haque, "Experimental investigation of an airfoil with multiple dimples on the upper surface," in *International*

Conference on Mechanical Engineering and Renewable Energy, Chittagong, 2017.

[34] C. Eastlake, "An aerodynamicist's view of Lift, Bernoulli, and Newton," *The Physics Teacher*, vol. 40, no. 3, pp. 166-173, 2002.

[35] O. Tietjens, *Applied hydro- and aeromechanics*. New York: Dover, 1934.

[36] H. Schlichting and K. Gresten, *Boundary-layer theory*, 9th ed. Berlin: Springer, 2017.

[37] K. Rozhdestvensky, *Aerodynamics of a lifting system in extreme ground effect*. Berlin: Springer, 2000.

[38] M. Kim, H. Yoon, J. Jung, H. Chun and D. Park, "Hydrodynamic characteristics for flow around wavy wings with different wave lengths," *International Journal of Naval Architecture and Ocean Engineering*, vol. 4, no. 4, pp. 447-459, 2012.

[39] R. Cummings, S. Morton, W. Mason and D. McDaniel, *Applied computational aerodynamics*. New York: Cambridge University Press, 2015.

[40] A. Priyanto, A. Maimun, S. Noverdo, J. Saeed, A. Faizal and M. Waqiyuddin, "A study on estimation of propulsive power for wing in ground effect (WIG) craft to take-off," *Jurnal Teknologi*, vol. 59, no. 1, 2012.

[41] S. Lee and J. Lee, "Aerodynamic characteristics of a rectangular wing in ground proximity," *Journal of Aircraft*, vol. 51, no. 2, pp. 688-693, 2014.

[42] Y. Moon, H. Oh and J. Seo, "Aerodynamic investigation of three-dimensional wings in ground effect for aero-levitation electric vehicle," *Aerospace Science and Technology*, vol. 9, no. 6, pp. 485-494, 2005.

[43] J. Lee, B. Kim and K. Park, "Aerodynamic characteristics and shape optimization of airfoils in WIG craft considered ground effect," *Transactions*

of the Korean Society of Mechanical Engineers B, vol. 30, no. 11, pp. 1084-1092, 2006.

[44] M. Holloran and S. O'Meara, "Wing in ground effect craft review," Royal Melbourne Institute of Technology, Contract Report CR-9802, Melbourne, 1999.

[45] G.S. Baker, "Some experiments in connection with the design of floats for hydro-aeroplanes," Aeronautical Research Council, London, R&M no. 70, 1912.

[46] W. Sottorf, "Experiments with planing surfaces," National Advisory Committee for Aeronautics, NACA-TM-739, Washington, 1934.

[47] J. Shoemaker, "Tanks tests of flat and vee-bottom planing surfaces," National Advisory Committee for Aeronautics, NACA-TM-848, Washington, 1934.

[48] A. Sambraus, "Planing surfaces tests at large Froude numbers - airfoil comparison," National Advisory Committee for Aeronautics, NACA-TM-509, Washington, 1938.

[49] L. Sedov, "Scale effect and optimum relation for sea surface planing," National Advisory Committee for Aeronautics, NACA-TM-1097, Washington, 1947.

[50] F. Locke, "Tests of a flat bottom planing surface to determine the inception of planing," US Navy, Report no.1096, 1948.

[51] B. Korvin-Kroukovsky, D. Savitsky and W. Lehman, "Wetted area and center of pressure of planing surfaces," Steven Institute of Technology, Davidson Laboratory Report No. 360, Hoboken, 1949.

[52] A.B. Murray, "The hydrodynamics of planing hulls," Paper presented at the February 1950 meeting of the New England Section of SNAME,

[53] D. Savitsky, "Hydrodynamic design of planing hulls," *Marine Technology*, vol. 1, no. 1, pp. 71-95, 1964.

[54] J. Almeter, "resistance prediction of planing hulls: state of the art," *Marine Technology*, vol. 30, no. 4, pp. 297-307, 1993.

[55] W. Vorus, *Hydrodynamics of planing monohull watercraft*. Switzerland: Springer, 2017.

[56] J. Masri, L. Dala and B. Huard, "A review of the analytical methods used for seaplanes' performance prediction," *Aircraft Engineering and Aerospace Technology*, vol. 91, no. 6, pp. 820-833, 2019.

[57] R. Ibrahim and I. Grace, "Modeling of ship roll dynamics and its coupling with heave and pitch," *Mathematical Problems in Engineering*, vol. 2010, pp. 1-32, 2010.

[58] K. Rawson and E. Tupper, *Basic ship theory*, 5th ed. Boston: Butterworth-Heinemann, 2001.

[59] R. Yousefi, R. Shafaghat and M. Shakeri, "Hydrodynamic analysis techniques for high-speed planing hulls," *Applied Ocean Research*, vol. 42, pp. 105-113, 2013.

[60] M. Morabito, "*On the spray and bottom pressures of planing surfaces*," Ph.D. Thesis, Scha. Sch. Eng. & Sci., Steven Institute of Technology, Hoboken, 2010.

[61] M. Iacono, "*Hydrodynamics of Planing Hulls by CFD*," M.Sc. Dissertation, University of Naples, 2015.

[62] A. Perelmuter, "On the Determination of the Take-Off Characteristics of a Seaplane," National Advisory Committee for Aeronautics, NACA-TM-863, Washington, 1938.

[63] D. Chambliss and G. Boyd, "The planing characteristics of two v-shaped prismatic surfaces having angles of dead rise of 20 degrees and 40 degrees," National Advisory Committee for Aeronautics, Technical Report no. 2876, Langley, 1953.

[64] P. Payne, "Contributions to planing theory," *Ocean Engineering*, vol. 22, no. 7, pp. 699-729, 1995.

[65] W. Perring and L. Johnston, "Hydrodynamic forces and moments on a simple planing surface and on a flying boat hull," Aeronautical Research Council, London, R&M no. 1646, 1935.

[66] W. Sottorf, "Analysis of experimental investigations of the planing process of the surface of water," National Advisory Committee for Aeronautics, NACA-TM-1061, Washington, 1937.

[67] W. Siler, "*Lift and moment of flat rectangular low aspect ratio lifting surfaces*," M.Sc. Dissertation, Steven Institute of Technology, Hoboken, 1949.

[68] B. Korvin-Kroukovsky, "Lift of Planing Surfaces," *Journal of the Aeronautical Sciences*, vol. 17, no. 9, pp. 597-599, 1950.

[69] E. Schnitzer, "Theory and procedure for determining loads and motions in chine-immersed hydrodynamic impacts of prismatic bodies," National Advisory Committee for Aeronautics, NACA-TM-1152, Washington, 1953.

[70] C. Shufford, "A review of planing theory and experiment with a theoretical study of pure-planing lift of rectangular flat plates," National Advisory Committee for Aeronautics, NACA-TM-3233, Washington, 1954.

[71] D. Farshing, "*The lift coefficient of flat planing surfaces*," M.Sc. dissertation, Steven Institute of Technology, Hoboken, 1955.

[72] C. Shufford, "A theoretical and experimental study of planing surfaces including effects of cross section and plan form," National Advisory Committee for Aeronautics, NACA-TM-1355, Washington, 1958.

[73] P. Brown, "An experimental and theoretical study of planing surfaces with trim flaps," Steven Institute of Technology, Report SIT-DL-71-1462, 1971.

[74] A. Browning, "*A Mathematical Model to Simulate Small Boat Behaviour*," Ph.D. Thesis, Bournemouth Polytechnic, 1990.

[75] M. Abkowitz, *Stability and motion Control of ocean vehicles*. Cambridge: M.I.T. Press, 1969.

[76] I. Young, *Wind Generated Ocean Waves*. Burlington: Elsevier, 1999.

[77] S. Thornton and J. Marion, *Classical dynamics of particles and systems*, 5th ed. Belmont: Brooks/Cole, 2004.

[78] L. Meirovitch, *Methods of Analytical Dynamics*. New York: McGraw-Hill, 1970.

[79] L. Marshall, A. Nayfeh and D. Mook, "Forward speed effects in the equations of ship motion," *Journal of Sound and Vibration*, vol. 85, no. 3, pp. 303-313, 1982.

[80] A. Nayfeh, D. Mook and L. Marshall, "Perturbation-energy approach for the development of the nonlinear equations of ship motion," *Journal of Hydronautics*, vol. 8, no. 4, pp. 130-136, 1974.

[81] L. Landau and E. Lifshitz, *Quantum mechanics*, 2nd ed. Oxford: Pergamon Press, 1965.

[82] H. Goldstein, C. Poole and J. Safko, *Classical mechanics*, 3rd ed. Harlow: Pearson, 2001.

[83] S. Ueng, D. Lin and C. Liu, "A ship motion simulation system," *Virtual Reality*, vol. 12, no. 1, pp. 65-76, 2008.

[84] A. Nayfeh, D. Mook and L. Marshall, "Nonlinear coupling of pitch and roll modes in ship motions," *Journal of Hydronautics*, vol. 7, no. 4, pp. 145-152, 1973.

[85] A. Nayfeh and D. Mook, *Nonlinear oscillations*. New York: John Wiley & Sons, 1979.

[86] B. Suleiman, "*Identification of finite-degree-of-freedom models for ship motions*," Ph.D. Thesis, Virginia Polytechnic Institute and State University, 2000.

[87] T. Fossen, *Guidance and control of ocean vehicles*. Chichester: John Wiley & Sons, 1994.

[88] S. Pradeep, "Derivation of perturbed equations of motion of aircraft," *Aircraft Design*, vol. 1, no. 4, pp. 205-215, 1998.

[89] E. Lewandowski, *The dynamics of marine craft*. Singapore: World Scientific, 2004.

[90] T. Ogilvie, "The development of ship-motion theory," University of Michigan, Report no. 021, Michigan, 1969.

[91] N. Salvesen, E. Tuck and O. Faltinsen, "Ship motions and sea loads," Paper presented at the annual meeting of SNAME, New York, 1970.

[92] J. Wu and J. Sheu, "An exact solution for a simplified model of the heave and pitch motions of a ship hull due to a moving load and a comparison with some experimental results," *Journal of Sound and Vibration*, vol. 192, no. 2, pp. 495-520, 1996.

[93] E. Lewis, *Principles of naval architecture*, 3rd ed. New Jersey: SNAME, 1989.

[94] A. Fitriadhy and N. Adam, "Heave and pitch motions performance of a monotricat ship in head-seas," *International Journal Of Automotive And Mechanical Engineering*, vol. 14, no. 2, pp. 4243-4258, 2017.

[95] B. Korvin-Kroukovsky, "Investigation of ship motions in regular waves," Paper presented at the annual meeting of SNAME, New York, 1955.

[96] M. Tuveri, A. Ceruti and P. Marzocca, "Added masses computation for unconventional airships and aerostats through geometric shape evaluation and meshing," *International Journal of Aeronautical and Space Sciences*, vol. 15, no. 3, pp. 241-257, 2014.

[97] W. Lata and K. Thiagarajan, "Comparison of added mass coefficients for a floating tanker evaluated by conformal mapping and boundary element methods," in *16th Australian Fluid Mechanics Conference*, Gold Coast, Australia, 2007, pp.1388-1391.

[98] H. Ghassemi and E. Yari, "The added mass coefficient computation of sphere, ellipsoid and marine propellers using boundary element method," *Polish Maritime Research*, vol. 18, no. 1, pp. 17-26, 2011.

[99] R. Steidel, *An introduction to mechanical vibrations*, 3rd ed. New York: John Wiley & Sons, 1989.

[100] B. Tongue, *Principles of vibration*. New York: Oxford University Press, 2019.

[101] X. Wu, L. Tao and Y. Li, "Nonlinear roll damping of ship motions in waves," *Journal of Offshore Mechanics and Arctic Engineering*, vol. 127, no. 3, pp. 205-211, 2005.

[102] O. Faltinsen, *Sea loads on ships and offshore structures*. Cambridge: Cambridge University Press, 1990.

[103] A. Bhange, "Simpson’s rules and its application in ship stability," *International Journal of Computer & Mathematical Sciences*, vol. 6, no. 2, pp. 22-28, 2017.

[104] T. Fossen and H. Nijmeijer, *Parametric Resonance in Dynamical Systems*. New York, NY: Springer New York, 2012.

[105] I. Kovacic and M. Brennan, *The Duffing Equation: Nonlinear Oscillators and their Behaviour*. Chichester: John Wiley & Sons, 2011.

[106] X. Li, L. Zhang, H. Zhang and K. Li, "Singularity analysis of response bifurcation for a coupled pitch–roll ship model with quadratic and cubic nonlinearity," *Nonlinear Dynamics*, vol. 95, no. 4, pp. 2659-2674, 2019.

[107] A. Kleiman and O. Gottlieb, "Nonlinear Dynamics and Internal Resonances of a Ship with a Rectangular Cross-Section in Head Seas," *Journal of Offshore Mechanics and Arctic Engineering*, vol. 131, no. 4, 2009.

[108] S. Shaw and B. Balachandran, "A Review of Nonlinear Dynamics of Mechanical Systems in Year 2008," *Journal of System Design and Dynamics*, vol. 2, no. 3, pp. 611-640, 2008.

[109] L. Cveticanin, "The Approximate Solving Methods for the Cubic Duffing Equation based on the Jacobi Elliptic Functions," *International Journal of Nonlinear Sciences and Numerical Simulation*, vol. 10, no. 11-12, 2009.

[110] J. Sunday, "The Duffing Oscillator: Applications and Computational Simulations," *Asian Research Journal of Mathematics*, vol. 2, no. 3, pp. 1-13, 2017.

[111] N. Bogolubov and Y. Mitropolski, *Asymptotic methods in the theory of nonlinear oscillations*. Moscow: Hindustan Publishing Corporation, 1961.

[112] H. Babazadeh, D. Ganji and M. Akbarzade, "He's Energy Balance Method to Evaluate the Effect of Amplitude on the Natural Frequency in Nonlinear

Vibration Systems," *Progress In Electromagnetics Research M*, vol. 4, pp. 143-154, 2008.

[113] A. El-Naggar and G. Ismail, "Analytical solution of strongly nonlinear Duffing oscillators," *Alexandria Engineering Journal*, vol. 55, no. 2, pp. 1581-1585, 2016.

[114] Y. Farzaneh and A. Akbarzadeh Tootoonchi, "Global Error Minimization method for solving strongly nonlinear oscillator differential equations," *Computers & Mathematics with Applications*, vol. 59, no. 8, pp. 2887-2895, 2010.

[115] J. He, "Variational iteration method – a kind of non-linear analytical technique: some examples," *International Journal of Non-Linear Mechanics*, vol. 34, no. 4, pp. 699-708, 1999.

[116] J. He, "Homotopy perturbation method: a new nonlinear analytical technique," *Applied Mathematics and Computation*, vol. 135, no. 1, pp. 73-79, 2003.

[117] K. Guo and S. Cao, "Modified Lindstedt-Poincaré method for obtaining resonance periodic solutions of nonlinear non-autonomous oscillators," *Transactions of Tianjin University*, vol. 20, no. 1, pp. 66-71, 2014.

[118] M. Holmes, *Introduction to perturbation methods*, 2nd ed. New York: Springer, 2013.

[119] A. Nayfeh, *Perturbation methods*. New York: John Wiley & Sons, 1973.

[120] A. Nayfeh, *Introduction to perturbation techniques*. New York: John Wiley & Sons, 1981.

[121] J. Murdock, *Perturbation theory and methods*. New York: John Wiley & Sons, 1991.

[122] A. Fetter and J. Walecka, *Nonlinear mechanics: a supplement to theoretical mechanics of particles and continua*. New York: Dover Publications, Inc, 2006.

[123] J. Kevorkian and J. Cole, *Perturbation methods in applied mathematics*. Heidelbers: Springer-Verlag, 1981.

[124] J. Logan, *Applied Mathematics*, 4th ed. Hoboken, New Jersey: John Wiley & Sons, 2013.

[125] N. Staff, *Twenty-First Symposium on Naval Hydrodynamics*. Washington: National Academies Press, 1997.

[126] P. Drazin, *Nonlinear systems*. Cambridge: Cambridge University Press, 1992.

[127] A. Sayma, *Computational Fluid Dynamics*. Bookboon, 2009.

[128] P. Kundu, I. Cohen, D. Dowling, P. Ayyaswamy and H. Hu, *Fluid mechanics*, 5th ed. Waltham, MA: Academic Press, 2012.

[129] A. Williams, "*Aerodynamic Forces on High-Speed Multihulled Marine Vehicles*," Ph.D. Thesis, Sch. of Eng., Cranfield University, 2008.

[130] W. Oberkampf and T. Trucano, "Verification and validation in computational fluid dynamics," *Progress in Aerospace Sciences*, vol. 38, no. 3, pp. 209-272, 2002.

[131] R. Cosner, "The importance of uncertainty estimation in computational fluid dynamics," in *41st AIAA Aerospace Science Meeting and Exhibit*, St. Louise, MO, 2003.

[132] J. Anderson, *Computational fluid dynamics*. New York: McGraw-Hill, 1995.

[133] C. Liu, G. Zhou, W. Shyy and K. Xu, "Limitation principle for computational fluid dynamics," *Shock Waves*, vol. 29, no. 8, pp. 1083-1102, 2019.

[134] J. Shang, "Landmarks and new frontiers of computational fluid dynamics," *Advances in Aerodynamics*, vol. 1, no. 1, 2019.

[135] C. Fletcher, *Computational techniques for fluid dynamics*, 2nd ed. Berlin: Springer-Verlag, 1991.

[136] J. Tu, G. Yeoh and C. Liu, *Computational fluid dynamics: a practical approach*, 3rd ed. Amsterdam: Butterworth-Heinemann, 2018.

[137] J. Ferziger and M. Perić, *Computational methods for fluid dynamics*, 3rd ed. Berlin: Springer-Verlag, 2002.

[138] J. Matsson, *An introduction to ANSYS Fluent 2019*. Mission, KS: SDC Publications, 2019.

[139] C. Yue, S. Guo and M. Li, "ANSYS FLUENT-based Modeling and Hydrodynamic Analysis for a Spherical Underwater Robot," in *International Conference on Mechatronics and Automation*, Takamatsu, Japan, 2013.

[140] Gourlay, Tim, Alexander von Graefe, Vladimir Shigunov, and Evert Lataire. "Comparison of AQWA, GL RANKINE, MOSES, OCTOPUS, PDSTRIP and WAMIT with model test results for cargo ship wave-induced motions in shallow water," in *ASME 2015 34th International Conference on Ocean, Offshore and Arctic Engineering*. American Society of Mechanical Engineers Digital Collection, Newfoundland, Canada 2015.

[141] N. Javanmardi and P. Ghadimi, "Hydroelastic analysis of a semi-submerged propeller using simultaneous solution of Reynolds-averaged Navier–Stokes equations and linear elasticity equations," *Proceedings of the Institution of Mechanical Engineers, Part M: Journal of Engineering for the Maritime Environment*, vol. 232, no. 2, pp. 199-211, 2017.

[142] Y. Ozdemir and B. Barlas, "Numerical study of ship motions and added resistance in regular incident waves of KVLCC2 model," *International*

Journal of Naval Architecture and Ocean Engineering, vol. 9, no. 2, pp. 149-159, 2017.

[143] A. Hellsten, "Some improvements in Menter's k - ω SST turbulence model," in *29th AIAA Fluid Dynamics Conference*, Albuquerque, NM, 1998.

[144] F. Menter, "Two-equation eddy-viscosity turbulence models for engineering applications," *AIAA Journal*, vol. 32, no. 8, pp. 1598-1605, 1994.

[145] S. Mahdi Sajedi, P. Ghadimi, M. Sheikholeslami and M. Ghassemi, "Experimental and numerical analyses of wedge effects on the rooster tail and porpoising phenomenon of a high-speed planing craft in calm water," *Proceedings of the Institution of Mechanical Engineers, Part C: Journal of Mechanical Engineering Science*, vol. 233, no. 13, pp. 4637-4652, 2019.

[146] L. Wang, R. Quant and A. Kolios, "Fluid structure interaction modelling of horizontal-axis wind turbine blades based on CFD and FEA," *Journal of Wind Engineering and Industrial Aerodynamics*, vol. 158, pp. 11-25, 2016.

[147] M. Hosain, U. Sand and R. Fdhila, "Numerical Investigation of Liquid Sloshing in Carrier Ship Fuel Tanks," *IFAC-PapersOnLine*, vol. 51, no. 2, pp. 583-588, 2018.

[148] H. Wang and Z. Zou, "Numerical study on hydrodynamic interaction between a berthed ship and a ship passing through a lock," *Ocean Engineering*, vol. 88, pp. 409-425, 2014.

[149] T. Tezdogan, Y. Demirel, P. Kellett, M. Khorasanchi, A. Incecik and O. Turan, "Full-scale unsteady RANS CFD simulations of ship behaviour and performance in head seas due to slow steaming," *Ocean Engineering*, vol. 97, pp. 186-206, 2015.

[150] B. Venkatachari, G. Cheng, B. Soni and S. Chang, "Validation and verification of Courant number insensitive CE/SE method for transient

viscous flow simulations," *Mathematics and Computers in Simulation*, vol. 78, no. 5-6, pp. 653-670, 2008.

[151] S. He, D. Liu and D. Tan, "Comparison of Various Spatial Discretization Schemes in Numerical Simulation for Ship Airwakes," *Applied Mechanics and Materials*, vol. 627, pp. 63-68, 2014.

[152] S. Samaei, F. Azarsina and M. Ghahferokhi, "Numerical simulation of floating pontoon breakwater with ANSYS AQWA software and validation of the results with laboratory data," *Bulletin de la Société Royale des Sciences de Liège*, vol. 85, pp. 1487-1499, 2016.

[153] H. Ye, Z. Shen and D. Wan, "Numerical prediction of added resistance and vertical ship motions in regular head waves," *Journal of Marine Science and Application*, vol. 11, no. 4, pp. 410-416, 2012.

[154] M. Liu, L. Lu, B. Teng, M. Zhao and G. Tang, "Numerical modeling of local scour and forces for submarine pipeline under surface waves," *Coastal Engineering*, vol. 116, pp. 275-288, 2016.

[155] L. Holthuijsen, *Waves in oceanic and coastal waters*. Cambridge: Cambridge University Press, 2015.

[156] J. Fenton, "A high-order cnoidal wave theory," *Journal of Fluid Mechanics*, vol. 94, pp. 129-161, 1979.

[157] M. Maâtoug and M. Ayadi, "Numerical simulation of the second-order Stokes theory using finite difference method," *Alexandria Engineering Journal*, vol. 55, no. 3, pp. 3005-3013, 2016.

APPENDIX A

Strip Theory Calculations

Strip theory calculations are applied in which the coefficients of the heave and pitch equations (equations 3.7 and 3.8) will be determined next for a planing hull with the geometrical data given in Table 10. The wave characteristics are considered to be regular which means that the wavelength is assumed to be equal to the length of the planing hull, wave amplitude is 0.2 ft and wave velocity is 9.9 ft/s [6]. The speed of the hull is assumed to be 4.788 ft/s.

Table 10. Planing hull geometrical characteristics [6]

Parameter	Value
Length of model	19.2 ft
Maximum beam length	2.592 ft
Maximum draft	1.144 ft
Displacement	2837.76 lb
Radius of gyration	4.588 ft

In order to calculate the encounter frequency, the wave frequency is calculated first from the following equation:

$$\omega_w = \sqrt{\frac{2\pi g}{L_w}} \tag{A.1}$$

Then:

$$\omega_w = \sqrt{\frac{2 * 3.14 * 32.2}{19.2}} = 3.245\ rad/s$$

The encounter frequency can be found from equation (3.5) as follows:

$$\omega_e = 3.245 - \frac{3.245^2 * 4.788}{32.2}\cos(180) = 4.811\ rad/s$$

The planing hull is now divided into 4 segments as shown in Figure 89. The area between stations 1, 2 and 3 is assumed to have a rectangular shape which means that the beam length is equal in the three stations.

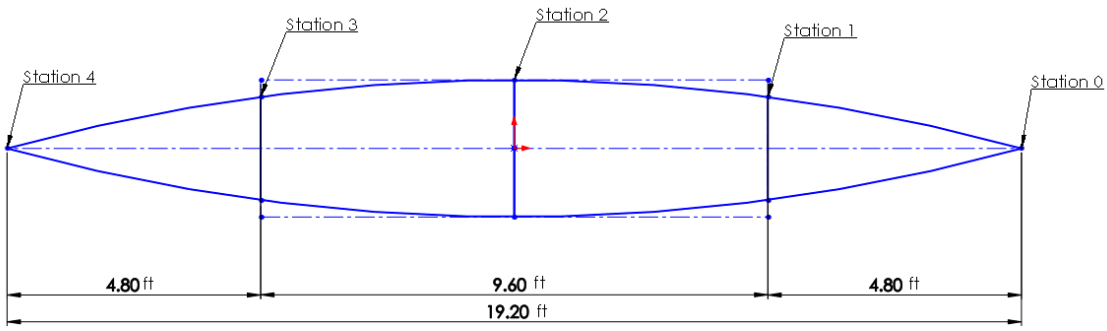

Figure 89. Planing hull segments

The calculations will be performed next and will be presented in form of tables. In Table 11, the added mass coefficient in the heave direction due to motion in the heave (added mass force for heaving A_{33}) and the added mass coefficient in the pitch direction due to motion in the pitch (added mass moment for pitching A_{55}) will be calculated. After that, in Table 12, damping coefficients due to heaving and pitching motions in heave and pitch axes respectively will be determined (B_{33} and B_{55}). Next, the hydrostatic restoring force and moment due to the same action as the two previous coefficients will be calculated in Table 13 (C_{33} and C_{55}). Afterwards, the cross-coupling coefficients A_{35}, A_{53}, B_{35}, B_{53}, C_{35} and C_{53} will be determined in Table 14. Finally, in Table 15, the exciting force function $F(t)$ and moment function $M(t)$ of the two equations are calculated.

Table 11. Calculations for A_{33} and A_{55}

(1) Station No.	(2) Beam length B	(3) Draft length T	(4) Sectional area A_s	(5) Distance from station to LCB	(6) $\omega_e^2 \times \frac{B}{2g}$	(7) $\frac{B}{T}$
0	0	1.144	0	9.12	0	0
1	2.592	1.144	2.965	4.32	0.932	2.266
2	2.592	1.144	2.965	-0.48	0.932	2.266
3	2.592	1.144	2.965	-5.28	0.932	2.266
4	0	1.144	0	-10.08	0	0

(8) $B \times T$	(9) $\frac{A_s}{B \times T}$	(10)* Added mass coefficient C_a	(11) Beam length squared	(12) $\rho\pi \times \frac{B^2}{8}$	(13) Sectional added mass a_n (10)×(12)	(14)** Simpson's Multiplier
0	0	0	0	0	0	1
2.965	1	0.98	6.718	5.115	5.0127	4
2.965	1	0.98	6.718	5.115	5.0127	2
2.965	1	0.84	6.718	5.115	4.296	4
0	0	0	0	0	0	1

(15) (13)×(14)	(16) Distance from station to LCB squared	(17) (13)×(16)	(18) Simpson's Multiplier	(19) (17)×(18)
0	83.174	0	1	0
20.05	18.662	93.547	4	374.188
10.025	0.230	1.1529	2	2.305
17.184	27.878	119.763	4	479.052

0	101.606	0	1	0
SUM_1: 47.259				SUM_2: 855.545

*The added mass coefficient C_a depends on the speed of the planing hull, the beam-to-draft ratio and the encounter frequency. It is given in [6] based on previous experimental investigations.

**Simpson's Multiplier is a method used to approximate the area of a curved figure. There are three rules of this method. The first rule is usually used in ship stability when the hull is divided into an odd number of stations. More details about the derivation of this method can be found in [103].

The added mass for heaving A_{33} and the added mass for pitching A_{55} can be found as follows:

$$A_{33} = \frac{1}{3} \times S \times SUM_1 = \frac{1}{3} \times 4.8 \times 47.259 = 75.6144\ lb.sec^2/ft$$

$$A_{55} = \frac{1}{3} \times S \times SUM_2 = \frac{1}{3} \times 4.8 \times 855.545 = 1368.872\ lb.sec^2.ft$$

Where S is the distance between each segment.

Table 12. Calculations for B_{33} and B_{55}

(1) Station No.	(2) $\omega_e^2 \times \frac{B}{2g}$	(3) $\frac{B}{T}$	(4) $\frac{A_s}{B \times T}$	(5)* Amplitude ratio for heaving $\check{A}$	(6) Amplitude ratio for heaving $\check{A}$ squared	(7)** Sectional damping coefficient b_n
0	0	0	0	0	0	0
1	0.932	2.266	1	0.57	0.325	5.87
2	0.932	2.266	1	0.57	0.325	5.87

3	0.932	2.266	1	0.66	0.436	7.87
4	0	0	0	0		0
(8) Simpson's Multiplier	(9) (7)×(8)	(10) Distance from station to LCB squared	(11) (7)×(10)	(12) Simpson's Multiplier	(13) (11)×(12)	
1	0	83.174	0	1	0	
4	23.48	18.662	109.545	4	438.18	
2	11.74	0.230	1.35	2	2.7	
4	31.48	27.878	219.34	4	877.36	
1	0	101.606	0	1	0	
	SUM_3: 66.7				SUM_4: 1318.24	

*The amplitude ratio for a two-dimensional body in heaving motion $\check{A}$ depends on the speed of the planing hull, the beam-to-draft ratio and the encounter frequency. It is given in [6] based on previous experimental investigations.

**The Sectional damping coefficient b_n is calculated from the following equation:

$$b_n = \frac{\rho g^2 \check{A}^2}{\omega_e^3}$$

The damping coefficients due to heaving B_{33} and pitching B_{55} can be calculated as follows:

$$B_{33} = \frac{1}{3} \times S \times SUM_3 = \frac{1}{3} \times 4.8 \times 66.7 = 106.72\ lb.sec/ft$$

$$B_{55} = \frac{1}{3} \times S \times SUM_4 = \frac{1}{3} \times 4.8 \times 1318.24 = 2109.184\ ft.lb.sec/rad$$

Table 13. Calculations for C_{33} and C_{55}

(1) Station No.	(2) Beam length B	(3)* Sectional restoring force coefficient c_n	(4) Simpson's Multiplier	(5) (3)×(4)	(6) Distance from station to LCB squared	(7) (3)×(6)
0	0	0	1	0	83.174	0
1	2.592	161.91	4	647.64	18.662	3021.56
2	2.592	161.91	2	323.82	0.230	37.24
3	2.592	161.91	4	647.64	27.878	4513.723
4	0	0	1	0	101.606	0
				SUM_5: 1619.1		

(8) Simpson's Multiplier	(9) (7)×(8)
1	0
4	12086.24
2	74.48
4	18054.892
1	0
	SUM_6: 30215.612

*The Sectional restoring force coefficient c_n is calculated from the following equation:

$$c_n = \rho g b_n$$

The hydrostatic restoring force due to heaving C_{33} can be found as follows:

$$C_{33} = \frac{1}{3} \times S \times SUM_5 = \frac{1}{3} \times 4.8 \times 1619.1 = 2590.56\ lb/ft$$

Table 14. Calculations of A_{35}, A_{53}, B_{35}, B_{53}, C_{35} and C_{53}

(1) Station No.	(2) Distance from station to LCB	(3) Sectional added mass a_n	(4) (2)×(3)	(5) Simpson's Multiplier	(6) (4)×(5)	(7) Sectional damping coefficient b_n
0	9.12	0	0	1	0	0
1	4.32	5.0127	21.655	4	86.62	5.87
2	-0.48	5.0127	-2.406	2	-4.812	5.87
3	-5.28	4.296	-22.68	4	-90.72	7.87
4	-10.08	0	0	1	0	0
					SUM_7: -8.912	
(8) (2)×(7)	(9) Simpson's Multiplier	(10) (8)×(9)	(11) Sectional restoring force coefficient c_n	(12) (2)×(11)	(13) Simpson's Multiplier	(14) (12)×(13)
0	1	0	0	0	1	0
25.358	4	101.432	161.91	699.45	4	2797.8
-2.8176	2	-5.6352	161.91	-77.72	2	-155.44
-41.55	4	-166.2	161.91	-854.88	4	-3419.52
0	1	0	0	0	1	0
		SUM_8: -70.4				SUM_9: -777.16

The cross-coupling coefficients can then be calculated as follows:

$$A_{35} = -\frac{1}{3} \times S \times SUM_7 = -\frac{1}{3} \times 4.8 \times -8.912 = 14.256\ lb.sec^2$$

$$A_{35} = A_{53} = 14.256\ lb.sec^2$$

$$B_{35} = -\frac{1}{3} \times S \times SUM_8 + V \times A_{33} = -\frac{1}{3} \times 4.8 \times -70.4 + 4.788 \times 75.6144$$
$$= 474.7\ lb.sec$$

$$B_{53} = -\frac{1}{3} \times S \times SUM_8 - V \times A_{33} = -\frac{1}{3} \times 4.8 \times -70.4 - 4.788 \times 75.6144$$
$$= -249.4\ lb.sec$$

$$C_{35} = -\frac{1}{3} \times S \times SUM_9 + V \times B_{33} = -\frac{1}{3} \times 4.8 \times -777.16 + 4.788 \times 106.72$$
$$= 1754.43\ lb$$

$$C_{53} = -\frac{1}{3} \times S \times SUM_9 = -\frac{1}{3} \times 4.8 \times -777.16 = 1243.456\ lb$$

$$C_{55} = \frac{1}{3} \times S \times SUM_6 - V \times B_{53} = \frac{1}{3} \times 4.8 \times 30215.612 - 4.788 \times -249.4$$
$$= 49539.1\ lb.ft/rad$$

Table 15. Calculations for exciting forces and moments

(1) Station No.	(2) Distance from station to LCB *D*	(3) $\frac{2\pi}{L_w} \times$ (2)	(4) sin((3))	(5) cos((3))	(6) Draft length *T*	(7) $\frac{2\pi}{L_w} \times$ (6)
0	9.12	2.983	0.158	-0.987	0	0
1	4.32	1.413	0.987	0.157	1.144	0.374
2	-0.48	-0.157	-0.156	0.987	1.144	0.374
3	-5.28	-1.727	-0.987	-0.155	1.144	0.374

4	-10.08	-3.297	0.155	-0.987	0	0
(8) $e^{((7))}$	(9) Sectional restoring force coefficient c_n	(10) (9)×wave amplitude	(11) Sectional added mass a_n	(12) (11)× ω_e^2 × -1×wave amplitude	(13) (12) + (10)	(14)* Slope of the added mass curve
1	0	0	0	0	0	-1.044
0.68785	161.91	32.382	5.0127	-23.2	9.182	-0.522
0.68785	161.91	32.382	5.0127	-23.2	9.182	0.075
0.68785	161.91	32.382	4.296	-19.89	12.492	0.522
1	0	0	0	0	0	0.895
(15) (14)× V × ω_e×wave amplitude	(16) Sectional damping coefficient b_n	(17) (16)× ω_e× wave amplitude	(18) (17) – (15)	(19) (13)×(4)	(20) (18)×(5)	(21) (19) + (20)
-4.811	0	0	4.811	0	-4.75	-4.75
-2.4	5.87	5.65	8.05	9.063	1.263	10.326
0.344	5.87	5.65	5.306	-1.432	5.237	3.805
2.4	7.87	7.57	5.17	-12.33	-0.801	13.131
4.12	0	0	-4.12	0	4.066	4.066
(22) (13)×(5)	(23) (18)×(4)	(24) (22) – (23)	(25) (21)×(8)	(26) Simpson's Multiplier	(27) (25)×(26)	(28) (24)×(8)
0	0.76	-0.76	-4.75	1	-4.75	-0.76
1.44	7.95	-6.5	7.1	4	28.4	-4.47
9.064	-0.82	9.88	2.61	2	5.22	6.8
-1.945	-5.1	3.155	-9.04	4	-36.16	2.17
0	-0.64	0.64	4.075	1	4.075	0.64
					SUM_{10}:	

					-3.215	
(29) Simpson's Multiplier	(30) (28)×(29)	(31) (25)×(2)	(32) Simpson's Multiplier	(33) (31)×(32)	(34) (28)×(2)	(35) Simpson's Multiplier
1	-0.76	-43.32	1	-43.32	-6.9312	1
4	-17.88	30.672	4	122.688	-19.3104	4
2	13.6	-1.25	2	-2.5	-3.264	2
4	8.68	47.73	4	190.92	-11.5	4
1	0.64	-41	1	-41	-6.5	1
	SUM_{11}: 4.3			SUM_{12}: 226.8		

(36) (34)×(35)
6.9312
-77.2416
-6.53
-46
-6.5
SUM_{13}: -143.2

*The slope of the added mass curve at the leading edge of the planing hull can be found as follows:

$$\frac{da_n}{dD} = \left(\frac{a_{n5} - a_{n0}}{D_5 - D_0}\right) = \left(\frac{5.0127 - 0}{4.32 - 9.12}\right) = -1.044$$

At the central stations, the added mass curve can be found as follows:

$$\frac{da_n}{dD} = \frac{1}{2}\left(\frac{a_{n5} - a_{n0}}{D_5 - D_0} + \frac{a_{n10} - a_{n5}}{D_{10} - D_5}\right) = \frac{1}{2}\left(\frac{5.0127 - 0}{4.32 - 9.12} + \frac{5.0127 - 5.0127}{-0.48 - 4.32}\right)$$
$$= -0.522$$

Finally, the excitation loads can be calculated as follows:

$$F_1 = \frac{1}{3} \times S \times SUM_{10} = \frac{1}{3} \times 4.8 \times -3.215 = -5.2\ lb$$

$$F_2 = \frac{1}{3} \times S \times SUM_{11} = \frac{1}{3} \times 4.8 \times 4.3 = 6.9\ lb$$

$$M_1 = \frac{1}{3} \times S \times SUM_{12} = \frac{1}{3} \times 4.8 \times 226.8 = 363\ ft.lb$$

$$M_2 = \frac{1}{3} \times S \times SUM_{13} = \frac{1}{3} \times 4.8 \times -143.2 = -229.12\ ft.lb$$

$$F_R = \sqrt{F_1^2 + F_2^2} = \sqrt{(-5.2)^2 + (6.9)^2} = 8.64\ lb$$

$$M_R = \sqrt{M_1^2 + M_2^2} = \sqrt{(363)^2 + (-229.12)^2} = 429.26\ ft.lb$$

The phase lag angles of the exciting force and moment can be calculated as follows:

$$\sigma = (\tan^{-1}\frac{F_2}{F_1} + 180) = (\tan^{-1}\frac{6.9}{-5.2} + 180) = 127°$$

$$\tau = \tan^{-1}\frac{M_2}{M_1} = \tan^{-1}\frac{-229.12}{363} = -32°$$

The mass of the planing hull m and the mass moment of inertia I_{55} can be found as follows:

$$m = \frac{Disp.}{g} = \frac{2837.76}{32.2} = 88.13\ slug$$

$$I_{55} = (0.234 \times L)^2 \times m = 1779\ ft.lb.sec^2$$

With all of the coefficients calculated, the equations of heave and pitch can be written as follows:

$$(88.13 + 75.6144) \times \ddot{\eta}_3 + 14.256 \times \ddot{\eta}_5 + 106.72 \times \dot{\eta}_3 + 474.7 \times \dot{\eta}_5 + 2590.56 \times \eta_3 + 1754.43 \times \eta_5 = -5.2\cos(4.811t) + 6.9\sin(4.811t) = 8.64\cos(4.811t + 127)$$

$$14.256 \times \ddot{\eta}_3 + (1368.872 + 1779) \times \ddot{\eta}_5 - 249.4 \times \dot{\eta}_3 + 2109.184 \times \dot{\eta}_5 + 1243.456 \times \eta_3 + 49539.1 \times \eta_5 = 363\cos(4.811t) - 229.12\sin(4.811t) = 429.26\cos(4.811t - 32)$$

APPENDIX B

User Defined Function (UDF) used to obtain the CFD results

The UDF used to restrict the motion of the hull and record the structural response is shown below:

```
#include "udf.h"

#include "math.h"

DEFINE_SDOF_PROPERTIES(mov, prop, dt, time, dtime)

{

prop[SDOF_MASS]= 1296;

prop[SDOF_IXX] = 62;

prop[SDOF_IYY] = 3455.07;

prop[SDOF_IZZ] = 3517.08;

prop[SDOF_ZERO_TRANS_X]= TRUE;

prop[SDOF_ZERO_TRANS_Y]= FALSE;

prop[SDOF_ZERO_TRANS_Z]= TRUE;

prop[SDOF_ZERO_ROT_X]= TRUE;

prop[SDOF_ZERO_ROT_Y]= TRUE;

prop[SDOF_ZERO_ROT_Z]= FALSE;

}
```

Note this is the UDF used to produce the results of the hull presented in [6]. The mass and mass moment of inertia of the other hull examined are different.

APPENDIX C

The Visual Basic code developed to perform the strip theory calculations

The code developed in shown below:

```
Public Class Form1

    Private Sub Form1_Load(sender As Object, e As EventArgs) Handles
MyBase.Load

    End Sub

    Private Sub Button1_Click(sender As Object, e As EventArgs) Handles
Button1.Click
        Dim a1, b1, F1, M1, M2, C35, m, A33, C53, A55, Iyy, FR, Ma, Mb, wo,
C55, C33 As Double

        C35 = textC35.Text
        m = textm.Text
        A33 = textA33.Text
        C53 = textC53.Text
        A55 = textA55.Text
        Iyy = textIyy.Text
        FR = textFR.Text
        Mb = textMb.Text
        Ma = textMa.Text
        C55 = textC55.Text
        C33 = textC33.Text



        a1 = C35 / (m + A33)
        b1 = C53 / (A55 + Iyy)
        F1 = FR / (m + A33)
        M1 = Ma / (A55 + Iyy)
        M2 = Mb / (A55 + Iyy)
        wo = (C33 / (m + A33)) ^ 0.5


        texta1.Text = a1
        textb1.Text = b1
        textF1.Text = F1
        textM1.Text = M1
        textM2.Text = M2
        textwo.text = wo



    End Sub
```

```
    Private Sub Button2_Click(sender As Object, e As EventArgs) Handles
Button2.Click
        texta1.Text = ""
        textb1.Text = ""
        textF1.Text = ""
        textM1.Text = ""
        textM2.Text = ""
        textwo.Text = ""
        textC35.Text = ""
        textm.Text = ""
        textA33.Text = ""
        textC53.Text = ""
        textA55.Text = ""
        textIyy.Text = ""
        textFR.Text = ""
        textMb.Text = ""
        textMa.Text = ""
        textC55.Text = ""
        textC33.Text = ""
    End Sub

    Private Sub Button3_Click(sender As Object, e As EventArgs) Handles
Button3.Click
        textC35.Text = 1753.2
        textm.Text = 88.8
        textA33.Text = 75.6
        textC53.Text = 1242.5
        textA55.Text = 1368.5
        textIyy.Text = 1780.2
        textFR.Text = 9.906
        textMb.Text = -231.79
        textMa.Text = 372.6
        textC55.Text = 49501.6
        textC33.Text = 2588.5

    End Sub

    Private Sub Label2_Click(sender As Object, e As EventArgs) Handles
Label2.Click

    End Sub

    Private Sub Button4_Click(sender As Object, e As EventArgs) Handles
Button4.Click
        textC35.Text = -28
        textm.Text = 1.031
        textA33.Text = 0.879
        textC53.Text = -17.2
        textA55.Text = 1.199
        textIyy.Text = 1.611
        textFR.Text = 1.1
        textMb.Text = 2
        textMa.Text = 3
        textC55.Text = 190.3
        textC33.Text = 147.1
    End Sub

    Private Sub Button5_Click(sender As Object, e As EventArgs) Handles
Button5.Click
```

```
        textC35.Text = -11.8
        textm.Text = 1.031
        textA33.Text = 0.939
        textC53.Text = 5.2
        textA55.Text = 1.399
        textIyy.Text = 1.611
        textFR.Text = 0.68
        textMb.Text = 2.27
        textMa.Text = 3.27
        textC55.Text = 226.1
        textC33.Text = 160.2
    End Sub

    Private Sub Button6_Click(sender As Object, e As EventArgs) Handles
Button6.Click
        textC35.Text = -7.5
        textm.Text = 1.031
        textA33.Text = 0.939
        textC53.Text = 5.2
        textA55.Text = 1.399
        textIyy.Text = 1.611
        textFR.Text = 0.54
        textMb.Text = 2
        textMa.Text = 3
        textC55.Text = 226.6
        textC33.Text = 160.2
    End Sub
End Class
```

The window of the VB code is shown below:

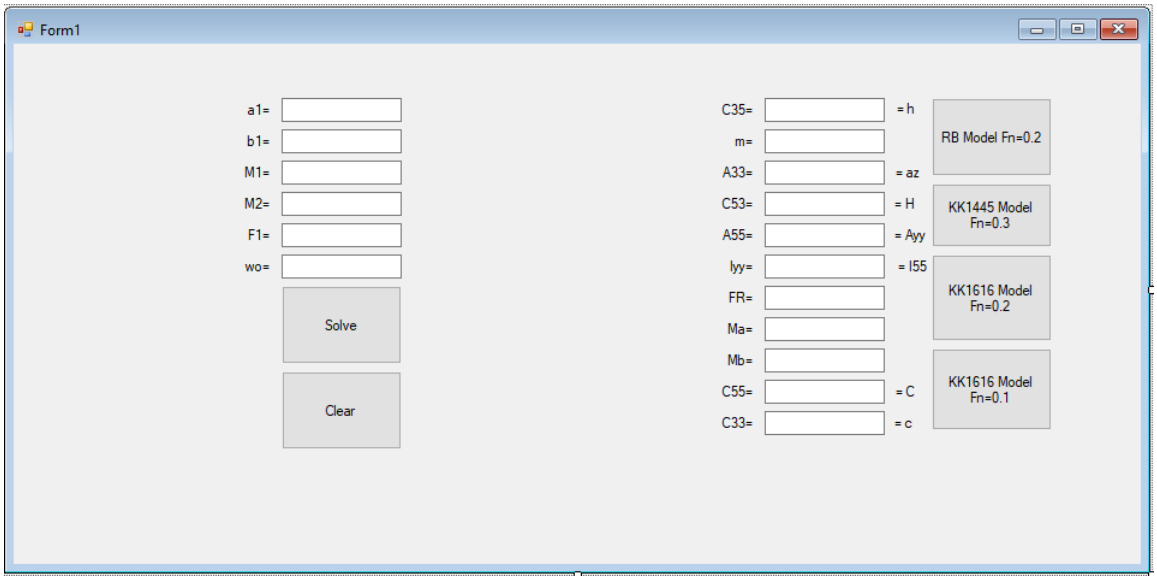

Figure 90. The VB code window

APPENDIX D

The MATLAB code used to obtain the analytical solution

The code used to get the heave and pitch motion history is shown below:

```
t=0:0.01:30;

%RB Model Fn= 0.2
% A=0.00181;
% w0=3.968;
% M1=0.118334550766983;
% M2= -0.0736145075745546;
% e=0.01;
% a1=10.6642335766423;
% a2=100;
% b1=0.394607298250071;
% b2=100;
% F1=0.0602554744525548;

% K-K model 1445 Fn=0.3
% A=0.01597;
% w0=8.77585932010551;
% M1=1.06761565836299;
% M2= 0.711743772241993;
% e=0.01;
% a1=-14.6596858638743;
% a2=100;
% b1=-6.12099644128114;
% b2=100;
% F1=0.575916230366492;

% K-K model 1616 Fn=0.2
% A=0.246;
% w0=2.6389;
% M1=1.08637873754153;
% M2= 0.754152823920266;
% e=0.01;
% a1=-5.98984771573604;
% a2=100;
% b1=1.72757475083057;
% b2=100;
% F1=0.09277664974619;

% % K-K model 1616 Fn=0.1
% A=0.02;
% w0=8;
% M1=0.996;
% M2= 0.664;
% e=0.01;
% a1=-3.8;
% a2=171144;
% b1=1.727;
```

```
% b2=171144;
% F1=0.07;

% RB Model Fn=0.1
A=0.265;
w0=3.0;
M1=0.6;
M2= 0.1;
e=0.01;
a1=6.811;
a2=100;
b1=0.394;
b2=100;
F1=0.5;

w1=((3*a2*A^3*M1)-(4*A*b1*F1)+(4*F1*M2))/(8*A*M1*w0);

w=w0+(e*w1)

% w=w0;

H=A*sin(w*t)-((e*a2*(A^3))/(32*w0*w0))*cos(3*w*t);

P= (F1/a1)*cos(w*t+3)+(F1*(M2-
A*b1)/(a1*M1))*sin(w*t+3)+((e*b2*(F1^3)*(A*b1-M2)*(M2^2-
2*A*b1*M2+A^2*b1^2-3*M1^2))/(32*a1^3*M1^3*w0^2))*sin(3*w*t+3)-
((e*b2*F1^3*(3*M2^2-6*A*b1*M2+3*A^2*b1^2-
M1^2))/(32*a1^3*M1^2*w0^2))*cos(3*w*t+3);

figure(1)
clf
plot(t,H), title('Heave vs Time'), xlabel('t (s)'), ylabel('Heave
(ft)')
legend({'Analytical Nonlinear'},'Location','northeast')
set(gca, 'FontName', 'Times')

figure (2)
clf
plot(t,P), title('Pitch vs Time'), xlabel('t (s)'), ylabel('Pitch
(rad)')
legend({'Analytical Nonlinear'},'Location','northeast')
set(gca, 'FontName', 'Times')

figure (3)
clf
plot(H,P), title('Pitch vs Heave'), xlabel('Heave (ft)'),
ylabel('Pitch (rad)')
legend({'Analytical Nonlinear'},'Location','northeast')
set(gca, 'FontName', 'Times')
```

APPENDIX E

The MATLAB ODE45 code used

The code used to obtain the numerical solution of the heave and pitch equations is shown below:

```
function [time, x, xdot, y, ydot]=
Duffingforced_numerical_heave_pitch_coupled_and_uncoupled

% x is the heave translational motion
% y is the pitch rotational motion

%values of initial conditions and time span

x0=-1.17690774082021e-11;
xdot0=0.00713441437119366;
y0=0.00565023949620481;
ydot0=-0.0141261033918153;
t0=0;
tf=10; % values of coefficients

% RB Model Fn=0.2
A=0.00181;
wo=3.968;
M1=0.118334550766983;
M2= -0.0736145075745546;
e=0.01;
a1=10.6642335766423;
a2=100;
b1=0.394607298250071;
b2=100;
F1=0.0602554744525548;
% wh=3.9653;
% wp=3.9653;

% KK Model 1445 Fn=0.3
% A=0.01597;
% wo=8.77585932010551;
% M1=1.06761565836299;
% M2= 0.711743772241993;
% e=0.01;
% a1=-14.6596858638743;
% a2=100;
% b1=-6.12099644128114;
% b2=100;
% F1=0.575916230366492;
% wh= 11.42;
% wp= 11.42;
```

```
% K-K model 1616 Fn=0.2
% A=0.01213;
% wo=9.01774899596982;
% M1=1.08637873754153;
% M2= 0.754152823920266;
% e=0.01;
% a1=-5.98984771573604;
% a2=100;
% b1=1.72757475083057;
% b2=100;
% F1=0.345177664974619;
% wp=9.82;
% wh=9.82;

% K-K model 1616 Fn=0.1
% A=0.00434;
% wo=9.01774899596982;
% M1=0.996677740863787;
% M2= 0.664451827242525;
% e=0.01;
% a1=-3.80710659898477;
% a2=5000;
% b1=1.72757475083057;
% b2=5000;
% F1=0.274111675126904;
% wp=8.25;
% wh=8.25;

%uncoupled system
% A=0.00434;
% wo=1;
% M1=5;
% M2= 0.5;
% e=0.01;
% a1=0;
% a2=2662;
% b1=0;
% b2=2758;
% F1=5;
% wp=1.25;
% wh=1.25;


 w1=((3*a2*A^3*M1)-(4*A*b1*F1)+(4*F1*M2))/(8*A*M1*wo);
 wh=wo+(e*w1);
 wp=wo+(e*w1);


tspan=[t0, tf]; % time span


% initial conditions
IC= [x0, xdot0, y0, ydot0];

% sdot = g(t,s)
sdot= @(t,s)[s(2);
```

```
 ((e*F1*cos(wh*t))-(wo*wo*s(1))-(e*a1*s(3))-(e*a2*((s(1))^3)));
 s(4);
 ((e*M1*cos(wp*t))+(e*M2*sin(wp*t))-(wo*wo*s(3))-(e*b1*s(1))-
(e*b2*((s(3))^3)))];

%(e*M2*sin(wp*t))

% call ode45 solver
[time, state_values ]= ode45(sdot,tspan,IC);

% extract individual values
x=state_values(:,1);
xdot=state_values(:,2);
y=state_values(:,3);
ydot=state_values(:,4);

% plot heave and pitch
figure(1)
clf
plot(time,x,'g'), title('Heave vs Time'), xlabel('t (s)'),
ylabel('Heave (ft)')
legend({'Numerical Nonlinear'},'Location','northeast')
set(gca, 'FontName', 'Times')

figure (2)
clf
plot(time,y,'g'), title('Pitch vs Time'), xlabel('t (s)'),
ylabel('Pitch (rad)')
legend({'Numerical Nonlinear'},'Location','northeast')
set(gca, 'FontName', 'Times')

figure (3)
clf
plot(x,y, 'g'), title('Pitch vs Heave'), xlabel('Heave (ft)'),
ylabel('Pitch (rad)')
legend({'Numerical Nonlinear'},'Location','northeast')
set(gca, 'FontName', 'Times')


end
```